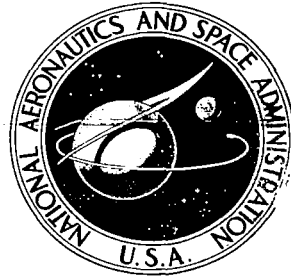


**NASA CONTRACTOR
REPORT**



NASA CR-1744
c.1

0060790



TECH LIBRARY KAFB, NM

NASA CR-1744

**LOAN COPY: RETURN TO
AFWL (DOGL)
KIRTLAND AFB, N. M.**

**MEASUREMENTS AND ANALYSIS
OF LIGHTNING-INDUCED VOLTAGES
IN AIRCRAFT ELECTRICAL CIRCUITS**

by K. J. Lloyd, J. A. Plumer, and L. C. Walko

Prepared by
GENERAL ELECTRIC COMPANY
Pittsfield, Mass.
for Lewis Research Center



0060790

1. Report No. NASA CR-1744	2. Government Accession No.	3. Recipient's Catalog No.	
4. Title and Subtitle MEASUREMENTS AND ANALYSIS OF LIGHTNING-INDUCED VOLTAGES IN AIRCRAFT ELECTRICAL CIRCUITS		5. Report Date February 1971	
		6. Performing Organization Code	
7. Author(s) K. J. Lloyd, J. A. Plumer, and L. C. Walko		8. Performing Organization Report No. HVL 69-161	
		10. Work Unit No.	
9. Performing Organization Name and Address General Electric Company Pittsfield, Massachusetts		11. Contract or Grant No. NAS 3-12019	
		13. Type of Report and Period Covered Contractor Report	
12. Sponsoring Agency Name and Address National Aeronautics and Space Administration Washington, D. C. 20546		14. Sponsoring Agency Code	
		15. Supplementary Notes	
16. Abstract <p>This report describes an experimental investigation of voltages induced by lightning in aircraft electrical circuits. An extensive series of measurements was made of voltages induced in circuits within a metallic aircraft wing by full-scale simulated lightning currents flowing through its skin and structure. The measured data were mathematically analyzed to enable determination of voltages across load impedances to which the circuits might be connected elsewhere in the aircraft. Relationships between induced voltages and lightning current, wing structural, and circuit parameters were determined. Induced voltages of magnitudes likely to cause damage or interference with avionics were measured.</p>			
17. Key Words (Suggested by Author(s)) Lightning, Aircraft, Induced voltages, Electrical circuits, Electrical equipment, Aircraft hazards		18. Distribution Statement Unclassified - unlimited	
19. Security Classif. (of this report) Unclassified	20. Security Classif. (of this page) Unclassified	21. No. of Pages 170	22. Price* \$3.00

FOREWORD

The research described in this report was conducted by the General Electric Company under NASA contract NAS 3-12019. Mr. Paul T. Hacker of the Lewis Research Center Aerospace Safety Research and Data Institute was the NASA Project Manager. The report was originally issued as General Electric report HVL 69-161.

TABLE OF CONTENTS

	Page
INTRODUCTION	1
EXPERIMENTAL INVESTIGATION	6
Description of Test Object	6
Physical Characteristics of F89J Wing	6
Wing Electrical Circuits	11
Test Setup	14
Experimental Conditions	28
Measurements	28
Lightning Simulation	30
Stroke Location Selections	32
Stroke Amplitude Selection	36
Stroke Wave Shape Selections	37
Circuit Conductor Selections	39
Experimental Results	42
Circuit Characteristics versus Induced Effects	43
Test Conditions versus Induced Effects	69
Special Tests	71
Other Observations	89
ANALYTICAL INVESTIGATION	94
Equivalent Circuits	94
Thevenin Voltage Source, e_T	97
Thevenin Impedance, Z_T	123
CONCLUDING DISCUSSION	139
Voltages Induced by Lightning	139
Circuit Characteristics	144
Analytical Method	145
Measurement of Induced Voltages in Operational Aircraft	146
APPENDIX	148
REFERENCES	163
BIBLIOGRAPHY	164

SUMMARY

The direct mechanical, thermal and electrical effects of lightning upon aircraft have been the subject of extensive studies during the past several decades; however, the induced or indirect electrical effects of lightning upon aircraft have not, until recently, received similar attention. Numerous incidents, however, have indicated that lightning currents which flow through the skin and structure of a metallic aircraft can induce hazardous voltages into electrical circuits within. Many incidents have been reported, for example, in which avionics equipments have been disabled as a result of lightning strokes to the aircraft. Accordingly, this program was undertaken to measure the level of voltages which lightning may induce in a variety of actual aircraft circuits, and determine the extent to which these voltages may be impressed across connected impedances representing various aircraft electrical components.

To accomplish this, the right-hand wing of an F89J aircraft, complete with all normally installed electrical circuits, was utilized as a test bed. Full-scale simulated lightning strokes were delivered to various locations on the wing, and measurements of induced voltages and currents were made at the electrical circuit terminals. Because only a wing was tested, an analytical technique was developed with which to determine the amount of induced voltage which these circuits would actually impress across connected electrical loads in other parts of the aircraft. From this analysis technique, relationships between the induced voltage and the applied lightning current parameters were also discovered.

Induced voltages measured ranged between several millivolts in well-shielded high-impedance circuits, and one hundred volts in poorly-shielded low-impedance circuits, which utilized the airframe as the circuit return path.

In all cases, the measured induced voltages were expressible mathematically in terms of a resistive voltage component, proportional to the

lightning current amplitude, and an inductive component, proportional to its rate of change. Effective wing resistances and mutual inductances relating these components to the lightning current amplitude and rate-of-change parameters were analytically derived from the test data, for each test condition and circuit.

From this investigation it has been determined that lightning may cause induced voltages of a magnitude probably sufficient to interfere with or damage sensitive aircraft electrical and avionics equipments. This is particularly likely if the results of these tests are extrapolated to correspond with larger aircraft dimensions or more severe lightning strokes. Substantial reduction in the level of induced voltages may be obtained, however, if certain shielding and grounding techniques can be utilized in the design and layout of aircraft electrical circuits.

Preliminary evaluations were made of a nondestructive test technique for possible use in determining the voltages which lightning may induce in the circuits of other aircraft. This technique utilizes a low-energy pulse generator known as a transient analyzer, in place of a full-scale simulated lightning current generator. When scaled upward, voltages induced by the transient analyzer tests agreed closely with those induced by full-scale simulated lightning currents of the same wave shape.

INTRODUCTION

The effects of lightning on aircraft have been the subject of extended investigations carried out during the past twenty years by various governmental agencies, aircraft industries and research laboratories (See Bibliography). To date these programs have concentrated on defining the thermal and mechanical effects of lightning on aircraft and associated hazards to surfaces, structures and fuel systems. Previous research has also been directed toward defining the effects of direct lightning contact with external electrical components, such as antennas and position lights.

Very little research had been accomplished, however, toward definition of the indirect or induced effects of lightning on aircraft electrical systems. It has been recognized that the magnetic fields associated with lightning currents passing through the aircraft skin and structure can link aircraft electrical circuits and cause resultant induced voltages. Similarly, lightning currents may also result in resistive voltage rises along the skin of an aircraft, which may be part of an electrical circuit if the skin is used as a return path for such circuits.

The magnitude of these voltages, or extent to which they interact with and affect aircraft electrical and electronic systems had not been determined. What has been evident is that sensitive avionics, as well as other equipment, have been increasingly affected by some characteristic of flight environment and communication equipments have failed. Electroexplosive devices (EED's) have also been actuated in similar environments (ref. 1). Nevertheless, for many years these hazards were lived with and few, if any, fatal accidents could be assigned to these effects. Induced effects, in the past, were probably not severe enough to cause extensive damage to electronic equipment, partially because such equipment has made extensive

use of vacuum tubes which, due to the vacuum gap between electrodes, have inherently high voltage breakdown characteristics. The latest and most modern aircraft, however, have equipment which used semiconductors and micro-circuitry, which are much less tolerant of transient overvoltages and currents. Increasing use of these devices and others such as integrated and hybrid circuits is evident in current development of advanced avionic equipments.

Some investigation has been accomplished to determine the transient voltage and current withstand capability of these new devices, and other work has been accomplished to determine the voltage breakdown characteristics of various electronic equipments and the inadvertent firing of EED's on aerospace vehicles (ref. 1). Very little work, however, had been accomplished to determine the magnitude of induced voltages arising in aircraft electrical circuits, or their relationships to characteristics of the lightning currents that cause them. It is necessary to know these voltage levels before the susceptibility of aircraft systems and components to interference or damage therefrom can be assessed.

Accordingly, this program was undertaken to determine the magnitude of magnetically-induced (and resistive) voltages which may arise in aircraft electrical circuitry within a metallic aircraft enclosure through which lightning current is flowing, and evaluate the factors affecting these voltages.

An understanding of these factors will permit an analysis of the susceptibility of sensitive avionics systems and components to these voltages, and determination of protective requirements and techniques.

For practical reasons, the experimental portion of this investigation had to be conducted on a structure of a single type of aircraft. While the same factors are likely to be effective in all aircraft, the degree to which each affects the induced voltages in other aircraft is not known. Therefore, this program has proceeded on the basis that a thorough study of

the mechanism of induced voltages in a single aircraft would permit satisfactory techniques to be developed with which to evaluate many other aircraft on a more rapid and economical basis. Thus, the specific objectives of this program were to:

- (1) Measure the voltages induced in actual aircraft circuits as a result of lightning current flow through a major structural assembly of an aircraft.
- (2) Determine the extent to which these voltages may be coupled into any loads (equipment) elsewhere in the aircraft, the input impedance of which is known.
- (3) Identify the factors affecting these voltages, and determine the significance of each.
- (4) Develop techniques for performing similar evaluations of the susceptibility of circuits within many different aircraft to lightning-induced effects.

The aircraft structural assembly used for this investigation was the complete right-hand wing of an F89J (Scorpion) all-weather fighter aircraft. The wing, supplied by NASA, was intact and had all normally installed electrical circuits in place.

A wing was chosen for this investigation for several reasons. First, the wings are among the locations most frequently struck by lightning, and lightning currents must flow along the length of the wing to reach the other extremities of the aircraft from which the stroke would likely exit. In addition, much electrical circuitry is present in a wing, and its orientation parallel with lightning current flow is likely to result in the greatest interaction with the resultant magnetic field. Finally, contrary to common belief, the noncylindrical geometry of a wing assures that, even though the wing surface is a conductor, some magnetic flux will be present within the wing.

Full-scale simulated lightning strokes of varying wave shapes and

amplitudes were delivered to various locations on the wing. Measurements were made of the induced voltages appearing at the terminals of the wing electrical circuits, located at the base of the wing, and correlations were made between these measurements and the lightning stroke and wing circuit characteristics.

In order to provide a means of determining the amount of induced voltage which these circuits would impress across the terminals of pieces of equipment to which they would be connected in a complete aircraft, measurements of voltages across the open wing circuit terminals, as well as currents flowing through the terminals when short circuited were made. From these measurements, equivalent circuits were determined analytically. These circuits are actually the Thevenin equivalents of the wing circuits, with respect to their terminals at the wing root. To these circuits, which consist of an ideal voltage source and a series impedance, any desired "load" impedance can be added and its voltage response calculated.

Additional analytical procedures were applied to derive relationships between the applied simulated lightning currents and the induced voltages.

Full-scale simulated lightning stroke currents were applied for most of the tests in this program; however, some comparison tests were also performed using very low amplitude currents associated with the Transient Analyzer, to evaluate the application of this instrument as a nondestructive means of determining the voltages which lightning would induce in circuits of other aircraft. The Transient Analyzer is a device developed by the G.E. High Voltage Laboratory for performing similar nondestructive tests on large-scale electric power apparatus.

The work described in this report represents, as far as is known, the first thorough experimental investigation of lightning-induced voltages in electric circuits within a major portion of an aircraft. Associated analytical work has permitted an understanding of some of the significant factors and relationships affecting these voltages. While the voltages

measured necessarily do not have direct significance to all other aircraft, the investigation has provided a significant insight into the problem of lightning hazards to aircraft electrical systems.

The main text of this report is divided into two sections, covering the Experimental Investigation and the Analysis of Results. Inasmuch as a large amount of data was gathered, only summaries or tables necessary to illustrate important points are included in the main text. The basic data are tabulated and presented in the Appendix.

EXPERIMENTAL INVESTIGATION

DESCRIPTION OF TEST OBJECT

Physical Characteristics of F89J Wing

The right-hand wing of an F89J (Scorpion) all-weather fighter served as the main test object for this program.

The Northrop F89J aircraft is a midwing all-weather interceptor fighter. Main features include a tricycle landing gear, combination aileron speed brakes, slotted wing flaps, wing tip fuel or combination fuel and rocket pads, and removable underwing pylons for fuel or armament stores.

The wing furnished had been removed from U.S. Air Force aircraft, Serial No. 53-2555. According to the USAF Technical Orders, this aircraft is in Group 60, Code Y. The wing is equipped with a 600 gallon tip fuel tank and an underwing pylon. No stores were present for the pylon.

The wing, shown in Figures 1 and 2, is of full cantilever, multispar construction using heavy, tapered alclad skin. The principal sections are the main wing panel, leading edge, trailing edge, inboard and outboard sections, wing flap and slot, aileron speed brakes, pylon, and a nonjettisonable wing tip pod. A fully retractable main landing gear and six fuel cells are housed in each wing.

The main wing panel consists of five heavily constructed spanwise spars, bulkheads, ribs, and aluminum honeycomb reinforced heavy tapered alclad skin. Access and inspection doors are provided throughout the wing surface.

The leading edge consists of a fabricated spar, formed ribs, heavy tapered alclad skin, a formed and perforated inner skin installed next to the outer skin between the spar and the extreme forward section, and a spanwise duct to distribute hot air to the leading edge for anti-icing. The leading edge is attached to the forward wing spar with high-strength flush-head screws and is removable for access to lines and equipment in that area.

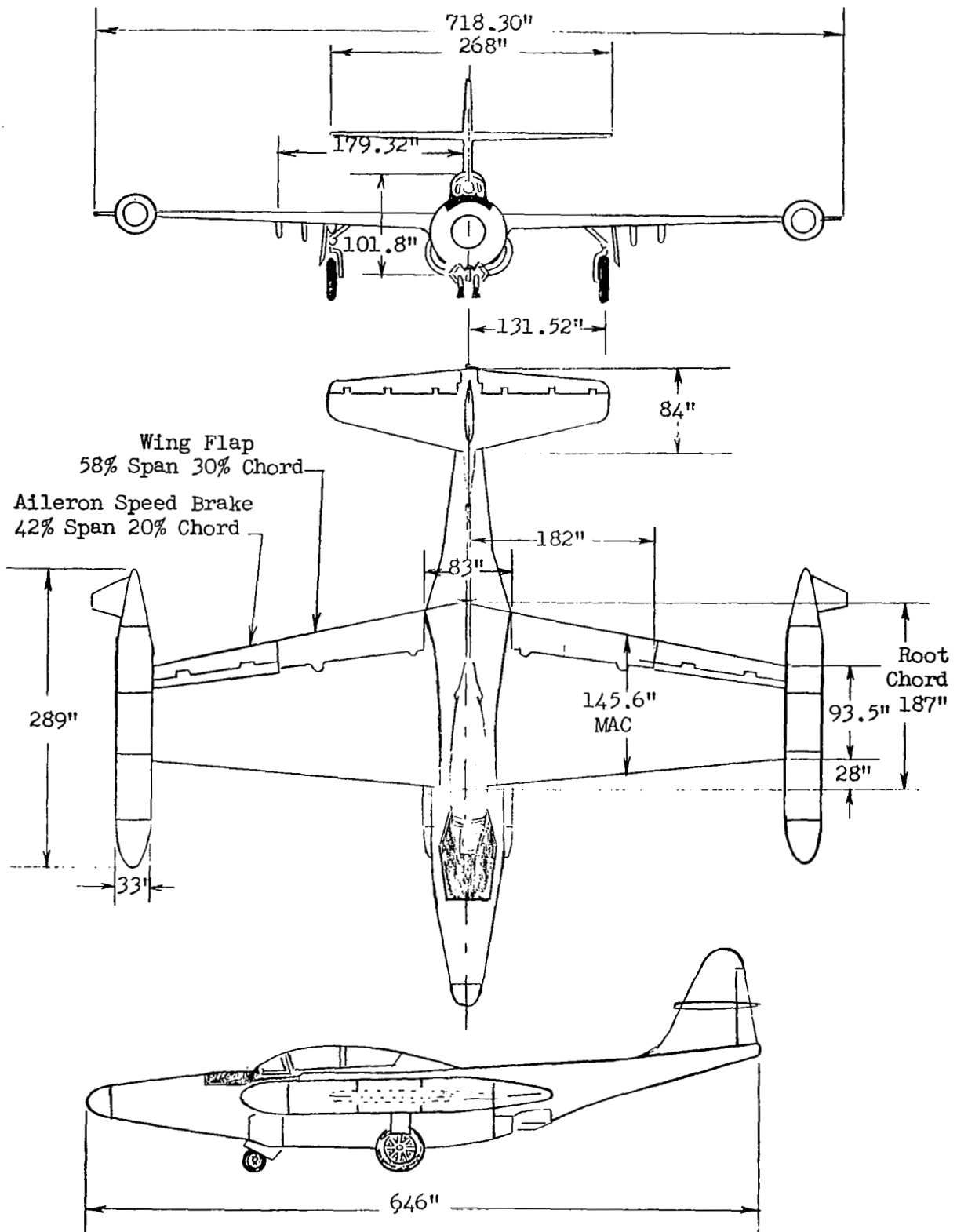


FIGURE 1. F89J PRINCIPAL DIMENSIONS



FIGURE 2. - F89J RIGHT WING SHOWN POSITIONED FOR TEST IN HIGH VOLTAGE LABORATORY TEST BAY. LIGHTNING CURRENT GENERATOR IS BENEATH TIP TANK.

The trailing edge section is located immediately aft of the main wing panel and consists of chordwise formers, diagonal built-up ribs, one spanwise spar in the outboard section, and alclad skin. Control units and lines for the flaps and aileron speed brakes are housed in the trailing edge section. Doors are provided on the lower skin surface for access to these units.

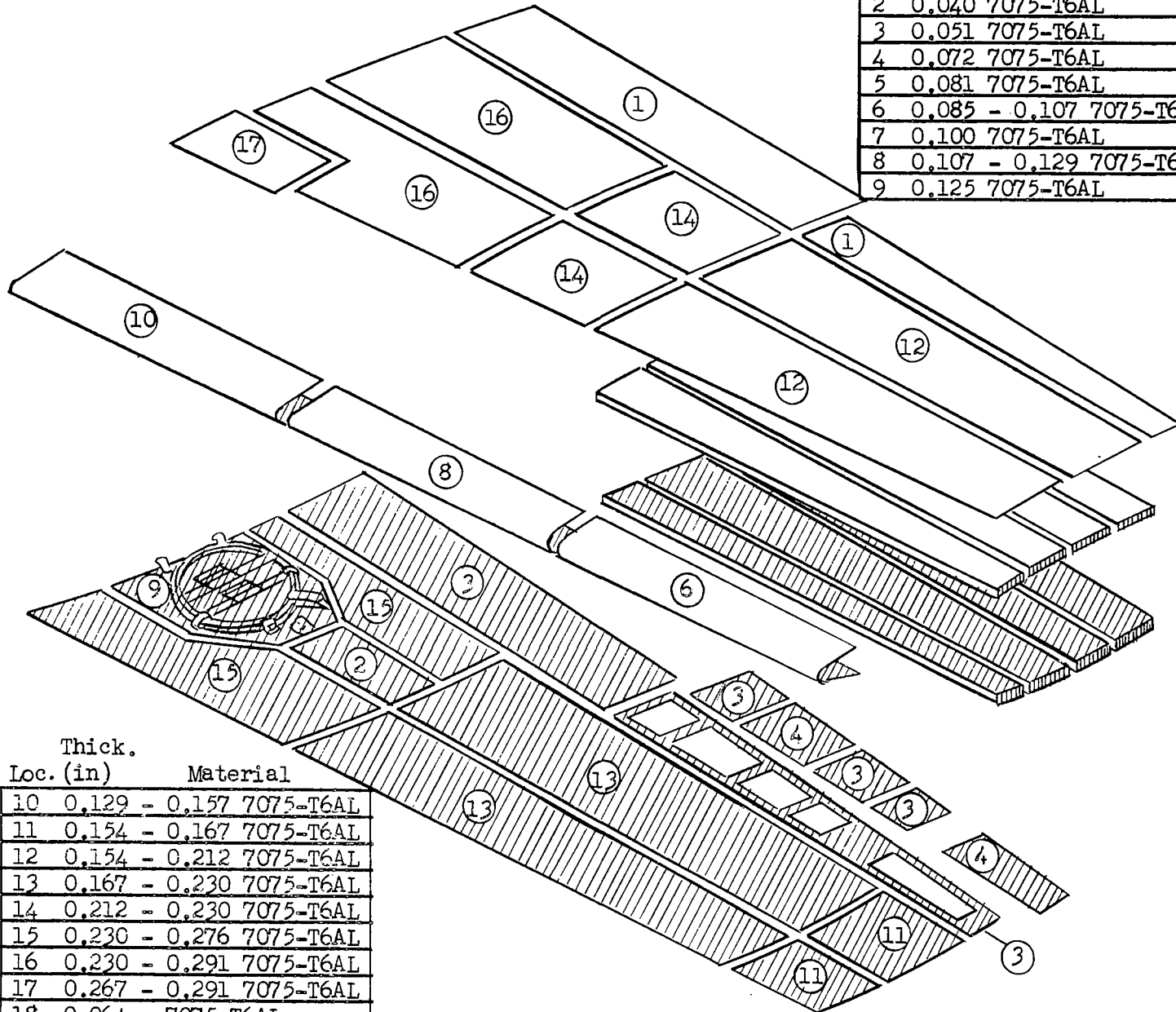
A slotted wing flap is mounted on the inboard portion of each wing trailing edge. The slots are installed on the leading edge of the flaps and are composed of formed ribs, extruded T-section caps and alclad skin. Access to the hinge bolts of the slats is gained through small doors located on the underside of each unit.

The aircraft is equipped with a combination aileron speed brake attached to the outboard section of each wing trailing edge. The aileron speed brake assembly is made up of three sections. The nose section is composed of a single cell structure having a main spar with ribs and skin forming the cell and housing the speed brake activating mechanism; the upper and lower movable speed brakes are of conventional skin and rib construction with doublers in the vicinity of the hinge points.

This wing is equipped with a 600 gallon wing tip fuel tank. This tank consists of a modified monocoque tail cone supporting an adjustable horizontal fin. The tank is mounted on the wing by two bolts and a pin. Flexible fuel hose and electrical cables provide necessary connections between the wing and tip tank.

Inasmuch as the electromagnetic shielding effectiveness of the wing is dependent in part on the composition and thickness of its skin, a description of the wing plating is provided in Figure 3. Each panel is made of alclad skin tapered in the lengthwise direction, as indicated in the tabulation of thicknesses in Figure 3. The wing plating is generally of substantial thickness, as required by the mission of the aircraft. These thicknesses are greater than some of those found in more recent commercial or military aircraft. As a result, the electromagnetic shielding effectiveness of this wing

Thick.	Loc. (in)	Material
1	0.051	2024-T4AL
2	0.040	7075-T6AL
3	0.051	7075-T6AL
4	0.072	7075-T6AL
5	0.081	7075-T6AL
6	0.085 - 0.107	7075-T6AL
7	0.100	7075-T6AL
8	0.107 - 0.129	7075-T6AL
9	0.125	7075-T6AL



Thick.	Loc. (in)	Material
10	0.129 - 0.157	7075-T6AL
11	0.154 - 0.167	7075-T6AL
12	0.154 - 0.212	7075-T6AL
13	0.167 - 0.230	7075-T6AL
14	0.212 - 0.230	7075-T6AL
15	0.230 - 0.276	7075-T6AL
16	0.230 - 0.291	7075-T6AL
17	0.267 - 0.291	7075-T6AL
18	0.064 -	7075-T6AL

FIGURE 3. WING PLATING

is likely to be greater than that of a wing plated with thinner skins.

The exterior of the wing plating was chromodized with Aladine 1000. The interior surfaces, and structural elements were Iridite 14-2 and chromic acid anodized and then covered with a green zinc chromate primer per NAI-1071, Type II. This treatment was given all surfaces, including the mating surfaces between elements. No treatment for improvement of electrical bonding between surfaces was applied. Thus, the resultant electrical bonding between structural elements is mainly accomplished via the fastening rivets and bolts.

Wing Electrical Circuits

The electrical circuits present in the wing generally run from connectors near the root end of the wing to components at various locations within the wing. Connections from these circuits to other aircraft circuits are made at these connectors, which permit breaking of the circuits when the wing is physically detached from the fuselage. Groups of connectors are located on panels within the root end of the leading edge and within a trailing edge space just aft of the landing gear wheel well. These groups of connectors will henceforth be referred to as the forward and aft connectors, respectively.

Table I lists the electrical circuits connected to each connector and the function of each. The identifying code numbers used are those given in U.S. Air Force Technical Order 1F-89J-2-10 (ref. 2). Each circuit may have from one to twenty or more conductors, and these may connect to one or more components within the wing. Electrical return paths may be through a single parallel conductor or through the wing structure itself. The complete circuit diagram of each is found in Reference 2.

There are a total of 29 functional circuits within the wing. In order to keep the data obtained within a manageable level, it was decided to perform induced effects measurements upon a reduced number of circuits selected

TABLE I. - F89J WING ELECTRICAL CIRCUITS

FORWARD CONNECTORS

Connector	Circuit No.	Description
UU	E.0701	Right fuel quantity indication
VV	E.0701	Right fuel quantity indication
AN/ARN 18	R.060	AN/ARN 18 glide path radio receiver
MJ 74		GAR-2 systems (Guided aircraft rocket)
MJ 33	A.100	Monitor and safety power
	A.120	Right special weapon armament power
	A.140	Right armament jettison
	S.220	Armament power supply
MJ 35	A.100	Monitor and safety power
	A.120	Right special weapon armament power
	S.220	Armament power supply
	S.4401	Special weapons heating system
WU	A.080	Fuel tank jettison
	Q.111	Right fuel control normal
	Q.121	Right fuel control manual
WN	Q.060	Right wing tank boosters
	Q.111	Right fuel control normal
	Q.170	Single point fueling master switches and lights
	Q.201	Single point fueling shutoff valves

- continued -

TABLE I. - F89J WING ELECTRICAL CIRCUITS (Continued)

AFT CONNECTORS

Connector	Circuit No.	Description
MJ 62	A.100	Monitor and safety power
TF	Q.170	Single point fueling master switches and lights
	Q.181	Single point fueling control
	Q.201	Single point fueling shutoff valves
	Q.210	Single point defueling
TB	A.010	Pod rocket firing
	D.020	Landing gear indication
	F.0511	Ell Autopilot
	G.010	Landing gear warning
TD	G.040	Anti-skid braking
	H.080	Pod doors, probe and vent heating controls
	Q.010	Fuel filter de-icing
	Q.060	Right wing tank booster pumps
	Q.110	Right fuel control normal
	Q.170	Single point fueling master switches and lights
	Q.200	Single point fueling shutoff valves
TH	A.030	Tip pod rocket door heating
TK	H.080	Pod doors, probe and vent heating control
	L.050	Position lights
	Q.020	Tip tank fuel dump and fuel pump warning lights
	Q.0401	Fuel vent valves

from this total. Thus, a group of eight circuits were selected for measurements in this program. The criteria used for selection of these eight circuits included:

- (1) Function of circuit
- (2) Location of circuit
- (3) Type of return path
- (4) Shielding
- (5) Applicability in other aircraft

In order to learn the relationship between these criteria and induced effects, circuits with varied characteristics were selected. Table II lists the selected circuits. The location and schematic diagram of each circuit is shown individually on Figures 4 through 11.

TEST SETUP

In order to permit passage of simulated lightning currents through the wing, it was positioned within an indoor test bay of the High Voltage Laboratory adjacent to a high-amplitude simulated lightning current generator. To maintain the shortest simulated lightning current circuit possible and thus obtain the maximum possible unidirectional current, the wing was positioned with its tip above the lightning current generator. In this manner, the output from the generator could be readily delivered, via a movable electrode, to desired stroke locations on the wing. To support the wing in this position, a wooden support carriage was constructed. The root end of the wing was joined to a double-screened instrument enclosure, into which the simulated lightning currents passed from the wing. A low-inductive aluminum foil return path along the floor connected the screened instrument enclosure with the impulse generator, completing the current flow circuit.

The wing is pictured set up in the test area in Figure 2. Figure 12 affords a graphic description of this arrangement, showing the wing mounted on its support carriage with the screened instrument enclosure attached to the wing root. The lightning current generator is situated underneath the wing tip and tip fuel tank. The electrode used to apply the simulated

TABLE II. - SUMMARY OF SELECTED CIRCUITS

Circuit Code	Name (Function)	General Location	Return Path	Shielding	Comments
A.140	Right Armament Jettison	Leading Edge and MB-1 Pylon	Airframe	Unshielded	Operates explosive bolts to jettison weapon
E.0711	Right Fuel Quantity Indication	Leading and trailing edges, fuel cells and tip tank	Isolated Conductors	Individual coaxial shielded	Connects fuel measurement probes to capacitance bridge
F.0511	E-11 Autopilot	Trailing edge	Isolated Conductors	Unshielded	Flap position monitor switch
L.050	Position Lights	Trailing edge and tip tank	Airframe	Conduit	Wing position light on tip tank
Q.0401	Fuel Vent Valves	Fuel cells and wing tip	Airframe	Conduit in fuel cells	Circuitous route through fuel cells to operate fuel vent valve
Q.060	Right Wing Tank Booster Pumps	Center and fuel cells	Airframe	Conduit in fuel cells	Operates fuel tank booster pumps
R.060	AN/ARN-18 Glide Path Radio Receiver	Leading edge	Coaxial Shield	Coaxial shielded	Glide path antenna in leading edge
S.220	Armament Power Supply	Leading edge and MB-1 pylon	Isolated Conductors	Individual shielded conductors	Connects time of flight ballistics computer to MB-1 weapon

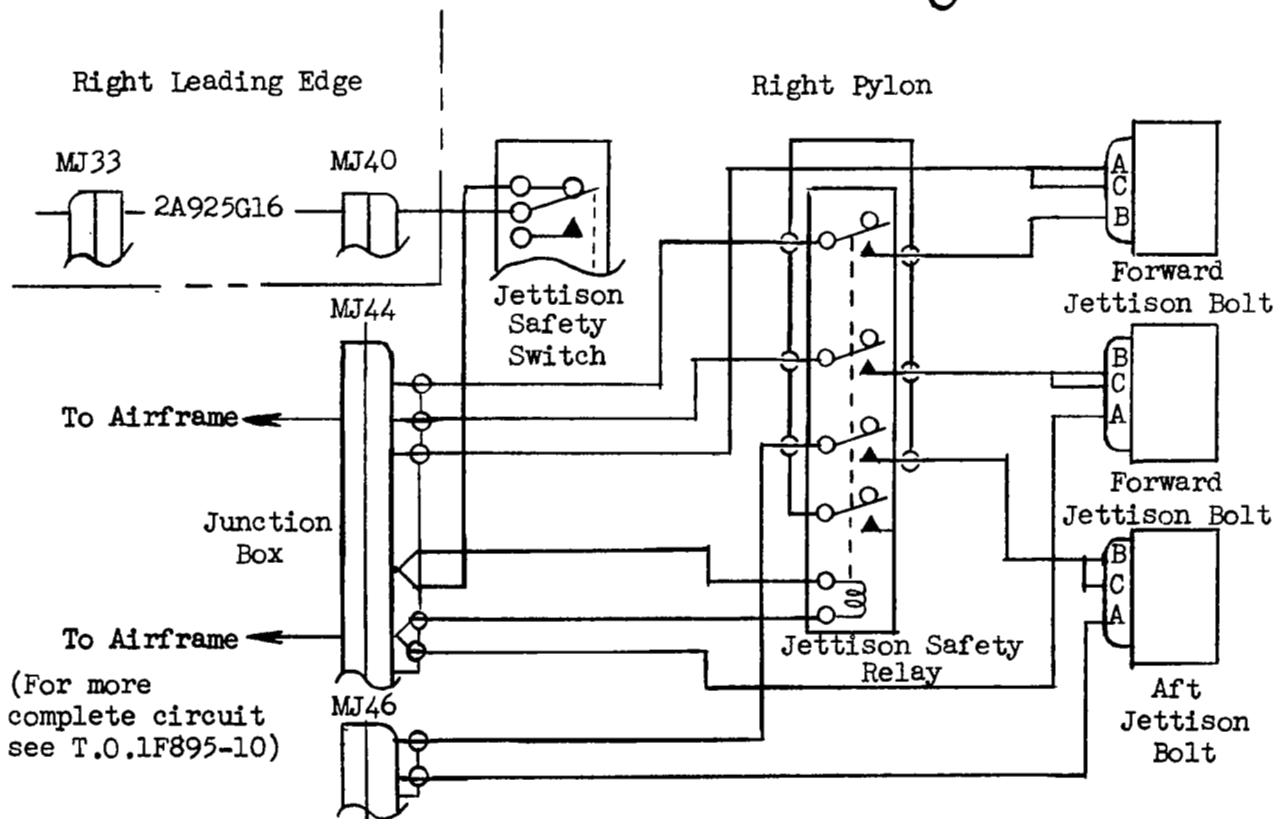
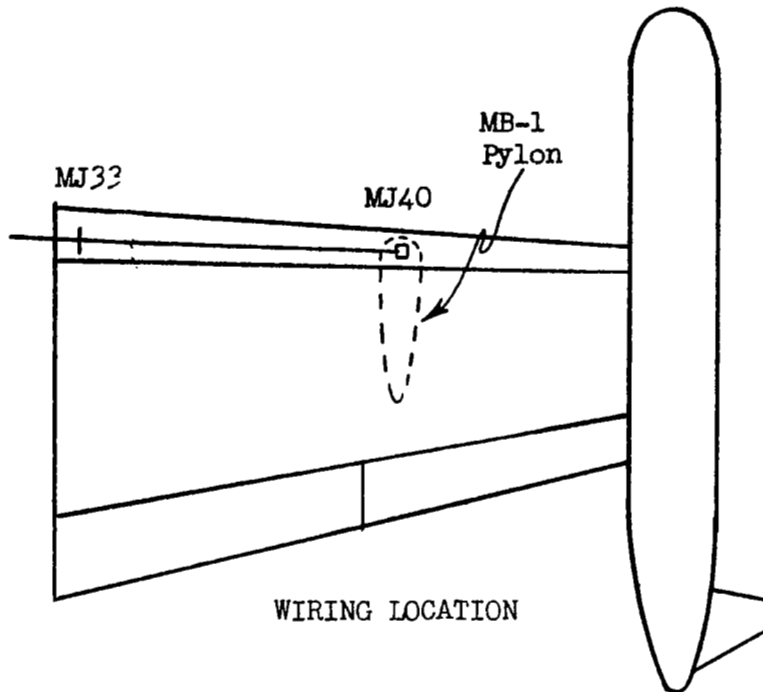
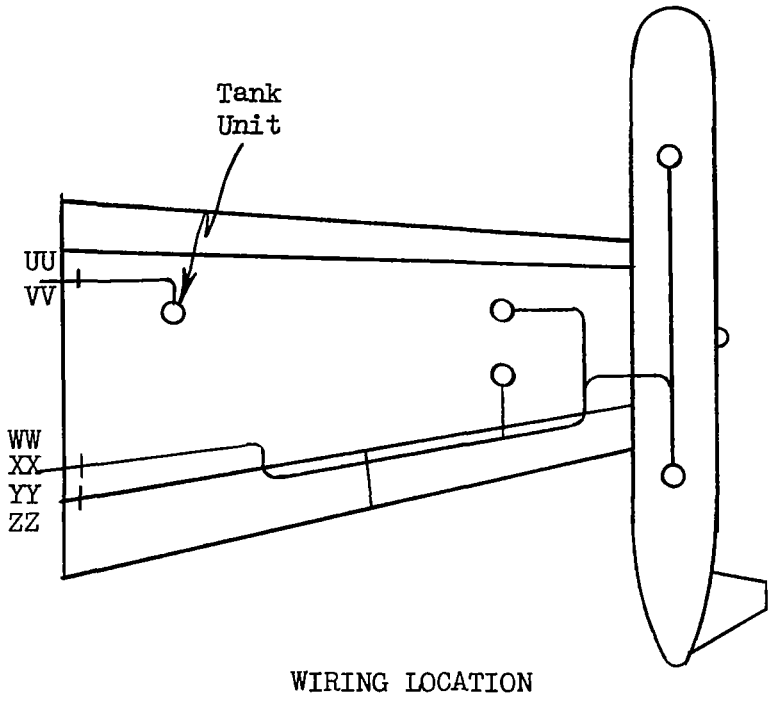


FIGURE 4. - CIRCUIT A.140 RIGHT ARMAMENT JETTISON
WIRING SCHEMATIC AND LOCATION
F89J RIGHT WING AND TIP FUEL TANK



WIRING LOCATION

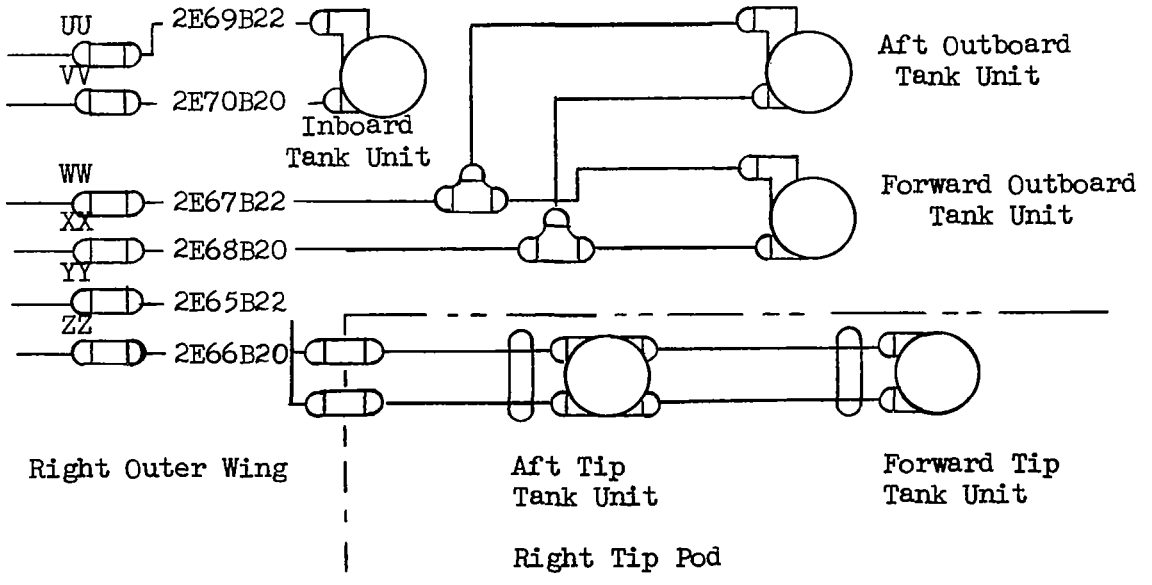
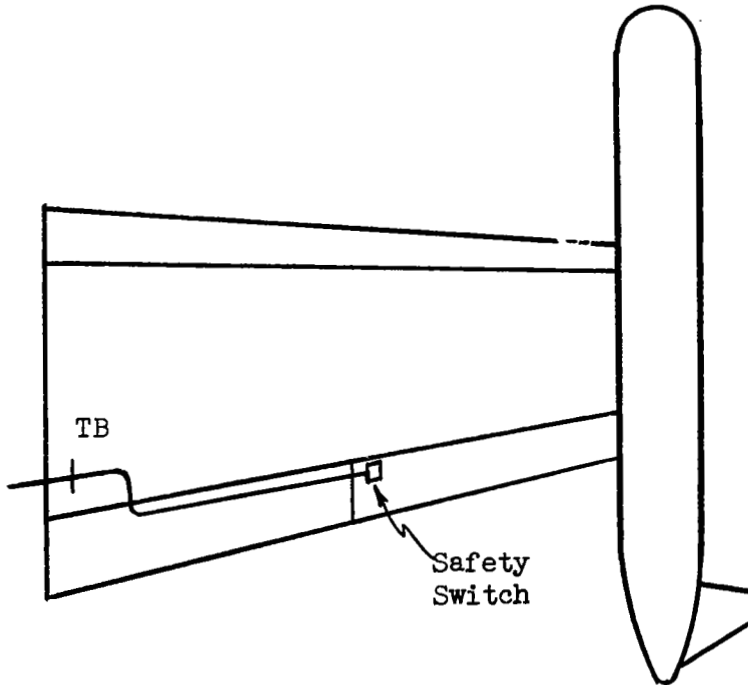


FIGURE 5. - CIRCUIT E.0711 RIGHT FUEL QUANTITY INDICATION
WIRING SCHEMATIC AND LOCATION
F89J RIGHT WING AND TIP FUEL TANK



WIRING LOCATION

RIGHT OUTERWING

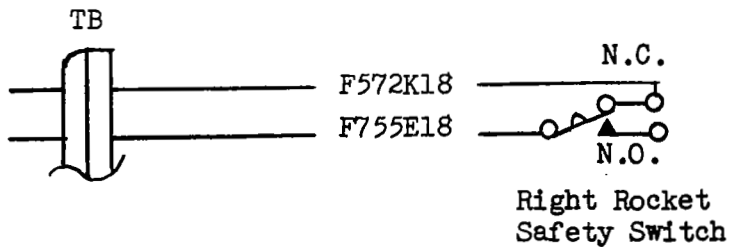
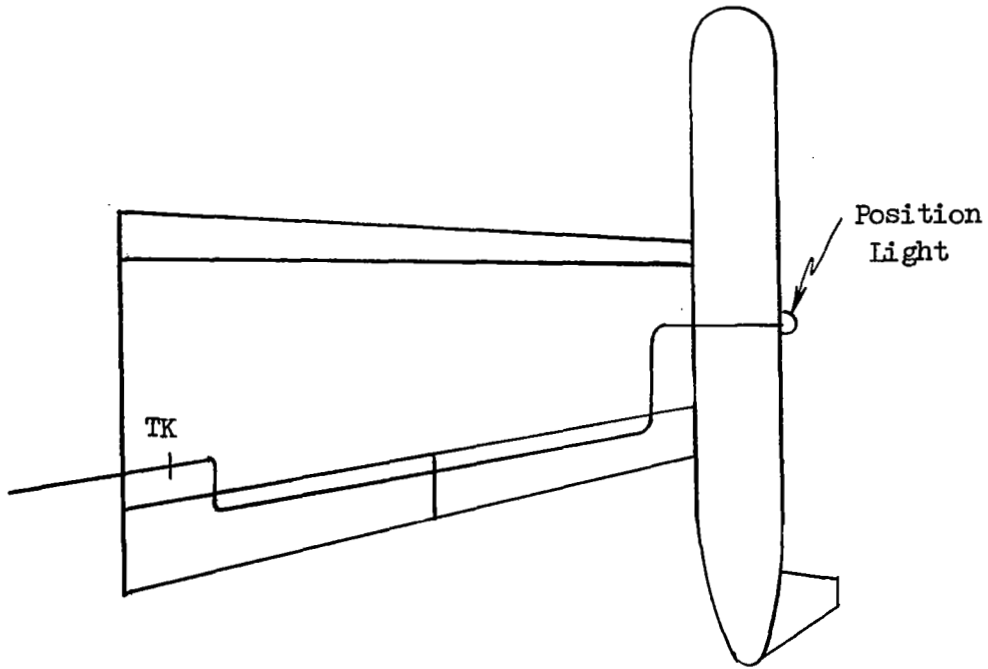


FIGURE 6. - CIRCUIT F.0511 E-11 AUTOPILOT FLAP POSITION MONITORING SWITCH WIRING SCHEMATIC AND LOCATION F89J RIGHT WING AND TIP FUEL TANK



WIRING LOCATION

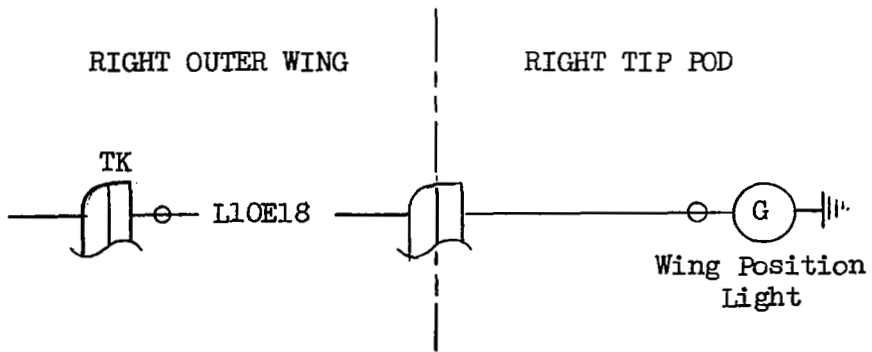
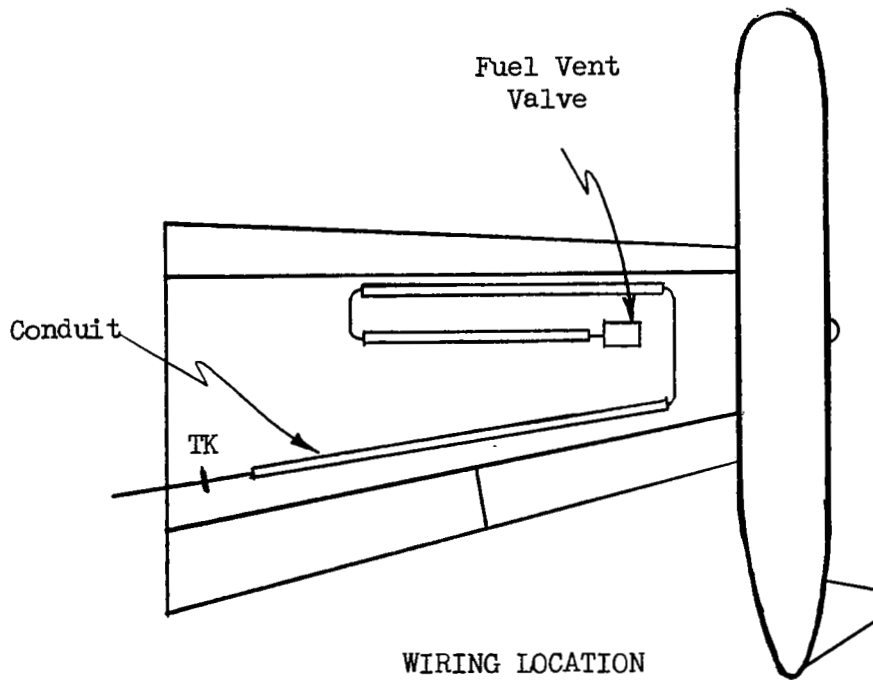


FIGURE 7. - CIRCUIT L.050 POSITION LIGHTS
 WIRING SCHEMATIC AND LOCATION
 F89J RIGHT WING AND TIP FUEL TANK



RIGHT OUTER WING

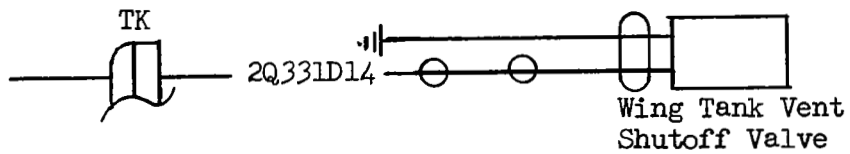


FIGURE 8. - CIRCUIT Q.0401 FUEL VENT VALVES
 WIRING SCHEMATIC AND LOCATION
 F89J RIGHT WING AND TIP FUEL TANK

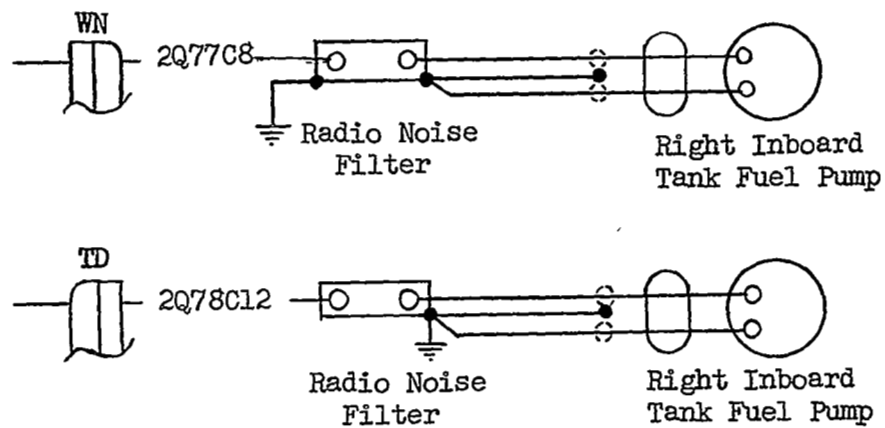
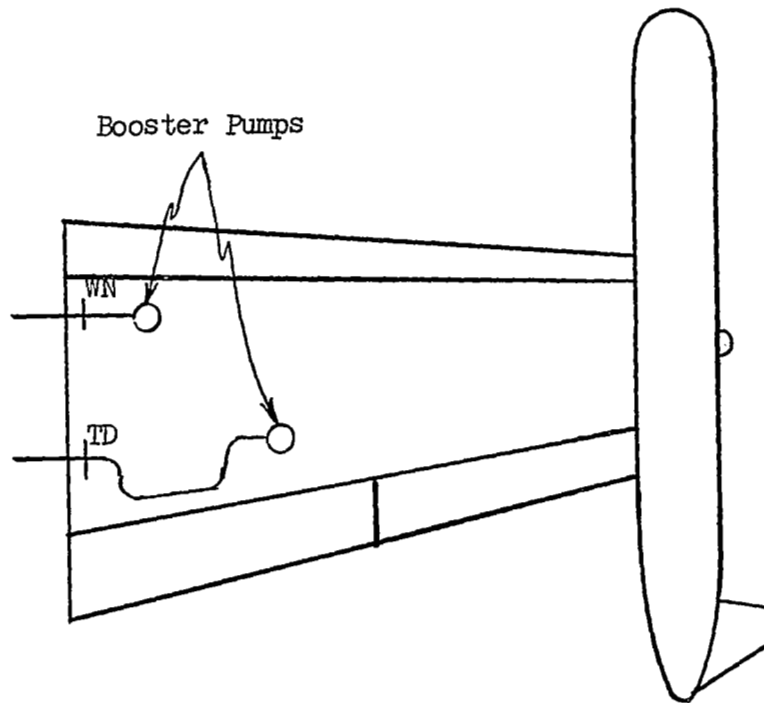


FIGURE 9. - CIRCUIT Q.060 RIGHT WING TANK BOOSTER PUMPS
WIRING SCHEMATIC AND LOCATION
F89J RIGHT WING AND TIP FUEL TANK

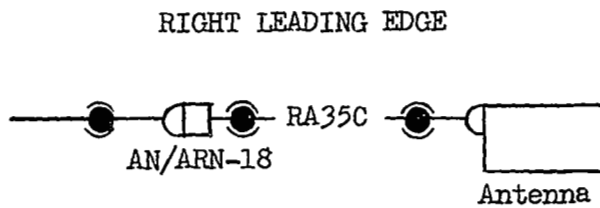
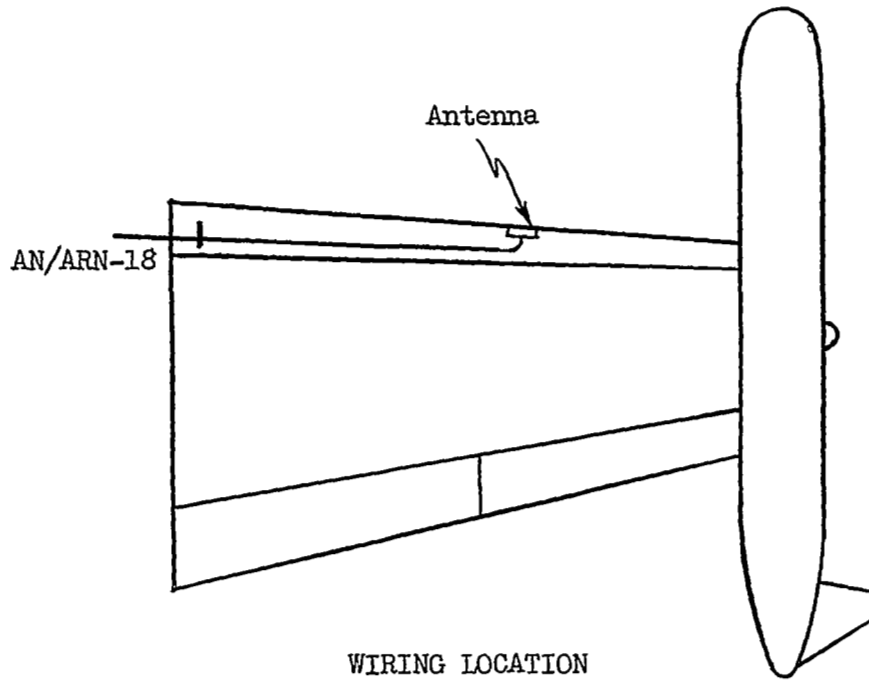


FIGURE 10. - CIRCUIT R.060 AN/ARN-18 GLIDE PATH RADIO RECEIVER
 WIRING SCHEMATIC AND LOCATION
 F89J RIGHT WING AND TIP FUEL TANK

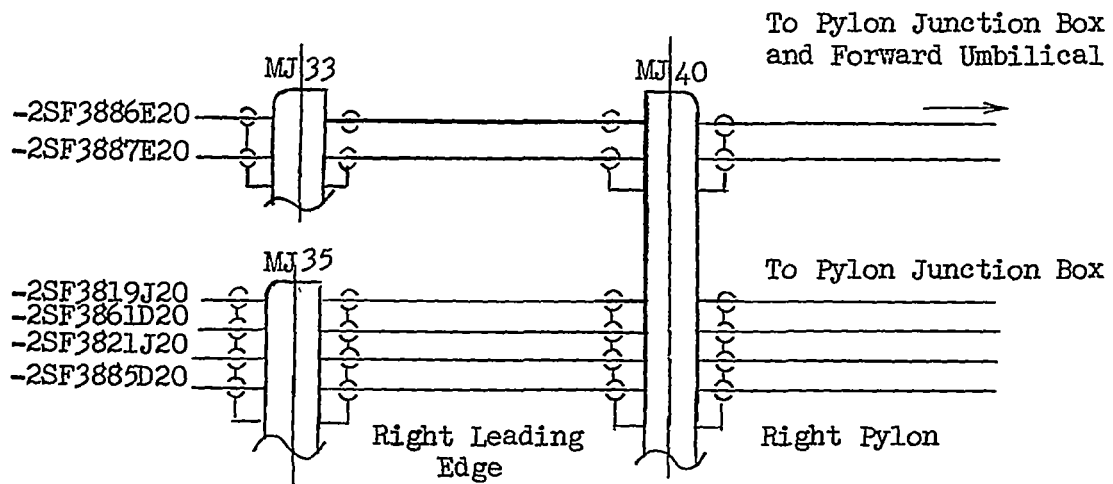
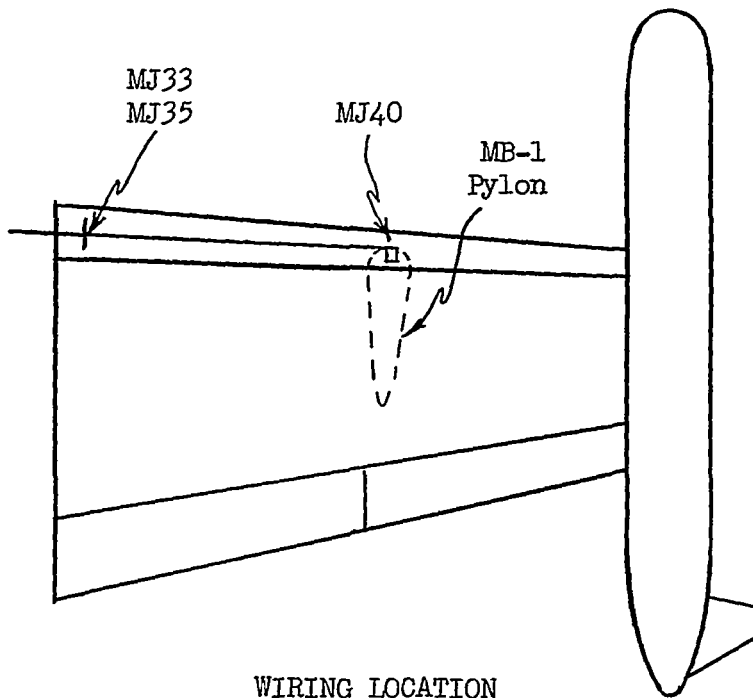


FIGURE 11. - CIRCUIT S.220 ARMAMENT POWER SUPPLY
WIRING SCHEMATIC AND LOCATION
F89J RIGHT WING AND TIP FUEL TANK

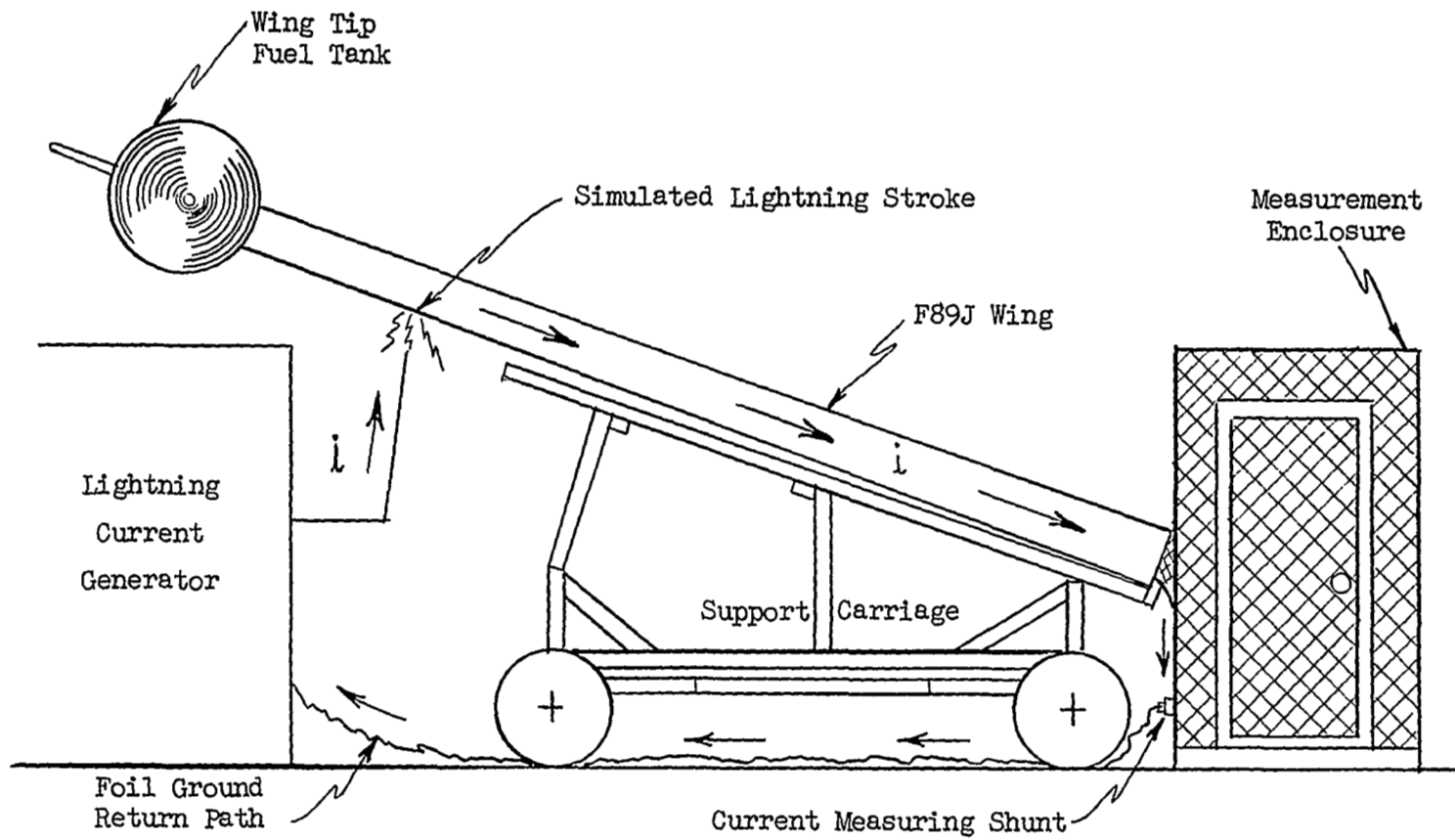


FIGURE 12. - F89J WING TEST SETUP

lightning stroke to the wing is shown in position adjacent to a desired stroke location. The figure also shows the path of the lightning stroke current proceeding along the wing to the screened instrument enclosure. A current measuring shunt between the enclosure and the return foil permitted measurement of the applied lightning stroke wave shape and magnitude.

Figure 13 is a detail description of the mating of the F89J wing and the screened enclosure. In order to remove current from the wing as naturally as possible, it was attached to the instrument enclosure, utilizing all of the attachment bolts located at the root end of the wing, in the same manner as the wing would be actually attached to the fuselage. This figure also illustrates the BNC connectors used to connect the oscilloscopes to the conductors coming from the wing circuit connectors. Figure 14 illustrates the attachment of the screened enclosure in the vicinity of the leading edge of the wing, and shows the BNC connectors fastened to a common bus mounted adjacent to the wing.

With the exception of the flap, which was removed to avoid contact with a nearby fence, and the MB-1 pylon which was removed for the main series of tests, the wing was tested intact with the tip fuel tank attached. Since this investigation was intended to be a basic study of induced effects within a wing, the pylon was removed to preclude introduction of additional effects. Later in the program a series of special tests were run, in which the effects of various modifications to the wing were evaluated. These modifications, which will be described in later paragraphs, included attachment of the pylon, application of a conducting strap along the leading edge seam, and intentional loosening of a main wing panel.

Prior to any tests, the wing and its electrical circuits were inspected to the extent possible. No abnormal conditions were found. Remaining traces of fuel were flushed from the system prior to application of simulated lightning currents.

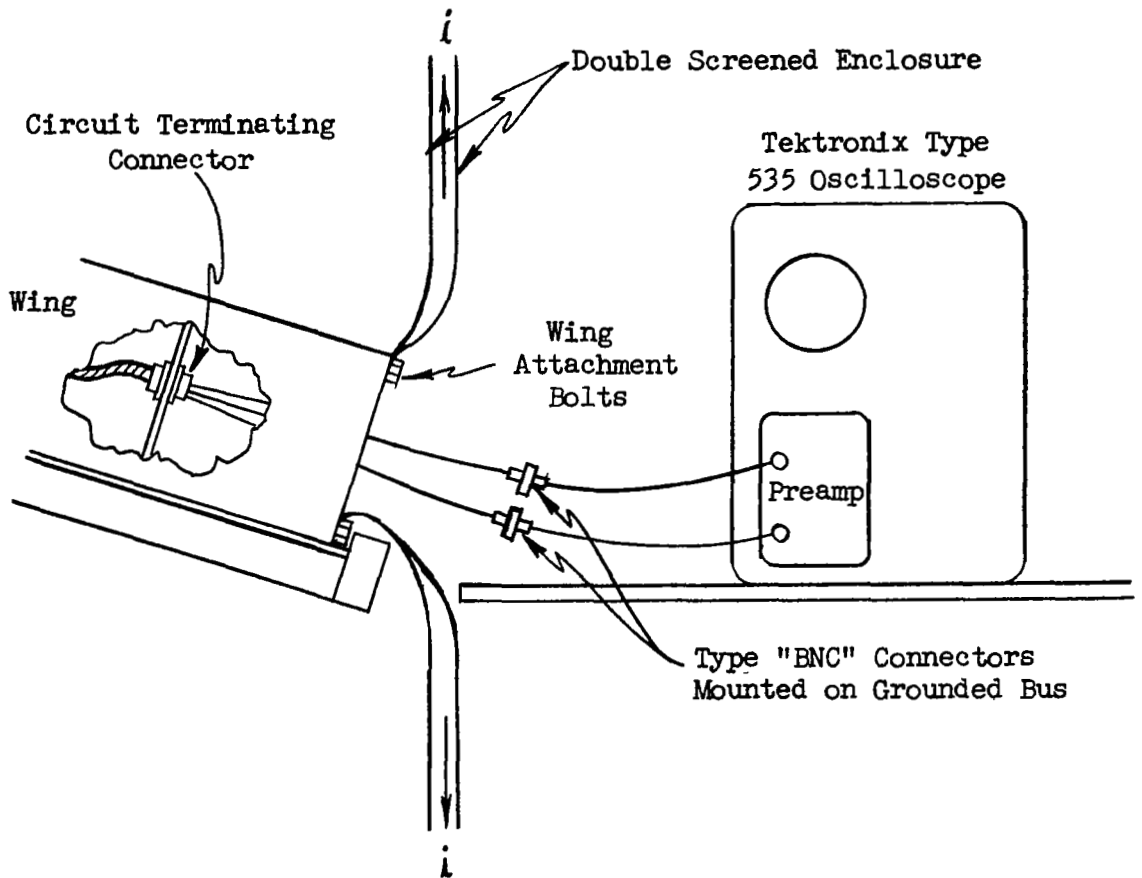
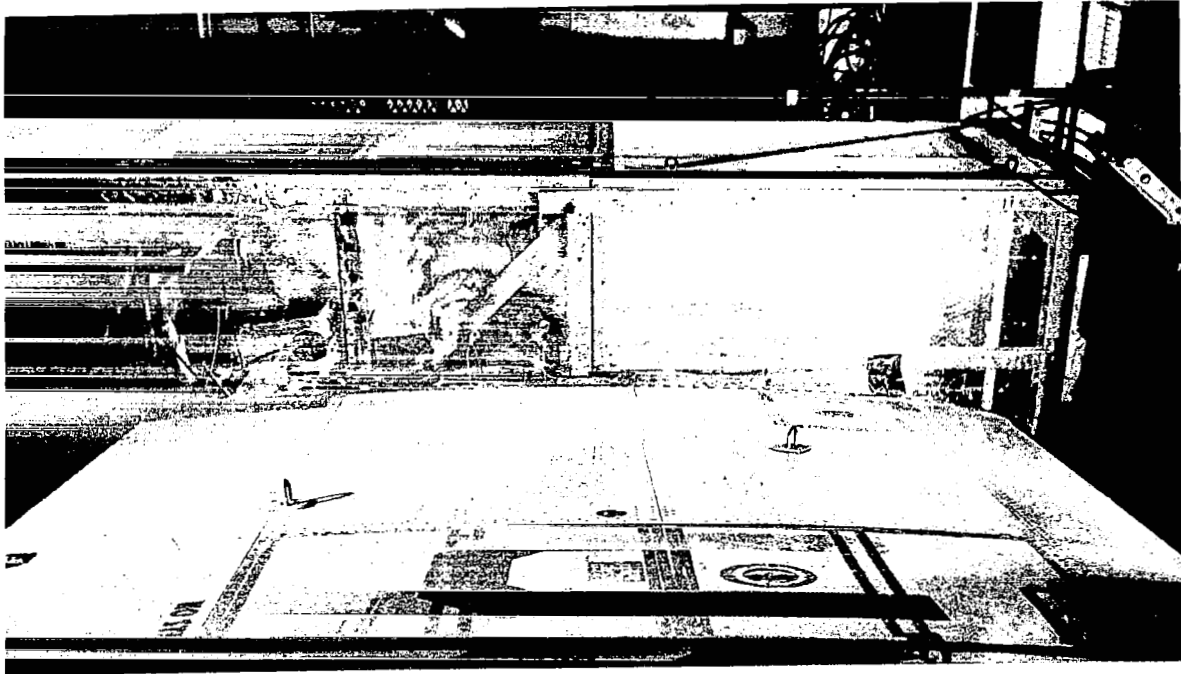
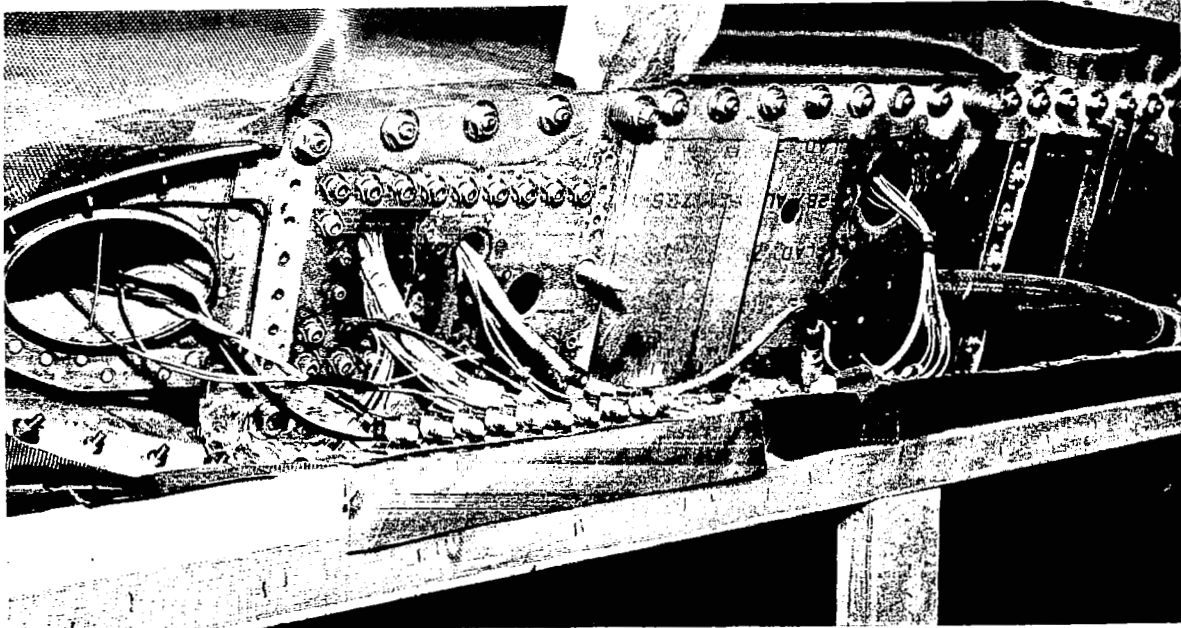


FIGURE 13
 DETAIL OF THE MATING OF THE F89J WING AND SCREENED ENCLOSURE
 SHOWING CURRENT DRAIN-OFF AND CONNECTIONS TO MEASURING EQUIPMENT



a. Inboard View Showing Wing Joined to Screened Instrument Enclosure



b. Interior of Instrument Enclosure, Showing Screen Joined to Leading Edge. Leading Edge Conductors and a Fuel Line are Visible. Newly Installed Special Measurement Circuits May be Seen Coming from Leading Edge Heating Duct.

FIGURE 14. - PHOTOGRAPHS OF F89J WING CONNECTION
TO SCREENED INSTRUMENT ENCLOSURE

EXPERIMENTAL CONDITIONS

Measurements

The objective of this test program was not only to obtain measurements of the voltages induced in the wing circuits by simulated lightning currents, but also to obtain sufficient additional measurements so that the amount of voltage arising across any load in the aircraft to which the wing circuits might be connected could be predicted. The mechanism selected to accomplish this was to determine the Thevenin equivalent circuits of each wing circuit under test. Since a Thevenin circuit consists of an induced voltage source in series with an impedance, another impedance (aircraft load) may be connected to this circuit to form a complete loop. The voltage arising across this load impedance can then be calculated by conventional means. By the Thevenin theorem, the Thevenin voltage source (e_T) is equal to the measured open-circuit (no load) voltage, e_{oc} , and the Thevenin impedance (Z_T) is obtained by making an additional measurement, i_{sc} , from which

$$Z_T = \frac{e_{oc}}{i_{sc}}$$

where i_{sc} (short circuit current) is the measured current flowing through the shorted wing circuit terminals.

From these measurements, the Thevenin equivalent circuit can be calculated. However, if either of the two required measurements were not measured correctly, the calculated Thevenin circuit would have been incorrect. In order to preclude this possibility and perform a check on the validity of the measurements, a third measurement was made with a finite impedance, usually 1 ohm, connected to the terminals, during which both the terminal voltage and current were measured. This set of measurements provided a check which was compared with a calculated response to the same impedance using the Thevenin equivalent circuit determined from the open and closed circuit tests. A further discussion of the analytical processes is given in the Analytical Investigation section of this report.

Measurements of e_{oc} and i_{sc} were made oscillographically, with instruments located within the double-screen shielded enclosure attached to the root end of the wing. This enclosure provided a magnetic shielding of the oscilloscopes and measurement leads, into which extraneous voltages could otherwise be induced by the strong magnetic field presented by the lightning currents. To assure that this shielding was effective, a series of checkout tests were made to assure that no such effects were present. These included zero-signal measurements, using the measurement system in its various configurations, as well as measurements of magnetic flux within the enclosure. These measurements showed that the instrumentation system was not being influenced by these extraneous effects.

Open-circuit voltages, e_{oc} , were measured by a Tektronix Type 535 oscilloscope with a Type 1A1 plug-in. For open-circuit voltage measurements the wing circuits were not otherwise terminated, and thus actual impedance with which the circuits were terminated was the preamplifier input impedance of 1 megohm of resistance paralleled by approximately 15 picofarads of capacitance. The Type 1A1 preamplifier has a rise time of less than 50 nanoseconds, depending upon the deflection scale selected.

The customary series of measurements made at each set of circuit terminals for each applied stroke condition included:

- (1) Open-circuit voltage, e_{oc}
- (2) Short-circuit current, i_{sc}
- (3) Voltage across a terminating dummy load, e_L
- (4) Current through a terminating dummy load, i_L

These measurements were made at one or more oscilloscope sweep settings as necessary to define the wave shape of the signals being measured.

The amplitude and wave shape of the applied lightning current were monitored for all tests to assure that the desired wave shape was in fact being applied.

Lightning Simulation

The lightning currents which pass through an aircraft when it is struck by lightning are believed to be a combination (ref. 3, 4) of high-amplitude, short-duration "strokes" and low-amplitude, long-duration "continuing currents". The continuing currents are known to produce thermal erosion and resultant damage to aircraft skins (ref. 5, 6). However, these currents create very little magnetic flux, and that which is created does not change rapidly. Accordingly, these currents cannot produce significant induced voltages in internal circuitry. For this reason, these currents were not simulated in this program.

The high-amplitude, short-duration strokes, however, may have very high rates of rise, and the resultant rapidly-changing magnetic flux (ϕ) can induce large voltages in magnetically coupled circuits, since

$$E_{\text{induced}} = \frac{d\phi}{dt}$$

Therefore, the high-amplitude, short-duration strokes were simulated for all of the tests in this program.

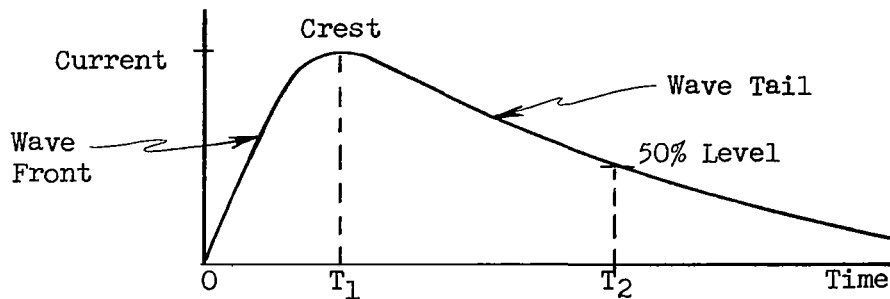
The simulated lightning currents were delivered to the wing by means of an arc approximately 8" long from an electrode positioned adjacent to desired stroke locations on the wing or tip tank.

Since natural lightning currents are nearly always unidirectional (ref. 3, 4 and Bibliography), the currents applied in this program were critically damped or overdamped to obtain a unidirectional wave shape. In order to calculate the lightning current generator circuit constants required to achieve this condition for the various wave shapes desired, the inductance of the lightning current circuit was determined experimentally. This was accomplished by measurement of the frequency and decrement of a damped oscillatory wave form, and subsequent calculation of the inductance by means of the classical differential equations for

an R-L-C circuit. The circuit inductance was found to be 11 microhenrys.

Description of the wave shape of the applied current is facilitated by use of the standard wave shape notation for current impulses. An impulse current, simulating a high-amplitude, short-duration lightning stroke is ideally an aperiodic transient current which rises rapidly to a maximum value and falls less rapidly to zero. The wave shape of such an impulse is defined by:

- (1) polarity
- (2) front time (T_1)
- (3) time to half value on the tail, T_2



The wave shape is then described by the notation:

$$(T_1 \times T_2)$$

where T_1 and T_2 are usually expressed in terms of microseconds (μs). Thus, a wave rising to crest in 5 μs and decaying to 50% level in 10 μs is referred to as a 5 x 10 μs wave.

Since natural lightning strokes may vary in wave shape, amplitude, polarity and attachment location, it was desired to evaluate, insofar as possible, the effect of each of these variables upon the voltages induced in internal circuits.

To evaluate the significance of stroke location variations, identical

strokes were delivered to a large number (10) of locations on the wing, and resultant induced voltages were measured in each of two wing circuits. From these data, the five most significant locations were selected and subsequent tests were made at each of these.

Another series of preliminary tests was made to ascertain the number of stroke amplitude variations necessary to establish the relationship between lightning stroke amplitude and amplitude of induced effects. If this relationship is linear, as was expected, subsequent tests could all be made at the same amplitude, and the results scaled upward or downward to correspond to other stroke amplitudes.

These preliminary tests permitted establishment of test conditions to be subsequently applied for systematic measurements of induced effects in all eight circuits. These measurements then permitted a determination of the effect of stroke location and wave shape upon induced voltages in each of the eight circuits.

Stroke Location Selections

To obtain a preliminary evaluation of the relationship between stroke location and induced effects, and to identify those locations creating the most severe induced voltages, identical strokes were applied to each of the ten locations shown on Figure 15. An identical 14 kiloampere, 12 x 24 μ s simulated lightning discharge was applied to each location. Open-circuit voltages and short-circuit currents were measured at the terminals of circuit L.050 (position lamp) and A.140 (armament jettison) located in the trailing edge and leading edges of the wing, respectively. These measurements are tabulated in Tables III and IV.

For the position lamp circuit (Figure 7) which extends to the extremity of the tip tank and incorporates an airframe return, it is evident that stroke locations on the tank itself create the greatest induced voltages.

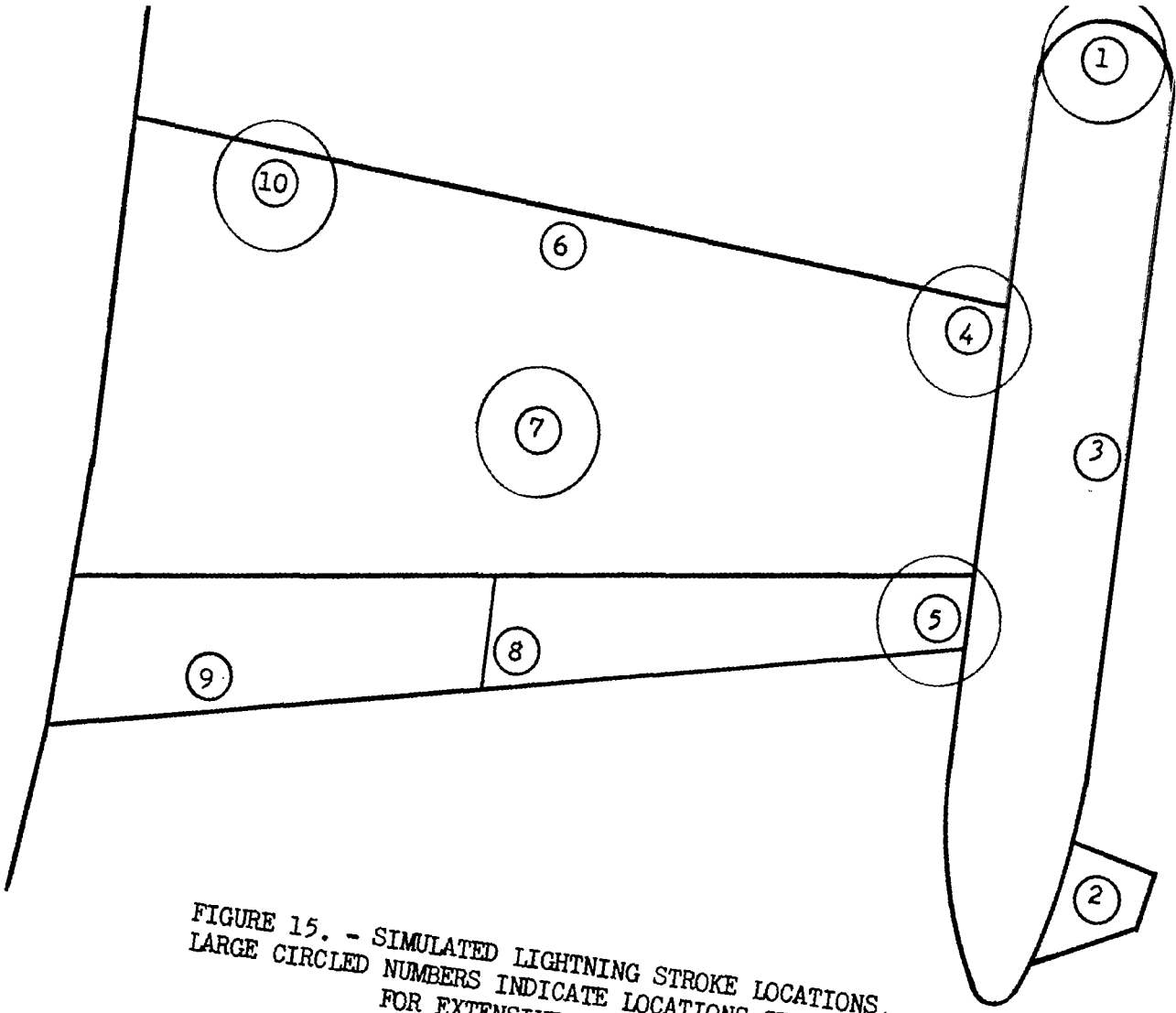


FIGURE 15. - SIMULATED LIGHTNING STROKE LOCATIONS.
LARGE CIRCLED NUMBERS INDICATE LOCATIONS SELECTED
FOR EXTENSIVE TESTING.

TABLE III. - EFFECT OF STROKE LOCATION ON INDUCED EFFECTS
 Circuit L.050 (Position Light)
 (Conductor 2L10E18 and Airframe)
 14 Kiloampere, 12 x 24 μ s Simulated Lightning Discharge

Stroke Location	Open Circuit Voltage (e_{oc}) (Maximums*, Volts)	Short Circuit Current (i_{sc}) (Maximum, Amps)
1	60/14	5.0
2	46/5	2.2
3	40/9	4.2
4	20/3	1.1
5	18/2.8	0.9
6	12/1	0.4
7 (Bottom)	20/1	0.39
8	12/0.8	0.32
9	16/0.8	0.32
10	24/0.8	0.32

* - Two 'maximum' voltages are listed. The first is the maximum amplitude reached by any half-cycle of the 'fast' oscillations appearing at the beginning of the open-circuit voltage. The second is maximum amplitude of the 'slow' component.

TABLE IV. - EFFECT OF STROKE LOCATION ON INDUCED EFFECTS
 Circuit A.140 (Armament Jettison)
 Conductor 2A925G16 and Airframe
 14 Kiloampere, 12 x 24 μ s Simulated Lightning Discharge

Stroke Location	Open Circuit Voltage (e_{oc}) (Maximums*, Volts)	Short Circuit Current (i_{sc}) (Maximum, Amps)
1	0.5/0.24	.003
2	0.3/0.23	.003
3	0.6/0.25	.003
4	0.6/0.25	.005
5	0.75/0.20	.003
6	0.6/0.35	.004
7 (Bottom)	0.60/0.28	.003
8	0.3/0.19	.004
9	0.5/0.15	.004
10	0.4/0.28	.003

* - Two maximum voltages are listed. The first is the maximum amplitude reached by any half-cycle of the 'fast' oscillations appearing at the beginning of the open-circuit voltage. The second is the maximum amplitude of the 'slow' component.

This undoubtedly reflects the maximum exposure of the circuit to magnetic flux and resistive voltage rises in the airframe. There is increased exposure at the junction between the tip tank and wing, due to the higher resistivity of the mechanical joint, as well as the crack between the tank and wing, which permits magnetic flux to directly couple the circuit. The effect of stroke location upon induced voltages in the armament jettison circuit (Figure 4) is less apparent, probably because this circuit was not terminated in the wing (the MB-1 pylon was not attached) and the voltage magnetically induced in it could not be measured at its terminals. In this case, a capacitive voltage rise between the conductor and airframe is all that would appear at the terminals. Such a voltage may arise from a potential difference between the airframe and the conductor - and this would not be as dependent upon stroke location.

From these results, five of the stroke locations of Figure 15 were selected for all subsequent tests. The following criteria were used for selection of these locations:

- Locations resulting in maximum induced effects
- Locations spread apart from others selected
- Locations known to be struck by actual lightning

The locations selected included numbers 1, 4, 5, 7 and 10, shown encircled on Figure 15.

Stroke Amplitude Selection

If the electrical characteristics of the wing and the mutual impedances between it and the circuits within are linear, then the relationship between lightning stroke amplitudes and amplitudes of induced voltages will be linear. In other words, changes in lightning amplitude will result in proportional changes in amplitude of induced voltages. To determine if this relationship exists, a series of tests were made wherein the amplitude of

the applied stroke was varied between 7 and 70 kiloamperes and the induced effects in the position lamp circuit were measured. Figure 16 illustrates the results of this experiment, which show an approximate linear relationship over the range of amplitudes applied. Based upon these results, subsequent tests were made at the single amplitude of 40 kiloamperes. This value was chosen because it is near the center of the linearity range of Figure 16, and because it is also near the average amplitude of measured natural lightning strikes (ref. 7).

Stroke Wave Shape Selections

Since magnetically induced voltages are proportional to the rate of change of magnetic flux linking a circuit, the effect of variations in lightning current wave shape (rate of rise and decay of current) are of considerable interest. Accordingly, the major portion of tests involved application of two different wave shapes, and tests and measurements were made on each of the eight selected circuits according to the following matrix:

Stroke Location	"Slow" Wave Shape				"Fast" Wave Shape			
	e_{oc}	i_{sc}	e_{load}	i_{load}	e_{oc}	i_{sc}	e_{load}	i_{load}
1								
3								
5								
7								
10								

The two wave shapes applied represented the slowest and fastest current wave shapes obtainable from the lightning generator at 40 kiloamperes for a unidirectional current through the relatively large inductance represented by the wing and return path. These wave shapes were as follows:

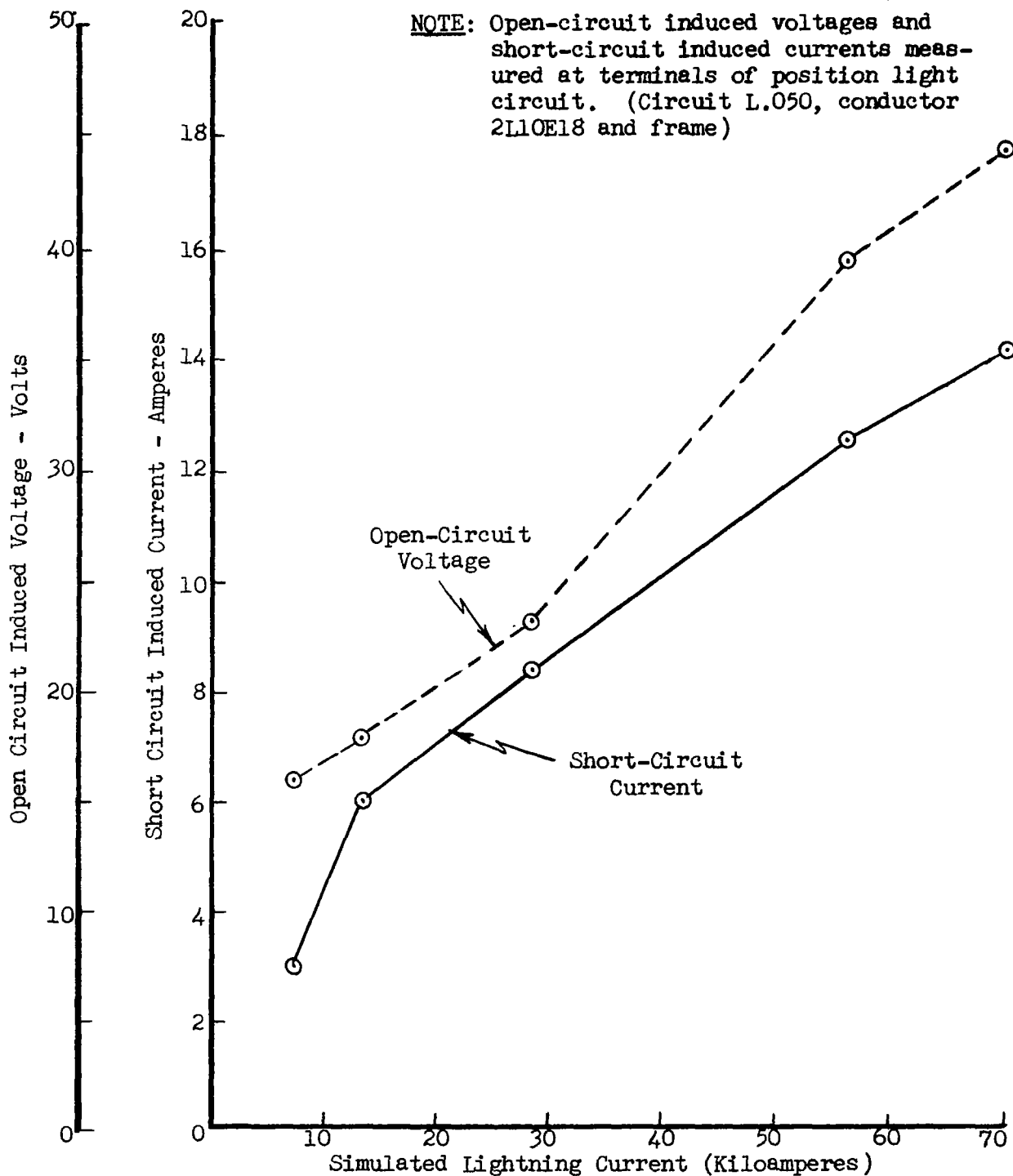
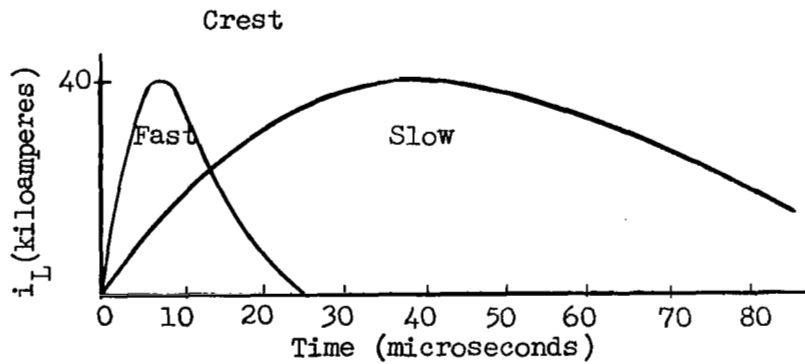


FIGURE 16. - AMPLITUDE OF INDUCED EFFECTS VERSUS AMPLITUDE OF SIMULATED $12 \times 24 \mu\text{s}$ LIGHTNING CURRENT Current Discharged to Location No. 1 (Fwd. End of Wing Tip Fuel Tank)

"Slow" Wave Shape = 36 x 82 μ s
 "Fast" Wave Shape = 8.2 x 14 μ s

Each of these wave shapes is within the range of wave shapes commonly measured from natural lightning strokes (ref. 7). Figure 17 shows oscillograms of each of these wave shapes.

The 8.2 x 14 μ s stroke provided a rate of change of current with respect to time (di/dt) of 8 kiloamperes per microsecond which is four times as fast as that characteristic of the 36 x 82 μ s stroke (2 kA/ μ s). A comparison of these two wave shapes when sketched on the same time base is illustrated below.

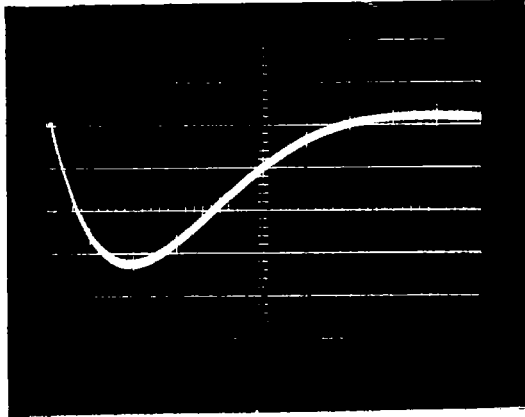


Simulated Lightning Currents

Circuit Conductor Selections

In circuits employing only a single conductor, in which the airframe or a coaxial shield is used as the return path, measurements were always made between the conductor and airframe, or shield, at the root end of the wing. Some circuits upon which measurements were made, however, have more than one conductor, and some do not employ the airframe as a return path.

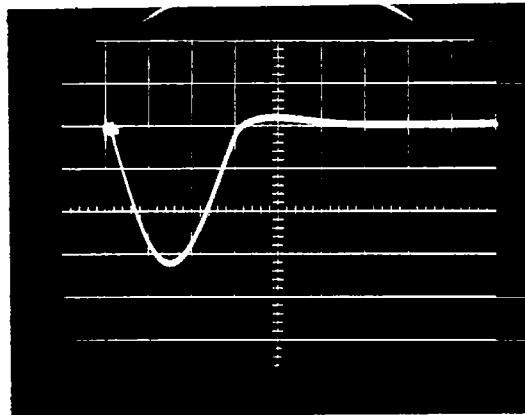
"Slow Wave Shape"
WAVE SHAPE: 36 x 82 μ s



12.5 Kiloamperes/Div.

20 μ s/Div.

"Fast Wave Shape"
WAVE SHAPE: 8.2 x 14 μ s

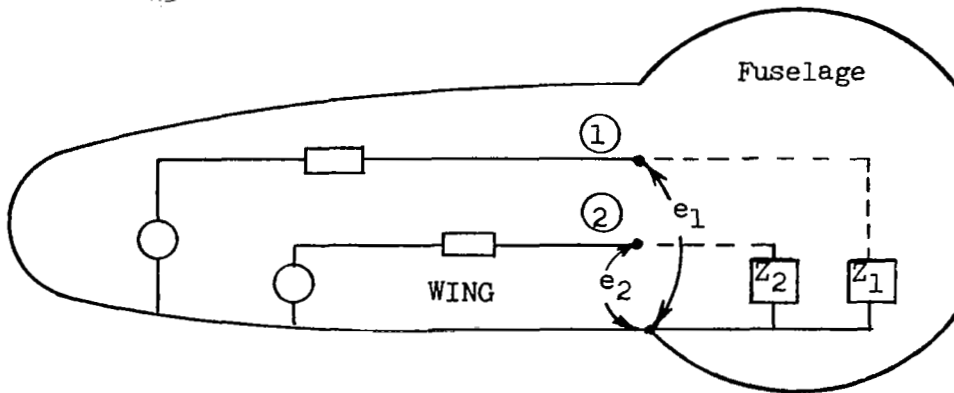


12.5 Kiloamperes/Div.

5 μ s/Div.

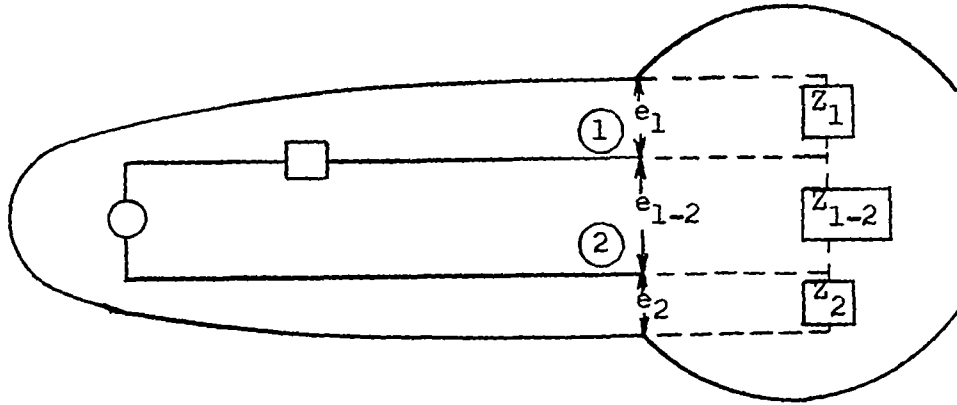
FIGURE 17. - SIMULATED LIGHTNING CURRENT WAVE SHAPES
(40 Kiloampere Strokes, Applied for Induced Effects Measurements)

In these cases, selection of measurement terminal pairs was dependent upon the function of each pair in the circuit, as well as the equipment to which the circuits are connected in the fuselage, with the criteria being the possibility of differences of potential being applied to a susceptible load. For example, consider the two-conductor and airframe return circuit shown in the following sketch:



If induced voltages e_1 and e_2 appear between conductors 1 and 2 and the frame, respectively, then the only voltage applied to load Z_1 is e_1 and the only voltage applied to Z_2 is e_2 . Even though there may be a voltage ($e_1 - e_2$) between conductors 1 and 2, it is not necessary to know this voltage in order to determine the response across the loads in question. Therefore, in the above example, the Thevenin equivalent circuits for circuits 1 and 2 are determined by appropriate measurements between conductor 1 and the airframe, and conductor 2 and the airframe.

In another example, consider the case where a circuit is isolated from the airframe, as is shown in the next sketch:



Even though the circuit is directly connected across a load, Z_{1-2} , in the fuselage, it is likely that there are other impedances to the airframe as represented by Z_1 and Z_2 . These may represent paths through power systems, for example. It is therefore clear that each of the voltages, e_1 , e_2 , and e_{1-2} , is of concern. If this is the case, the following Thevenin equivalent circuits must be determined:

- (1) conductor 1 and frame
- (2) conductor 2 and frame
- (3) conductor 1 and conductor 2

Determination of these circuits provided sufficient information to define the responses across any load or loads, Z_1 , Z_2 , and Z_{1-2} .

EXPERIMENTAL RESULTS

The maximum amplitudes of all open-circuit induced voltage and short-circuit current measurements made at each of the selected circuits and conductor pairs are tabulated in Table XVII in the Appendix. These values are

tabulated for each of the selected stroke location and wave shape variations described in the previous paragraphs. Oscillograms of the complete set of measurements made on circuit L.050 (position light) for example are also shown in Figures 21 and 22 (Pages 54 and 55). These oscillograms illustrate the effects of lightning stroke location and wave shape variations. The following paragraphs describe these effects in more detail.

Circuit Characteristics versus Induced Effects

The measurements made upon eight different wing circuits provided an excellent opportunity to determine the effect of circuit characteristics upon induced effects. The measurements showed that the circuit characteristics themselves are perhaps the most important factor governing the amount of voltage or current that will be induced therein.

The circuit characteristics found to be most significant were:

- Circuit routing and location
- Shielding
- Return path (airframe or separate conductor)
- Impedance of termination (load) at "far" end of circuit in wing

In general, it was found that circuits routed through the interior of the wing experienced lower induced voltage levels than did those which passed through portions of the wing open to the outside (unshielded). The addition of individual conductor shielding also significantly reduced the induced voltage level below that which was induced in similar unshielded circuits.

The type of electrical return path used and the nature of load (electrical equipment) impedances within the wing were of greater significance than routing and shielding, however. Greater open-circuit induced voltages and short-circuit currents were always measured in circuits that employ the

airframe as the return path than in those which do not. These circuits received not only a magnetically-induced voltage but also the resistive voltage rise created by the lightning currents flowing through (a portion of) the wing itself. The inherent low impedance of these circuits resulted in most of these voltages appearing at the open-circuited terminals at the wing root. Larger induced voltages were also measured in circuits of the greatest length, particularly if such circuits run lengthwise along the wing. These characteristics are more fully discussed in the analysis section of this report.

The following paragraphs describe the experimental results obtained from measurements on each of the eight selected circuits, for applications of 40-kiloampere simulated strokes of both the slow and fast wave shape to the five selected stroke locations shown on Figure 15.

Circuit A.140 Armament Jettison

This circuit, shown in Figure 4, provides power to energize the explosive jettison bolts in the pylon which jettison armament stores. Measurements were made initially on this circuit with the pylon removed, which rendered the circuit open-circuit terminated in the wing at plug MJ-40, located within the wing directly above the pylon station. Later, the pylon was installed and electrically connected to plug MJ-40.

With the pylon removed, open-circuit induced voltages measured between conductor 2A925G16 and the airframe under all test conditions remained within a minimum of 0.5 volt and a maximum of 1.0 volt. Oscillograms of the voltages created by the slow simulated lightning current were nearly identical in wave shape to that of the lightning current, indicating a resistive (in phase) voltage rise proportional to the resistive voltage rise along the wing structure itself. Since the conductor was not connected to the airframe at any place, this voltage must have been capacitively coupled from the airframe to the conductor.

When the fast wave shape was applied, more evidence of an inductive (out of phase) component was evident, resulting in a slight addition to the resistive component (which would have the same amplitude regardless of the lightning current wave shape).

There was little change in the induced voltages as a result of variation in stroke location. This fact would also tend to support a predominant capacitive coupling mechanism.

Since the circuit was open within the wing (except for its stray capacitances to the airframe), no currents could be measured with the terminals of the circuit shorted. The same was true with a 1-ohm resistor across the terminals, and this load also reduced the measurable induced voltage to zero.

When the pylon was attached, the circuit passes into it to the jettison safety relay coil and thence to the airframe, which serves as the return path. The explosive jettison bolts are not connected to this circuit until the jettison safety relay is energized. When this relay is energized, the same voltage (coming from conductor 2A925G16) which energizes it also, fires the explosive bolt as shown in Figure 4. When the relay was de-energized, an open-circuit induced voltage of 6 volts was measured as a result of a fast simulated lightning stroke delivered to the forward end of the tip tank. The oscillogram showed that this voltage was primarily inductive in nature, and the increase in amplitude is attributed to greater exposure to the lightning-caused magnetic field as a result of extension of the circuit down into the pylon, as well as the addition of the airframe return path. Another test was made under the same conditions except that the stroke was delivered to the forward tip of the pylon. This resulted in an increase in induced voltage to 70 volts. This increase is undoubtedly the result of stronger magnetic fields interacting with the circuit within the pylon, and possibly a resistive voltage caused by the lightning current

passing through the mechanical joint (6 bolts) between the pylon and the wing. No short-circuit currents were measurable with the pylon attached, even though a complete path existed through the relay coil to the airframe. Such a transient current is probably prevented by the large inductance of the relay coil.

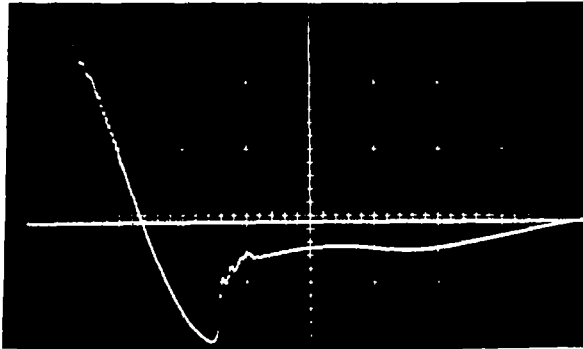
These tests were repeated with the relay coil energized by a 16-volt battery - sufficient to activate the jettison safety relay and connect the explosive jettison bolts to the circuit (See Figure 4). Since the relay is energized through the same circuit, it was not possible to measure an open-circuit voltage or a short-circuit current, due to presence of the battery. The amount of induced voltage arising across the battery impedance was measured, however, superimposed upon the battery voltage itself. The oscillogram of this voltage is shown on Figure 18, compared with corresponding open-circuit induced voltages (battery disconnected). Oscillograms are shown for strokes delivered to the forward end of the tip fuel tank (location 1) as well as to the tip of the pylon itself. A comparison of these oscillograms shows that a substantial portion of the (open circuit) induced voltage is impressed across the battery, even though the battery resistance was calculated to be only 0.045 ohm. While the impedance of the battery to such transients may not in fact be equal to its d-c resistance, the fact that a substantial portion of the voltage induced in this circuit may be impressed across such a low impedance is significant. Figure 18 shows that the negative portion of the induced voltage resulting from the stroke to the pylon was sufficient to depress the voltage across the battery to zero.

The negative undershoots characteristic of these induced voltages indicate that they are primarily inductive, and represent the differential of the applied lightning current. Since the latter is approximated by the first half-cycle of a sine wave, the differential thus approximates the same period of a cosine wave. This discussion is pursued in the analysis

Stroke to Forward Tip of Pylon

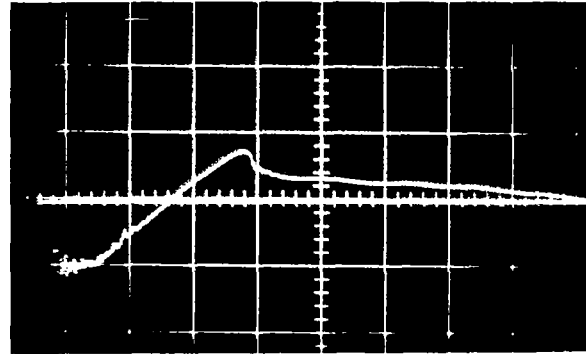
Stroke to Forward End of Wing Tip Tank

a. Induced Voltages Measured at Open Circuit Terminals.



20 volts/Div.

5 μ s/Div.

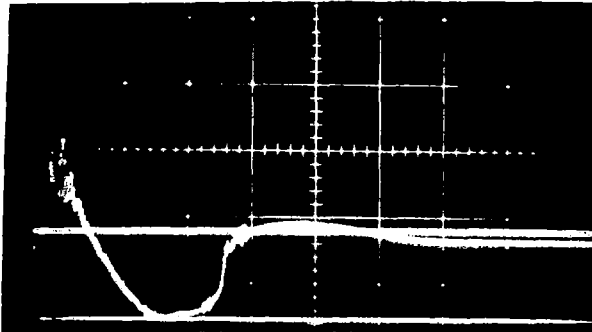


5 volts/Div.

5 μ s/Div.

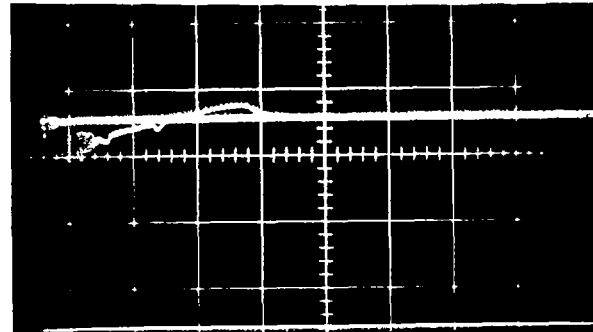
NOTE: Straight lines are zero lines.

b. Induced Voltages Measured Across Battery (Superimposed on 16-Volt Battery Voltage)



10 volts/Div.

5 μ s/Div.



5 volts/Div.

5 μ s/Div.

NOTE: Upper straight lines show 16-volt battery voltage.

Lower straight lines are zero lines.

Variable trace is induced voltage plus battery voltage.

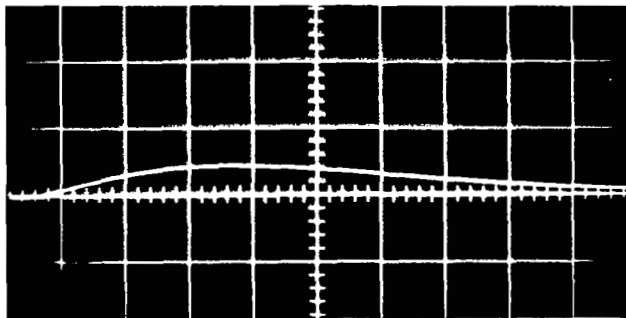
FIGURE 18. INDUCED VOLTAGES MEASURED (a) AT OPEN CIRCUIT TERMINALS (CONDUCTOR 2A925G16 TO AIRFRAME), AND (b) ACROSS 16-VOLT BATTERY CONNECTED TO TERMINALS TO ENERGIZE JETTISON SAFETY RELAY. CIRCUIT A.140 (RIGHT ARMAMENT JETTISON). 40 KILOAMPERE $8.2 \times 14 \mu$ s LIGHTNING CURRENTS APPLIED TO LOCATION 1 AND PYLON.

section of this report.

Circuit E.0711 Right Fuel Quantity Indication

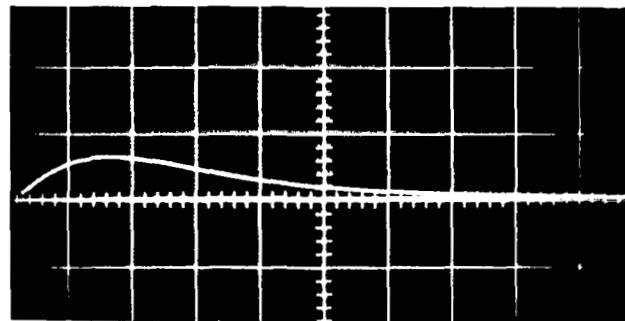
This circuit, shown in Figure 5, connects the fuel quantity probes located in the wing and wing tip fuel tanks to the capacitance bridge fuel quantity indication system within the fuselage. The fuel quantity probes are of the concentric cylinder type, with a dry capacitance of 15 picofarads. Variations in the height of the fuel between the cylinders results in changes in probe capacitance, the value of which is continuously measured by the bridge system and translated into an indication of fuel quantity. The circuit operates at very low voltage and is entirely isolated from the airframe. Two shielded conductors connect each probe, and some probes are connected in parallel. There are three pairs of conductors in the circuit. (See Figure 5). The shields are connected to the airframe via the probe frames, and also incidentally as they pass through bulkheads in the wing. Since the circuit employs isolated return paths, induced voltage measurements were made between each conductor pair and between each conductor of a pair and the airframe. The circuit is located entirely within the wing. For these measurements the shields were connected to the airframe at the wing root, and measurements were made under all stroke location and wave shape test conditions. The measured open-circuit voltages in all cases ranged between ± 3 volts. Little variation was evident in the amplitude of induced voltages as a result of stroke location or wave shape variations. This result is attributable to the extensive shielding provided these circuits, and to the use of isolated (and shielded) return paths.

Figure 19 shows an example of the measurements made on one conductor pair, illustrating the voltage measured between the pair, and between each conductor and the airframe. By definition, the difference between each of the conductor voltages to ground must equal the voltage between conductors. This relationship is apparent from the oscillograms of Figure 19.



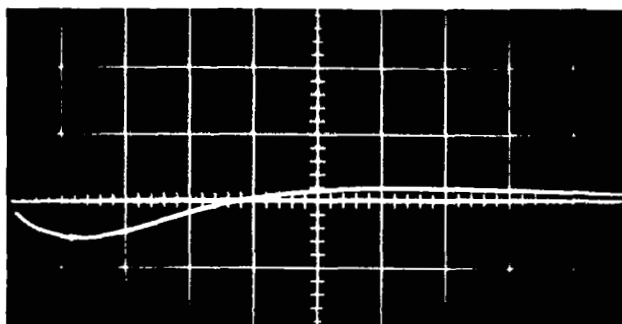
2 volts/Div. 20 μ s/Div.

a. Voltage Between Conductor 2E69B22 and Airframe.



2 volts/Div. 20 μ s/Div.

b. Voltage Between Conductor 2E70B22 and Airframe.



2 volts/Div. 20 μ s/Div.

c. Voltage Between Conductor 2E69B22 and 2E70B22 (a-b).

FIGURE 19. - RELATIONSHIP BETWEEN OPEN CIRCUIT INDUCED VOLTAGES MEASURED BETWEEN TERMINALS OF A FUEL PROBE CIRCUIT AND BETWEEN EACH TERMINAL AND THE AIRFRAME. CIRCUIT E.0711 (RIGHT FUEL QUANTITY INDICATION). 40 KILOAMPERE $36 \times 82 \mu$ s LIGHTNING STROKE TO LOCATION 10.

The voltage wave shape of Figure 19(a) is nearly identical to that of the lightning current itself ($36 \times 82 \mu\text{s}$), indicating a capacitance coupling between this conductor and the resistive voltage rise occurring in the airframe. The other conductor shows a delayed and sloped-off wave shape as compared with the lightning wave. This appears to represent a delayed capacitive coupling with the wing resistive voltage rise, possibly because this connector is connected to the inner concentric cylinder of the probe.

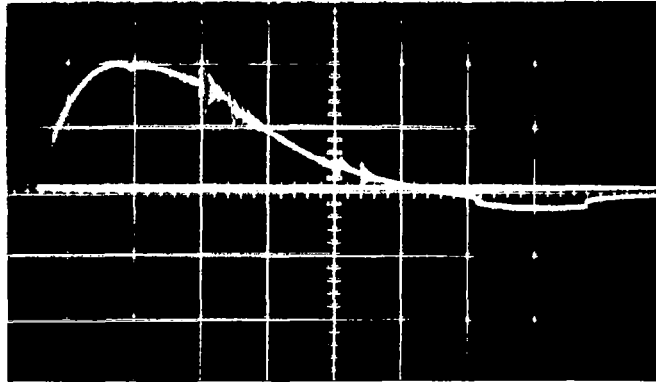
The (short circuit) currents flowing through the conductor shields to the airframe at the wing root were also measured, as was the voltage between the shields and the airframe when the shields were disconnected from the airframe at the wing root. Figure 20 shows an example of these measurements. It is interesting to note that, even though the shields are grounded to the airframe at several locations, a short-circuit current of approximately 15 amperes was measured. The wave shape of the current oscillogram (Figure 20(b)), is nearly identical to that of the applied lightning current, indicating that this current is directly conducted into the shield and not magnetically coupled.

Due to the very high impedance of the fuel probe circuits it was not possible to measure any short-circuit currents associated with the circuit conductors.

The induced voltages measured for all test conditions are tabulated in the Appendix.

Circuit F.0511 E-11 Autopilot

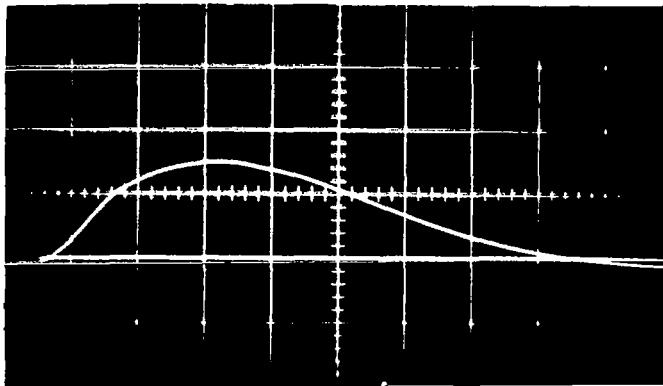
This circuit is shown in Figure 6. It is a portion of the autopilot circuit, extending to the rocket safety switch located adjacent to the leading edge of the aileron. This switch, mechanically actuated by movement of the aileron, is normally closed except when the aileron is in the neutral position. The switch prevents firing of the MB-1 rocket from the pylon unless the aileron is in this position, to assure that rocket exhaust will not



1 volt/Div.

20 μ s/Div.

a. Open Circuit Induced Voltage (Shield to Airframe)



10 amps/Div.

20 μ s/Div.

b. Short Circuit Current (Shield to Airframe)

FIGURE 20. - OPEN CIRCUIT INDUCED VOLTAGE AND SHORT CIRCUIT CURRENT MEASURED BETWEEN SHIELD OF CONDUCTOR 2E65B22 AND THE AIRFRAME AT THE WING ROOT. CIRCUIT E.0711 (RIGHT FUEL QUANTITY INDICATION). 40 KILOAMPERE 36 x 82 μ s LIGHTNING STROKE TO LOCATION 1.

damage the aileron. Connections to both sides of the switch are isolated from the airframe. In the fuselage, the circuit is connected to primary 28-volt d-c power and a relay coil, and to other portions of the autopilot system. The circuit is not shielded.

Since the safety switch and attached conductors are exposed to the outside of the wing, it is apparent that direct contact with a lightning stroke or even an intense corona streamer could result in considerable damage to the E-10 autopilot system. No direct strokes were applied to such components in this program, however, since the objectives were to study induced effects, and a direct stroke would have permanently damaged the circuit.

Since this circuit does not employ the airframe as a return path, measurements were made between the two conductors and between each one and the airframe. Measurements were made under all test conditions with the switch in the normally closed position.

As was the case with other circuits not employing the airframe as the return path, the voltages measured in this circuit were uniformly low, ranging from a few millivolts to a maximum of 5 volts. Open-circuit induced voltages measured between the two conductors were generally 0.5 volt or less, and short-circuit currents flowing through these conductors when shorted together were 0.5 ampere or less. In all cases, the voltage measured between conductors was equal to the difference between those measured from each conductor to the airframe.

Voltages measured between each terminal and the airframe (with the other terminal floating) ranged between 1 and 3 volts. Since the circuit was isolated from the airframe and the other conductor terminal was floating, no short-circuit currents were measurable between the measured conductor and the airframe.

Variations in stroke location did not cause significant changes in voltages induced into this circuit. As with other isolated circuits, the voltages appearing in this circuit are a combination of capacitively coupled resistive

voltages which are in phase with the lightning current wave shape, and magnetically induced voltages which resemble the differential of the applied lightning current wave shape. The latter component was more evident from the fast lightning current wave forms, which possess a rate of rise (differential) four times as great as the slow lightning current wave form.

Induced voltages and currents measured for all test conditions are tabulated in the Appendix.

Circuit L,050 Position Light

This circuit is shown in Figure 7. It provides 28-volt d-c power to the position lamp which is located on the outside of the wing tip fuel tank. The circuit is routed along the trailing edge main spar, and is partially exposed as it runs along the outside of this spar, forward of the flap. The circuit passes through the tip fuel tank to the position light on the outside. The bulb, of 2.5 ohms resistance, was installed. The airframe is used as the circuit return path. Perhaps because this circuit extends the longest, is partially exposed and employs the airframe as a return path, the induced voltages and currents measured were the greatest found in any of the circuits. As a result of this, and because this circuit is representative of a type found commonly in many aircraft, the position light circuit was more extensively studied than the others. Figures 21 and 22 show oscillograms of the open-circuit induced voltages and short-circuit currents measured between the single conductor 2L10E18 and the airframe.

Induced voltages measured in this circuit upon application of the slow light current wave ranged between 2 and 20 volts. Application of the fast lightning wave resulted in voltages and currents over twice as great. Variations in stroke location resulted in significant changes in induced voltages, as is evident in Figures 21 and 22. In general, delivery of strokes to locations farthest out on the wing and closest to the actual location of the circuit resulted in the highest voltages. The maximum voltages were obtained

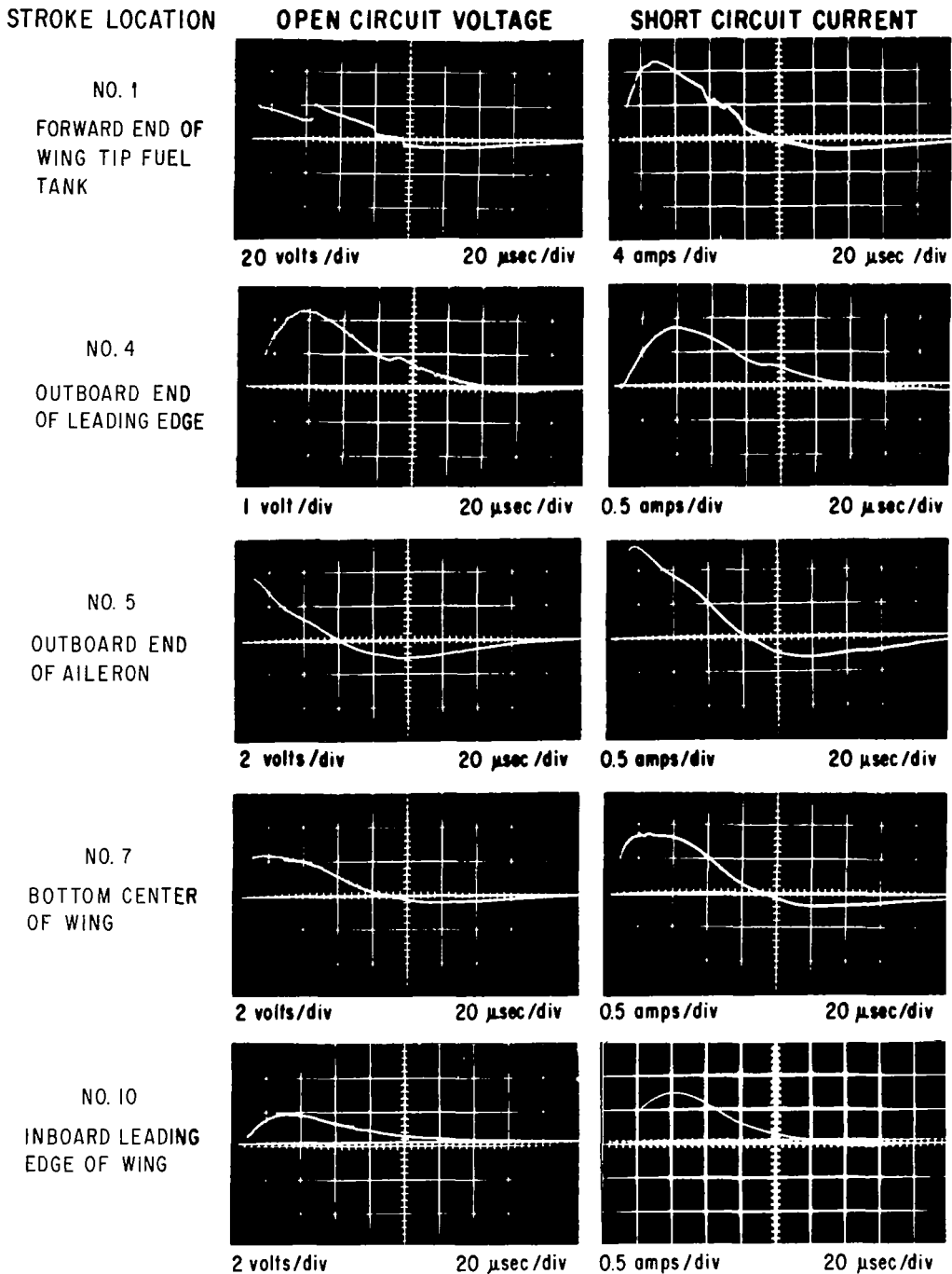


FIG. 21 OPEN CIRCUIT VOLTAGES AND SHORT CIRCUIT CURRENTS MEASURED ON TERMINALS OF CIRCUIT L.050 (POSITION LIGHT) CONDUCTOR 2L10E18 TO AIRFRAME.

36 x 82 μ sec 40 KILOAMPERE SIMULATED LIGHTNING CURRENT

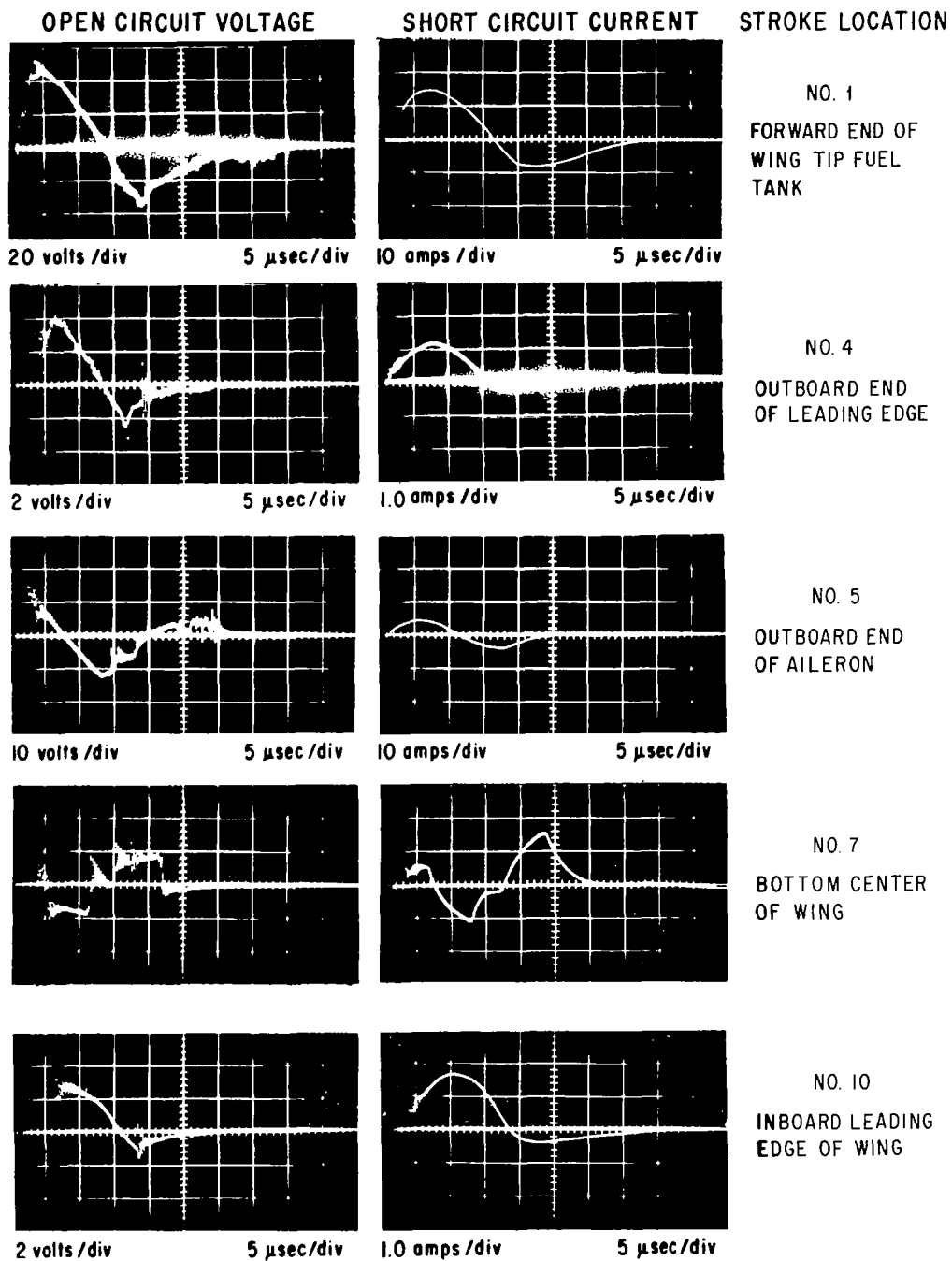


FIG. 22 OPEN CIRCUIT VOLTAGES AND SHORT CIRCUIT CURRENTS MEASURED ON TERMINALS OF CIRCUIT L.050 (POSITION LIGHT) CONDUCTOR 2L10E18 TO AIRFRAME.

8.2 x 14 μ sec 40 KILOAMPERE SIMULATED LIGHTNING CURRENT

from strokes to the tip tank. A comparison of the voltages induced from strokes delivered to locations 4 and 5, which are the same distance out on the wing, but at unequal distances from the circuit conductor location, shows that the stroke delivered closest to the conductor (location 5) causes the greatest voltage. Such a result would be expected, since strokes delivered closer will permit stronger magnetic fields to link the conductor.

All of the voltage wave shapes shown on Figures 21 and 22 are a composite of both a resistive voltage, in phase with the applied lightning current wave form, and a magnetically induced voltage, proportional to its differential. It can be seen that strokes to locations closest to the conductor (1 and 5) cause voltages with a greater inductive component (evidenced by higher initial rise and an undershoot) than do strokes to locations farther away, in which cases the resistive component seems to be predominant.

Occasionally, an induced voltage wave shape inconsistent with others is obtained, as occurred from strokes to location 1 (slow wave) and location 7 (fast wave). After some study, these inconsistencies have been attributed to loose connections within the circuit being measured; as, for example, a loose light bulb.

Since significant short-circuit currents could be obtained from this circuit, it was possible to attach a 1-ohm load resistor to its terminals and measure the induced voltage and current across this load. These measurements were made primarily to obtain a check on the validity of the open circuit voltage and short-circuit current measurements. However, they were also useful to show the effect of a load upon the measured induced voltages. The voltage measured across the 1-ohm resistor was about one-third of the open-circuit voltage, and correlation between load voltage and current measurements was excellent. All of these measurements are tabulated in the Appendix.

Circuit Q.0401 Fuel Vent Valves

This circuit conducts power to the solenoid-operated fuel vent valve located on the lower surface of the outer wing. It passes along a circuitous route through conduits extending through the forward and aft fuel cells, and between, as shown in Figure 8. The circuit applies power to close the normally open solenoid fuel vent valve prior to firing of rockets from the pylon. This circuit is not exposed and, due to its passage through conduits within the fuel cells, it receives some shielding not afforded other wing circuits.

The voltages induced in this circuit showed approximately the same relationship to test condition variations as did those measured in the position lamp circuit. The magnitudes, however, were lower; probably as a result of the greater shielding provided this circuit. Voltage magnitudes arising from the slow lightning wave ranged from 1.8 to 2.8 volts, while fast wave created induced voltages of between 1.9 and 6.5 volts. Due to the large inductance of the solenoid valve coil, very little short-circuit current was measured. For the same reason, the addition of the 1-ohm load resistor caused the measurable load voltage to drop nearly to zero.

As in other circuits employing the wing as the return path, the induced voltages consisted of a resistive as well as an inductive component. The inductive component was predominant in voltages induced by the fast lightning current wave form. The magnitudes of voltages and currents obtained under all test conditions are tabulated in the Appendix.

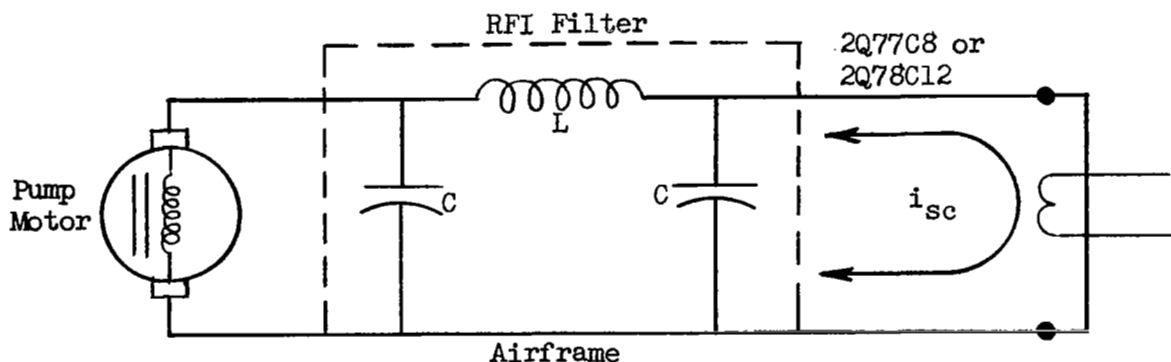
Circuit Q.060 Right Wing Tank Booster Pumps

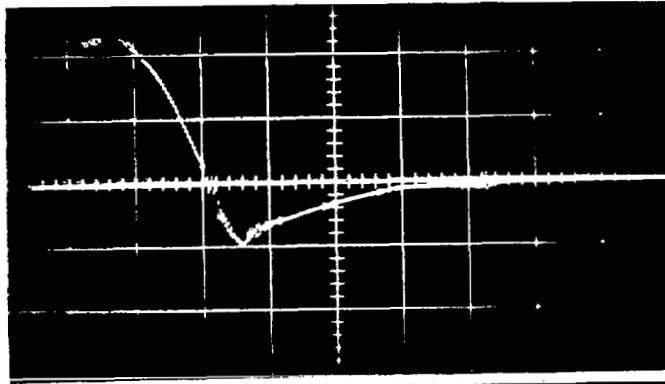
This circuit, shown in Figure 9, conducts power via two separate conductors to two fuel pump motors. The 28-volt d-c motors, which operate for extended periods of time, are equipped with radio frequency interference (RFI) filters to eliminate motor noise from interfering with other aircraft circuits and communication systems. The electrical description of these

filters was not obtainable; however, it is assumed that they were a standard pi-type filter employing a series inductance together with a pair of shunt capacitors.

Open-circuit induced voltage measurements showed relationships between induced voltages and test conditions similar to those found in other circuits employing the airframe as a return path. Since both of these circuits extended only a short way out into the wing, variations in stroke locations farther out on the wing did not significantly change the magnitude or wave shape of voltages induced in these circuits. Strokes to the locations nearest the circuits (7, 10) resulted in the highest induced voltages, as might be expected.

The induced voltage wave forms exhibited the same combination of resistive and inductive components which had been evidenced in other circuits using the airframe as the return path. The inductive component was predominant in voltages induced by the fast lightning wave forms. An example of such a voltage is shown in Figure 23(a). Also shown is the corresponding short-circuit current measurement, Figure 23(b). This current oscillates for an extended time, far exceeding the duration of the induced voltage itself (note the expanded time scale of Figure 23(b)). The short-circuit current oscillation is probably occurring between the inductive and capacitive elements in the circuit, as shown below:

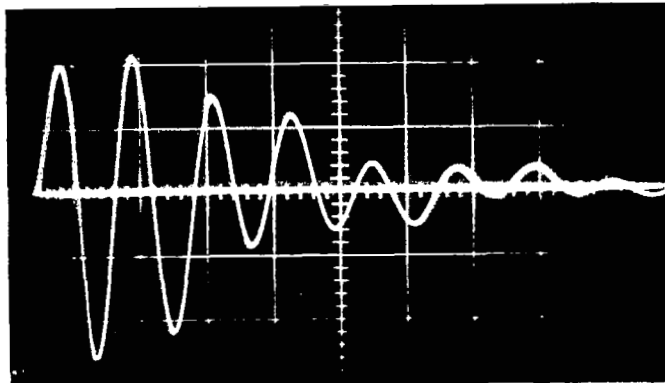




1 volt/Div.

5 μ s/Div.

a. Open Circuit Induced Voltage



1 amp/Div.

20 μ s/Div.

b. Short Circuit Current

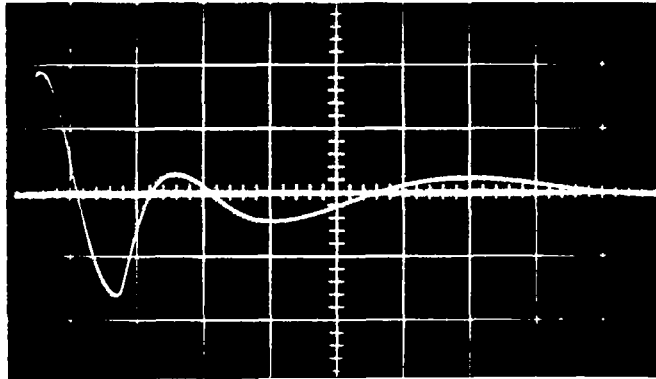
(Note extended time scale of oscillogram b)

FIGURE 23. - (a) OPEN CIRCUIT INDUCED VOLTAGE, AND
 (b) SHORT CIRCUIT CURRENT.
 MEASUREMENTS BETWEEN CONDUCTOR 2Q78C12 AND AIRFRAME.
 40 KILOAMPERE $8.2 \times 14 \mu$ s LIGHTNING CURRENT APPLIED
 TO LOCATION 10. CIRCUIT Q.060 (RIGHT WING TANK
 BOOSTER PUMPS).

It is believed that the RFI filter is located next to the pump motor, so that voltage is mostly being induced in the circuit conductor between the filter and the terminals at the wing root, where the voltage was measured. When these terminals are shorted together, the major portion of this voltage is impressed across the RFI filter. This voltage stores energy in the filter capacitances, exciting an oscillation between the L and C elements of the circuit which persist long after the exciting (induced) voltage has vanished. This phenomena was observed only in these circuits which have a combination of inductive and capacitive elements. This is an example of where the addition of a filter to eliminate one type of interference (motor noise) may aggravate the effect of interference created by another source (lightning).

Application of a 1-ohm load resistor to the terminals of this circuit resulted in a reduction in load voltage to approximately one-third of the open-circuit magnitude. The increased resistance of the circuit also increased the damping of the current oscillations, as would be expected. The voltage and current across the 1-ohm load resistor, for the same test conditions as applied for the open and short-circuit measurements of Figure 23, are shown in Figure 24. This figure also illustrates a comparison check between voltage and current measurement systems to assure reliability of measurements. The wave shape and amplitude of voltage and current across a 1-ohm resistor should be identical.

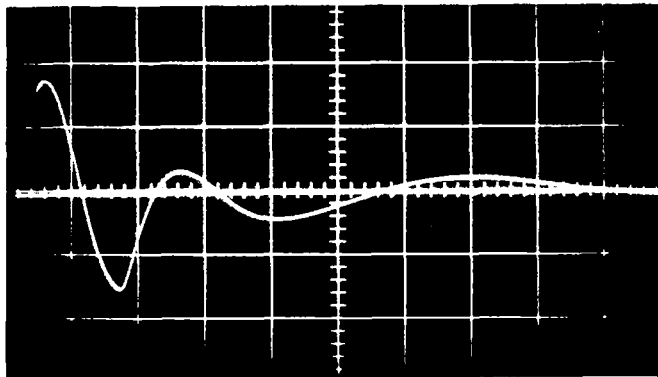
Since these tests were made with the motor inoperative, it was decided to perform a comparison test with the motor operating, to see if this condition had any effect upon the level of induced voltages. For this purpose, a 24-volt battery was attached to the circuit terminals, and the motor was operated. Measurements were made of the induced voltage and current across the battery. Since the resistance of the battery was very low, ($\approx .05$ ohm), the induced current measured thus constituted very nearly the short-circuit current. The current measured through the battery compared closely in



0.5 volt/Div.

10 μ s/Div.

a. Voltage Across 1-Ohm Resistor



0.5 amp/Div.

10 μ s/Div.

b. Current Through 1-Ohm Resistor

NOTE: Voltage measured by direct input to oscilloscope amplifier.

Current measured by pulse current transformer.

FIGURE 24. - INDUCED VOLTAGE AND CURRENT MEASURED ACROSS A 1-OHM LOAD RESISTOR CONNECTED BETWEEN CONDUCTOR 2Q78C12 AND AIRFRAME. 40 KILOAMPERE $8.2 \times 14 \mu$ s LIGHTNING CURRENT APPLIED TO LOCATION 10. CIRCUIT Q.060 (RIGHT WING TANK BOOSTER PUMPS)

amplitude and wave shape with the short-circuit current previously measured. Hence, the operating condition of the pump motor does not affect the voltages induced in the circuit.

The amplitude of all voltages and currents measured in this circuit are tabulated in the Appendix.

Circuit R.060 AN/ARN-18 Glide Path Radio Receiver

This circuit is shown in Figure 10. The glide path radio receiver antenna is located in the leading edge of the wing, and is a slot-type grounded antenna. The antenna is fed through an RG/11U, 75-ohm coaxial cable, the shield of which is connected to the airframe at the antenna end and at the forward connector panel. The cable runs within the leading edge of the wing. The center conductor of the cable connects to the antenna through a capacitor at the antenna connection. Inadvertently, this capacitor had been shorted and a complete series of measurements under all test conditions was made before this condition was discovered. Later, the antenna capacitor was unshorted and several more measurements were made with the circuit in this (correct) condition. However, most of the measurements made on this circuit were obtained with the circuit in an unnatural condition. The data was retained and analyzed, however, for its academic interest. Study of the voltages and currents induced in this circuit is of particular interest because it affords an opportunity to compare this shielded circuit, which is connected to the airframe through the shorted capacitor, with similar unshielded circuits (such as the position light circuit) which are also connected to the airframe through a low impedance.

The effect of lightning stroke location and wave shape was significant in determining the magnitude of voltages induced in this circuit. The stroke delivered to location 4 at the tip of the leading edge produced the highest induced voltages, as might be expected, since this condition would result in the highest concentration of current and magnetic flux around the leading edge, within which the circuit is housed. The open-

circuit induced voltages measured from strokes to this location are shown in Figure 25. This figure shows the voltages measured from both lightning wave shapes, and it is apparent that the fast wave shape induces voltages approximately four times as great as the slow wave shape does.

The magnitude of voltages induced by the slow lightning wave form ranged from 0.6 to 4 volts, while those induced by the fast wave form ranged from 1 to 20. These voltages are lower in magnitude than those induced under the same test conditions in the position light circuit (L.050), probably as a result of the shielding provided by the coaxial cable, and this circuit's shorter length. Short-circuit currents in this circuit were measured at between 3 and 12 amperes for the slow lightning wave, and were nearly twice as high for the fast wave. These current amplitudes are all higher than their counterparts in the position lamp circuit. This is undoubtedly due to the lower impedance of the antenna circuit, which was directly connected to the airframe through the shorted capacitor. The position light is connected to the airframe through its 2.5-ohm light bulb.

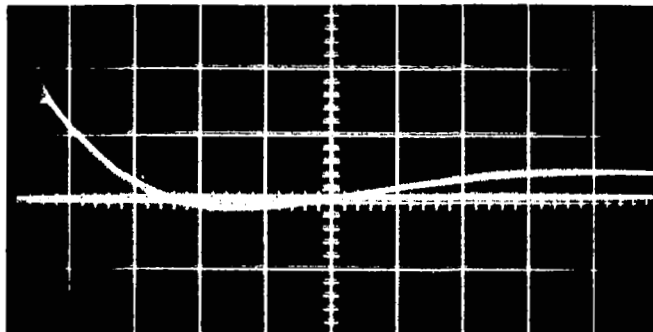
Some open-circuit induced voltages were measured on the antenna circuit with the coupling capacitor unshorted. These showed low-level capacitively coupled voltages of between 1 and 2 volts, similar to voltages measured in other circuits 'open' at the far end. No short-circuit currents could be measured under this condition.

As with many of the open-circuit voltages measured in other circuits, the presence of high-frequency oscillations was evident on the initial part of the induced voltage wave form (capacitor shorted). This portion of each induced voltage wave form is shown on an expanded time scale on Figure 25. Study of these oscillations shows that, unlike the low-frequency wave forms of the induced voltages which are related to the wave form of the lightning current, the high-frequency oscillations are not directly related to the lightning current wave shape. In fact, the fundamental frequency of these oscillations (about 6.5 megacycles) is the same for both lightning

Slow Lightning Wave Shape; 36 x 82 μ s

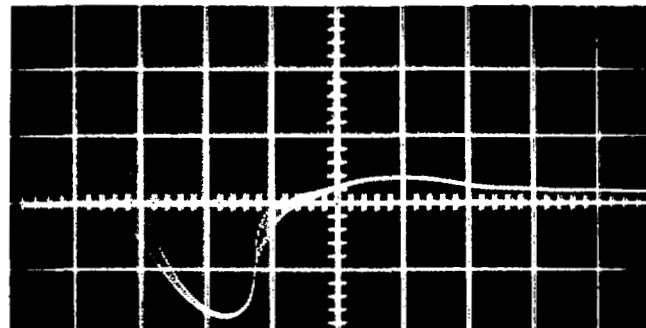
Fast Lightning Wave Shape; 8,2 x 14 μ s

Open Circuit Induced Voltage - Complete Wave Forms



2 volts/Div.

20 μ s/Div.

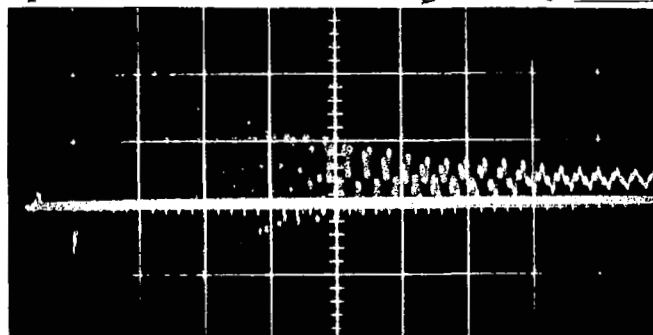


5 volts/Div.

5 μ s/Div.

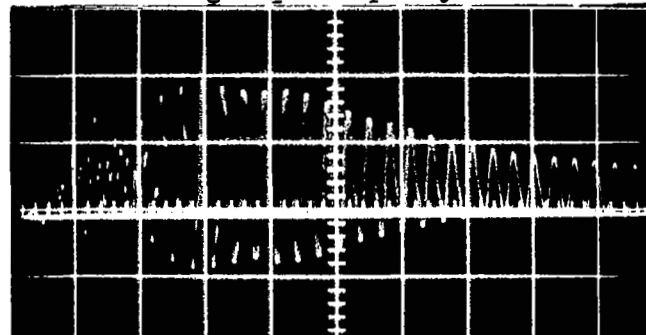
79

Open Circuit Induced Voltages - Expanded Time Scale Showing High Frequency Oscillations



10 volts/Div.

0.5 μ s/Div.



20 volts/Div.

0.5 μ s/Div.

FIGURE 25. - OPEN CIRCUIT INDUCED VOLTAGES MEASURED BETWEEN CONDUCTOR AN/ARN-18 AND THE AIRFRAME. 40 KILOAMPERE SLOW AND FAST STROKES TO LOCATION 4. CIRCUIT R.060 (AN/ARN-18 GLIDE PATH RADIO RECEIVER ANTENNA).

current wave shapes. If the amplitude of the low-frequency induced voltage component, upon which the oscillations are superimposed, is taken as the mean of the high-frequency oscillations in this region, then the amplitude of the high-frequency oscillations is found to be approximately twice that of the induced voltage (low frequency) component.

The above relationships, which are also found in other circuits, suggest that the high-frequency oscillations are not a component of the induced voltage itself, but are in fact the result of traveling voltage waves "ringing" back and forth along the transmission line of the wing circuit itself. The frequency of these oscillations is dependent on this transmission line, which in this case is the 75-ohm coaxial cable. If the velocity of traveling wave propagation in this cable is assumed to be 500 ft. per microsecond, then the time required for a traveling wave to make a round trip (down and back) through the cable is

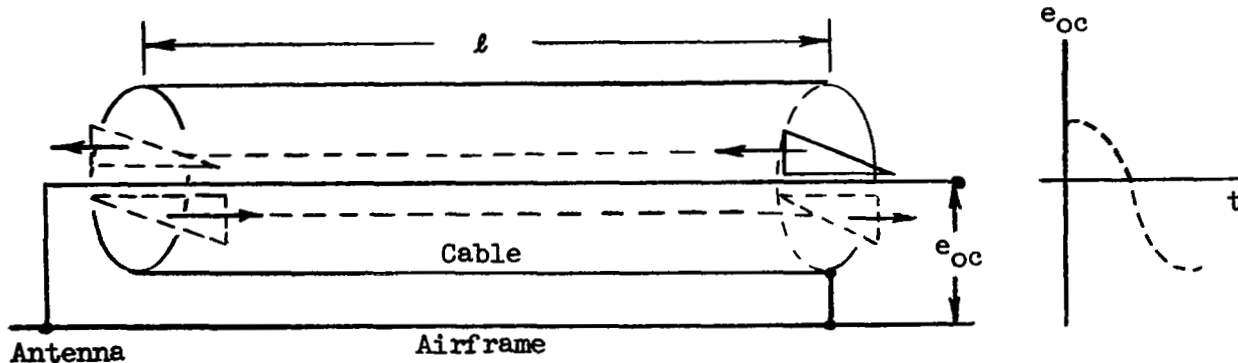
$$t = \frac{2 \times l}{v} = \frac{2 \times 17 \text{ ft}}{500 \text{ ft}/\mu\text{s}} = 0.068 \mu\text{s}$$

where t = traveling wave round trip time

l = length of cable = 17 ft

v = velocity of propagation = 500 ft/ μ s

In one round trip the traveling wave will result in one-half of a voltage oscillation cycle measured at the open circuit terminals, as shown below:



Thus, the period of a complete cycle will be:

$$\begin{aligned} T &= 2 \times t = 2 \times (.068 \mu\text{s}) \\ &= 0.136 \mu\text{s} \end{aligned}$$

and the frequency of this oscillation will be

$$f = \frac{1}{T} = \frac{1}{0.136 \times 10^{-6}} = 7.3 \times 10^6 \text{ hertz}$$

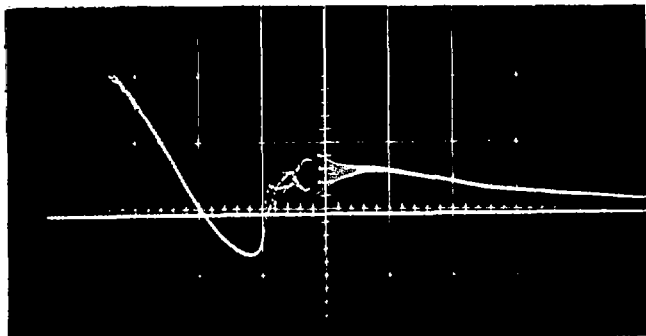
which compares favorably with the measured frequency at 6.5 megahertz.

If these oscillations are the result of traveling waves and successive reflections thereof at the ends of the transmission line formed by the circuit in the wing, the reflections may occur at the open-circuited termination since no energy can be absorbed at such a termination. On the other hand, if the line is terminated by a resistance equal to its surge impedance, the entire energy of the incident wave is absorbed in the resistor and no reflections will occur. For further verification, therefore, it was decided to terminate the cable with a resistor equal to its surge impedance (75 ohms) and measure the voltage appearing across the resistor. If the high-frequency oscillations are indeed traveling wave reflections, they should vanish when the circuit is terminated with its surge impedance (ref. 8). Figure 26 shows measurements made with and without the 75-ohm termination. It is apparent from these oscillograms that the termination largely eliminates the oscillations. The conclusion is therefore that the high-frequency oscillations are not part of the voltage induced in the circuit by the lightning, but are a secondary phenomenon excited by the induced voltage. The oscillations thus were not mathematically described as part of the induced voltage wave forms when the latter were analytically related to the lightning current wave form. The entire analytical process is described in the analysis section of this report.

Open Circuit Induced Voltage

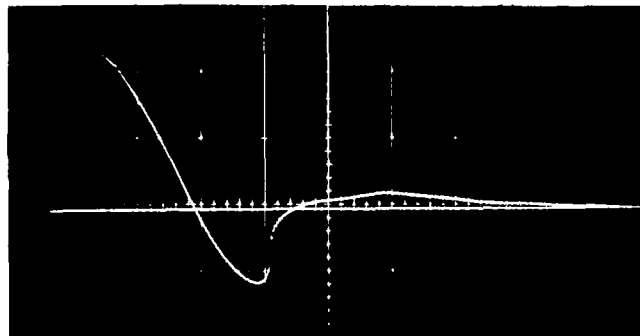
Voltage Across 75 Ohm Termination

Complete Induced Voltage Wave Forms



5 volts/Div.

5 μ s/Div.

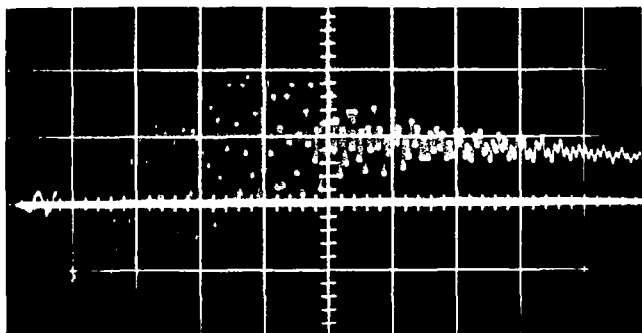


5 volts/Div.

5 μ s/Div.

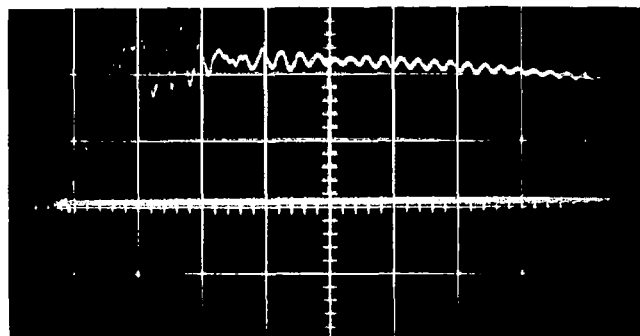
67

Expansion of Time Scale to Show Oscillations on Wave Fronts



10 volts/Div.

0.5 μ s/Div.



5 volts/Div.

0.5 μ s/Div.

FIGURE 26. - COMPARISON OF INDUCED VOLTAGES MEASURED ON CIRCUIT R.060 (GLIDE PATH ANTENNA) WITH AND WITHOUT A 75-OHM RESISTIVE TERMINATION. 40 KILOAMPERE $8.2 \times 14 \mu$ s SIMULATED LIGHTNING CURRENT TO LOCATION 1.

The antenna circuit was the logical one in which to study the origin of the high-frequency oscillations, since the surge impedance of this circuit is the known impedance of the 75-ohm cable. Similar studies would be less conclusive in other circuits, the surge impedance of which is variable and unknown. The oscillations in these other circuits were, however, generally eliminated or greatly reduced when a resistive load was placed across the circuit terminals.

The complete tabulation of measurements made on this circuit is given in the Appendix.

Circuit S.220 Armament Power Supply

This circuit is also located in the leading edge of the wing, and extends from the forward connector panel to the pylon connector MJ-40 located in the leading edge above the pylon location. The circuit diagram is shown in Figure 11. The circuit has a total of six individually-shielded connectors, which feed power to the MB-1 rocket carried on the pylon. The conductor shields are ultimately connected to the airframe in the fuselage and in the pylon when installed; however, they are not connected to the airframe in the wing. For these measurements, they were connected to the airframe at the instrument ground bus by the wing root.

Measurements were only made on this circuit as it is shown in Figure 11, without the pylon installed, since the weapon itself would have to have been installed on the pylon for these circuits to be complete. Measurements were made from each of the six individual conductors to the airframe. All of the induced voltages were very low, ranging from 20 to 60 millivolts as a result of the slow lightning current wave form, and from 20 to 200 millivolts when the fast stroke was applied. All of the conductors are of the same length and size, and the voltages induced in each were nearly the same. Variations in stroke location caused little change in the open-circuit voltages.

The fact that the voltages measured in this circuit were so low is due

to the shielding of the conductors. A very interesting comparison may be made between the voltages induced in any of these conductors and those induced in conductor 2A925G16 of the armament jettison circuit. This conductor runs parallel to the armament power supply conductors, and is the same length. In fact, when the pylon is removed, as for these tests, both circuits terminate at plug MJ-40 (see Figures 4 and 11).

For identical test conditions the voltage induced in the armament jettison circuit, conductor 2A925G16, is 20 times as great as that induced in armament power supply conductor 2SF3886E20 which runs parallel to conductor 2A925G16 but is shielded. This comparison is shown in Figure 27.

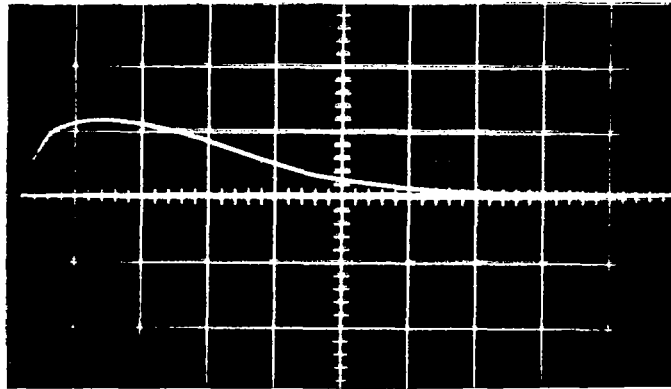
No short-circuit currents could be measured in these conductors, as a result of their being open at the far end. All of the voltages measured are tabulated in the Appendix.

Test Conditions versus Induced Effects

As is evident from the preceding discussion of test results obtained for each selected circuit, the electrical and physical characteristics of the circuit itself are not the only factors which determine the amount of voltage which will be induced in an aircraft electrical circuit. The applied test conditions have been found to be of equal significance. These include the lightning stroke parameters of amplitude and wave shape, as well as the location at which the stroke attaches itself to the aircraft. The preliminary tests showed that the amplitude of induced voltages is roughly proportional to the applied lightning current amplitude - at least within the range of amplitudes (7 to 70 kiloamperes) applied to determine this relationship.

The lightning current wave shape and, in particular, the rate of rise of current with respect to time (di/dt), is the other significant parameter. This factor was found to be significant to varying degrees in each of the eight circuits. In all circuits, the fast wave shape, which had a di/dt of

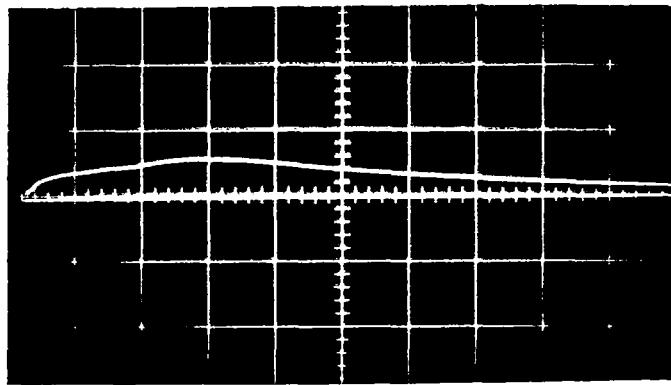
UNSHIELDED CONDUCTOR



0.5 volt/Div.

20 μ s/Div.

SHIELDED CONDUCTOR



0.05 volt/Div.

50 μ s/Div.

FIGURE 27. - COMPARISON OF VOLTAGES INDUCED IN UNSHIELDED AND SHIELDED CONDUCTORS OF OTHERWISE IDENTICAL DESCRIPTION AND LOCATION. 40 KILOAMPERE 36 x 82 μ s STROKE TO LOCATION 4. CONDUCTOR 2A925G16 AND AIRFRAME (CIRCUIT A.140 RIGHT ARMAMENT JETTISON) AND CONDUCTOR 2SF3886E20 AND AIRFRAME (CIRCUIT S.220 ARMAMENT POWER SUPPLY). BOTH CIRCUITS LOCATED IN LEADING EDGE OF WING

8 kiloamperes per microsecond, caused greater induced voltages than the slow wave shape, with a di/dt equal to 2 kiloamperes per microsecond. Definition of the relationship between induced voltages and the lightning current amplitude and rate of rise parameters was pursued analytically, based on the experimental data obtained. This procedure and the results thereof are discussed in the analysis section of this report.

The location of the stroke was also significant. In most circuits, the largest induced voltages were measured from strokes delivered to locations closest to the actual location of the circuit in the wing. In general also, the strokes delivered farthest out on the wing or tip tank resulted in the highest voltages, provided the circuit extended nearly as far. Since the wing is a complex mechanical structure, with numerous internal members and bonds, it is extremely difficult, if not impossible, to ascertain the paths of current concentration through the wing. As a result, definition of a meaningful quantitative relationship between stroke locations and induced effects is not possible, beyond simple recognition of the fact that circuits located in or near regions likely to be struck by lightning are more susceptible to induced effects than those in more protected locations. In particular, if a stroke is delivered to an extremity of the aircraft, such as the wing tip fuel tank which is fastened to the main airframe through temporary or movable joints, a large resistive or inductive voltage may arise across the joint. This voltage can enter a circuit if its airframe return path is through the joint.

Special Tests

While the majority of data obtained in this program was the result of systematic application of a set of standardized test conditions for each of the eight circuits selected for measurement, some additional tests and measurements were made to evaluate special conditions or interesting phenomena. These special tests included:

- (1) Installation of some additional circuits for evaluation of induced voltage reduction techniques.
- (2) Alteration of wing skin bonding to evaluate effect upon induced voltages.
- (3) Stroke polarity reversal test to determine if there were any polarity effect upon induced voltages.
- (4) High-amplitude stroke test, to see if any unexpected effects occurred as a result of a very high amplitude stroke.
- (5) Transient analyzer comparison tests, to compare and evaluate this instrument as a means of determining susceptibility of circuits to induced voltages.

These tests are discussed in the following paragraphs:

Installation of Additional Circuits

Several additional circuits were assembled and installed in the wing for the purpose of making some comparative measurements, which could not be made satisfactorily with circuits already existing in the wing. The measurements desired were:

- Comparison of voltages induced in circuits of different length which lead to the same location
- Comparison of voltages induced in a parallel pair and a twisted pair of conductors
- Comparison of voltages induced in a single unshielded conductor and a coaxial cable

For these tests, a group of conductors suitable for the above comparisons was assembled and installed in the wing. The conductors were passed from the instrument enclosure through the leading edge heating duct to the

wing tip, thence between the wing tip and tip fuel tank and along the outside of the trailing edge spar to the instrument enclosure. Both ends of each conductor were thus terminated in the enclosure.

Figure 28 shows the path of these circuits in the wing. They can be seen entering the heating duct in Figure 14. The circuits include a conductor bundle containing a single insulated #16 conductor, a single coaxial cable (RG 58A/U), a twisted pair of #16 insulated conductors, and a parallel pair of #16 insulated conductors. In order that the circuits would not be completely exposed anywhere along the path, part of the bundle was shielded by copper braid. This braid was placed over the conductor bundle for its entire path except where the bundle was within the heating duct. The copper braid did not cover the bundle within the heating duct because the duct itself provided shielding for the conductors within it. The braid was solidly connected to the airframe at the point where the bundle leaves the heating duct, and at various points along the trailing edge.

All measurements on these circuits were made with 40-kiloampere fast ($8.2 \times 14 \mu\text{s}$) simulated lightning strokes delivered to location 1 at the forward end of the tip fuel tank.

Two series of measurements were made. The first series consisted of measurements of the voltages induced in the entire length of each conductor. These measurements were obtained by measuring the voltages at each end of each conductor, with the other end connected to the airframe. For the second series of measurements, all conductors, including the coaxial cable shield and the copper braid, were solidly connected to the airframe at a point in the trailing edge between the aileron and flap positions, shown on Figure 28. This in effect created two sets of circuits terminating at the same point in the wing, but following different paths. The circuits passing through the heating duct and across the wing tip were the longest, at 38 feet. Those running out the trailing edge were only 12 feet long. Identical tests and measurements were made in each set of circuits. Measurements were made from

Lightning current stroke to the tank

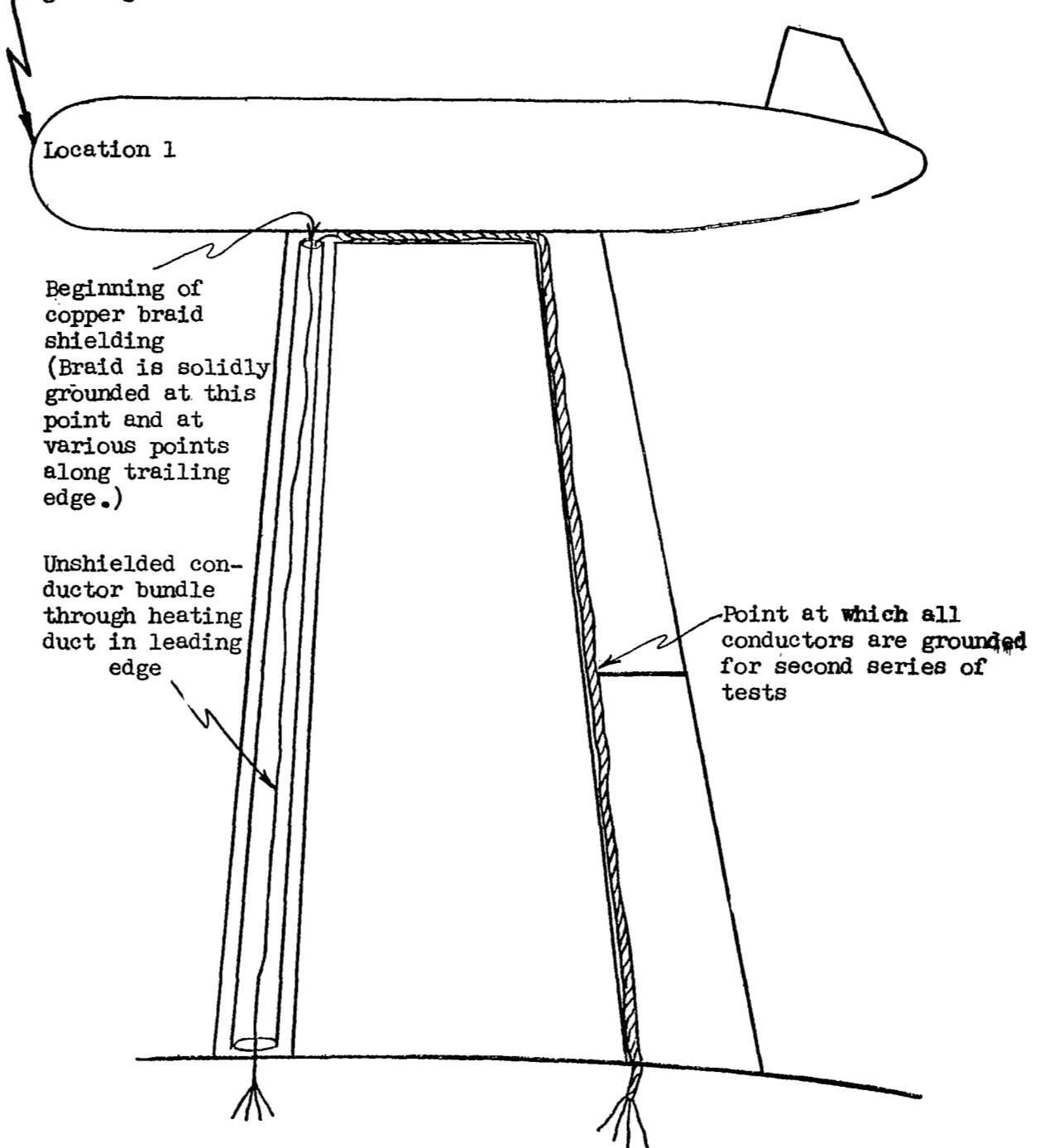


FIGURE 28. - F-89 WING SHOWING ADDITIONAL CIRCUITS PLACED IN THE WING FOR TEST.

all conductors to the airframe (line to airframe), and between each conductor of the twisted and parallel pairs. The open-circuit induced voltages and short-circuit currents measured in each conductor are listed in Tables V and VI. The maximum amount of voltage measured in any circuit was 6 volts. This relatively low value is probably due to the overall shielding provided all of the circuits. Placement of these circuits in the leading edge heating duct afforded them greater shielding than they would have if simply routed through the leading edge itself. Similarly, the addition of the copper braid around the rest of the circuit provided greater shielding than was afforded the existing aircraft circuits which followed the same path.

Comparison of voltages induced in the various circuits is of interest. When measured between individual conductors and the airframe, it was found that voltages induced in conductors of the parallel pair were three to six times greater than those induced in the twisted pair (Tables V and VI). Voltages measured between conductors of the parallel pair were between two and ten times greater than those measured in the twisted pair.

A comparison between conductor to airframe voltages measured from the individual #16 insulated conductor and the center conductor of the RG 58A/U coaxial cable shows little difference in voltage amplitudes (Tables V and VI). This is probably the result of the substantial attenuation in induced voltages provided both of these circuits by the heating duct and copper braid covering all circuits.

An additional interesting comparison is made between voltages and currents measured from the long (leading edge) circuits and the short (trailing edge) circuits, both of which terminate at the same point in the wing. Open-circuit voltages and short-circuit currents measured in the longer circuits were greater in all cases than those associated with the shorter ones. Such a result would be expected, since induced effects are believed to be proportional to circuit length (among other factors).

Similar comparisons were found for short-circuit currents, although the

TABLE V. - MAXIMUM INDUCED VOLTAGES AND CURRENTS IN NEW WING CIRCUITS

(Series 1 - Measurements at Leading Edge on Entire Length of Circuits.
Trailing Edge Terminations Connected to Airframe)

Conductor	Open Circuit Voltage (Volts)		Short Circuit Current (Amps)	
	Conductor-to-Airframe	Conductor-to-Conductor	Conductor-to-Airframe	Conductor-to-Conductor
Unshielded #16 Insulated Conductor	1.5	--	0.8	--
RG 58A/U Coaxial Cable	1.2	--	1.6	--
Twisted Pair of #16 Insulated Conductors	1.5	0.16	1.0	0.1
Parallel Pair of #16 Insulated Conductors	5.0	1.6	5.0	0.8

TABLE VI. - MAXIMUM INDUCED VOLTAGES AND CURRENTS IN NEW WING CIRCUITS

(Series 2 - All Circuits and Shields Connected to Airframe at Location Between Aileron and Flap on Trailing Edge. Identical Measurements on Circuits Terminating at Leading and Trailing Edges)

Conductor	Open Circuit Voltage (Volts)				Short Circuit Current (Amps)			
	Conductor-to-Airframe		Conductor-to-Conductor		Conductor-to-Airframe		Conductor-to-Conductor	
	Leading Edge*	Trailing Edge*	Leading Edge	Trailing Edge	Leading Edge	Trailing Edge	Leading Edge	Trailing Edge
Unshielded #16 Insulated Conductor	2.0	0.4	--	--	1.6	1.3	--	--
RG 58A/U Coaxial Cable	2.1	0.4	--	--	2.2	0.4	--	--
Twisted Pair of #16 Insulated Conductors	1.0	0.5	0.22	0.04	1.4	0.9	0.1	0.1
Parallel Pair of #16 Insulated Conductors	6.0	1.0	2.3	0.1	6.0	2.0	1.3	0.1

*NOTE: Circuits terminating at leading edge are 38 feet long.
Circuits terminating at trailing edge are 12 feet long.

comparison ratios for currents were not the same as corresponding voltage ratios. This would be expected for, while voltages are somewhat proportional to circuit length, currents would be proportional to voltages only to the extent they are not diminished by the additional circuit impedance provided by longer circuits.

These measurements illustrated some important facts, the most significant of which are that a twisted pair of conductors receives substantially less induced voltage than a parallel pair, and that circuits within a shielding braid or conduit are much less susceptible to induced voltages than those relying upon the wing skin itself for shielding.

Alteration of Wing Skin Bonding to Evaluate Effect upon Induced Voltages

With the realization that wing skin cracks, seams and structural bonds all afford an opportunity for magnetic flux leakage and coupling with electrical circuits, it was decided to investigate briefly the degree to which these factors are significant. For this purpose, two tests were made. The first consisted of application of a 1-inch wide aluminum foil tape pasted over the leading edge seams, as shown in Figure 29(a). Paint was sanded from the seams, and the aluminum foil tape was backed with a wider adhesive tape which secured it firmly over the seams. Induced voltage measurements were made on the glide path radio receiver circuit (R.060) and the armament jettison circuit (A.140) with a stroke delivered to location 1. The pylon was removed. The voltages measured with the tape applied were nearly the same as those measured earlier with no tape applied. Differences were not sufficient to show any evidence of increased electromagnetic shielding as a result of the tape being applied. This is probably due to the fact that the skin is fastened to the spars and ribs by means of lap joints, and thus the seams do not open directly into the wing interior. The joint itself thus provided a sufficient electromagnetic seal, and



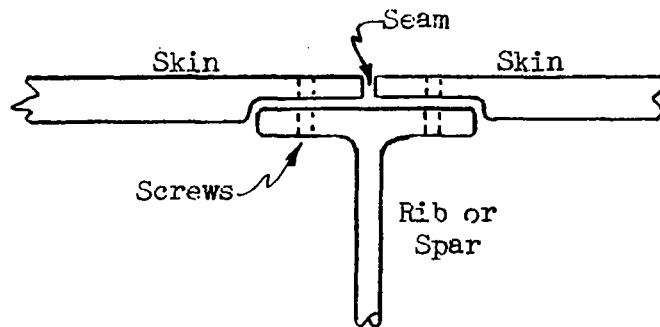
a. Aluminum Foil Tape Over Leading Edge Seams



b. Fastening Screws Removed from Upper Main Panel.
Lightning Stroke Electrode Shown Positioned
above Panel.

FIGURE 29. MODIFICATIONS TO WING BONDING.

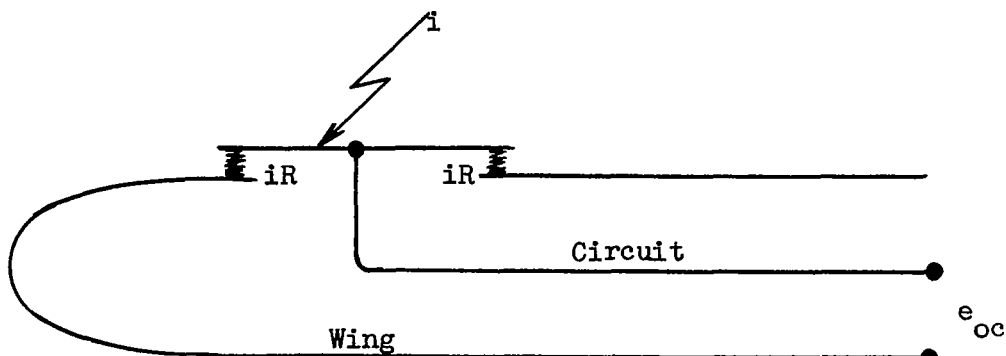
the addition of the tape was insignificant. A rough sketch of this type of joint is as follows:



The second test was made to evaluate the effects of lightning currents flowing through a poor bond, upon voltages induced in circuits within the wing. For this purpose, a 40-kiloampere fast stroke was delivered to one of the upper main panels from which all of the fastening screws had been removed, as shown in Figure 29(b). Stroke currents thus passed through the poor bonds to the rest of the wing. A similar stroke was delivered to the panel prior to removal of the screws, for comparison purposes. This panel covers the inboard fuel cells, and there are no electrical circuits in these cells. Measurements were made on nearby circuits, but all are separated from the fuel cells by metal spars and ribs. Thus, removal of the panel did not directly expose any electrical circuit. The circuits chosen for measurement all are located in the leading edge. These included the glide path antenna circuit (R.060); the fuel quantity indication circuit (E.0711), conductors 2E69B22 and 2E70B20; and the armament jettison circuit (A.140).

The induced voltages measured in these circuits were of approximately the same magnitude and wave shape as those delivered to nearby stroke locations (7 and 10) during the complete test series. Removal of the mounting bolts in the panel had little effect on any of the measurements. The

reason for this is that this panel does not cover any circuits. The metal spars and ribs which separate the fuel bay from the spaces housing electrical circuits provide magnetic shielding of these circuits. The high resistivity of the loosened joints likewise does not become a contributing factor to induced voltages because this resistance is not part of the wing electrical circuit in which voltage is being measured. If a wing circuit had been connected to the airframe at a point on the loosened panel, then the resultant high resistance bond would be included in the wing circuit. If a lightning stroke is delivered to this panel, the resultant resistive voltage rise will appear in the electrical circuit, as shown in the following sketch.



It was not possible to remove a panel to which a circuit was connected; hence, this situation could not be experimentally evaluated.

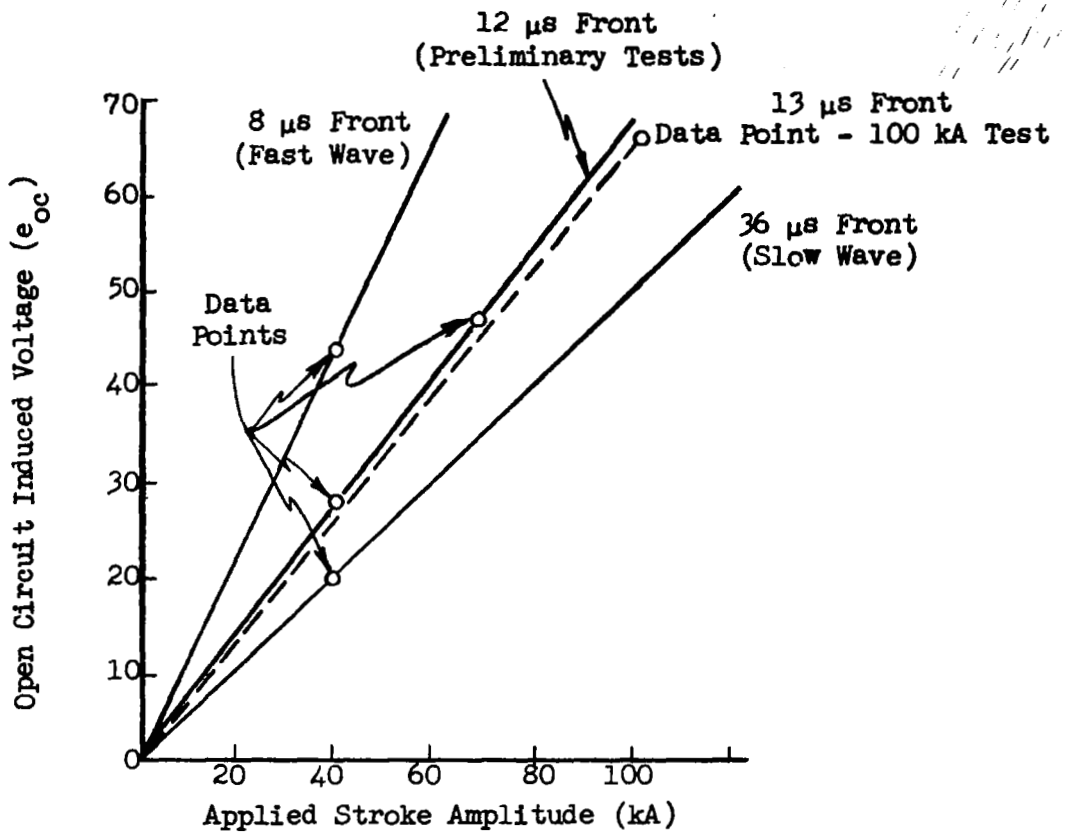
Lightning Stroke Polarity Reversal Test

All tests made in this program involved application of positive polarity simulated lightning strokes (the wing as cathode), since it was not expected that reversing the direction of lightning current flow would do any more than reverse the polarity of the induced voltages. To assure that this is so, selected tests were run in which negative polarity strokes were applied and the induced effects resulting therefrom were compared with the results of positive strokes under otherwise identical test conditions. The

results showed that reversing the polarity of the applied stroke simply reverses the polarity of the induced effects as had been expected. No other changes were detected.

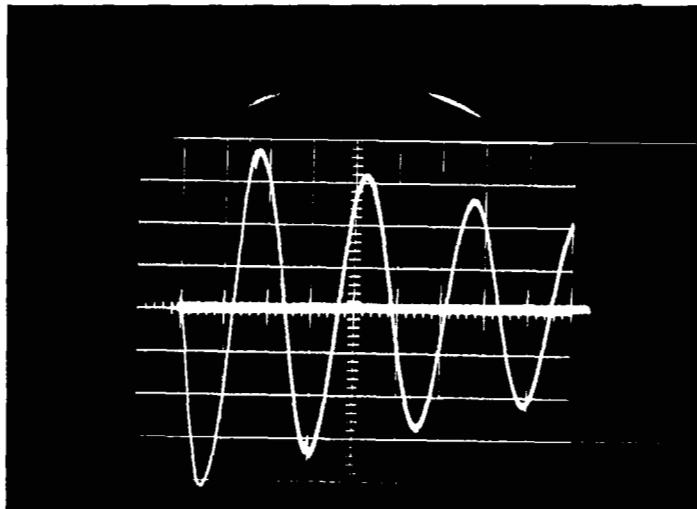
High Amplitude Stroke Test

With the exception of some 70-kiloampere strokes applied during the preliminary tests (Figure 16), all tests were made with 40-kiloampere strokes. To assure that no unexpected effects occur at higher stroke current amplitudes, a 100-kiloampere stroke was applied to locations 1 and 5. Due to test circuit impedance limitations, a current of 100 kiloamperes could not be obtained with a unidirectional wave form. A damped oscillatory wave form, shown in Figure 30(a), was thus applied. This wave form oscillated with a frequency of 21 kilohertz, and had an initial rate of rise (di/dt) of 10 kiloamperes per microsecond. The first half-cycle had a wave shape of $13 \times 23 \mu s$. Induced effects measurements were made on the position light circuit (L.050) and the E-11 autopilot circuit (F.0511). The voltages measured were higher than those obtained with the 40-kiloampere stroke. Comparison of these measurements with corresponding ones obtained from 40-kiloampere strokes is not possible by direct extrapolation, since the wave shapes applied at 40 kiloamperes were different. It has been learned, however, (Figure 16) that amplitudes of induced voltages are proportional to amplitudes of applied strokes at particular wave shapes. Thus, if straight lines are plotted through the zero and 40-kiloampere points obtained for each of the wave shapes previously tested, the following relationship is apparent:



AMPLITUDE OF INDUCED VOLTAGE VERSUS STROKE AMPLITUDE
(Stroke Wave Shapes Constant)

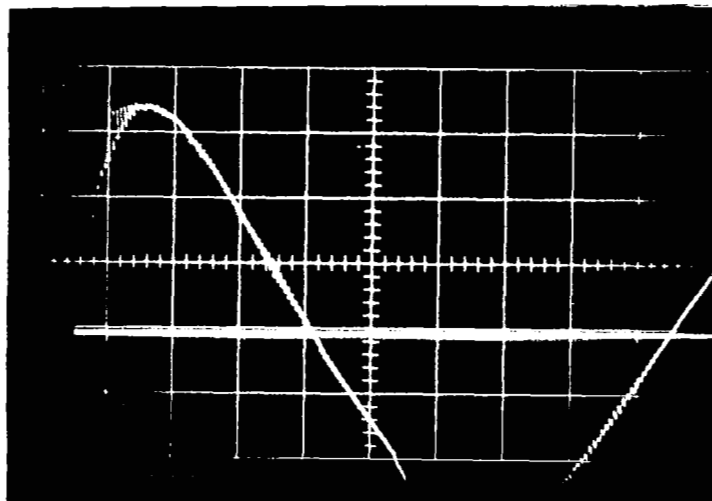
The 100-kiloampere stroke to location 1 induced 68 volts in the position light circuit. This data point falls on a line (dashed) just to the right of the 12 μs front line in the above graph. The dashed line would correspond to a 13 μs front line. It is therefore probable that induced voltages from strokes of 100 kiloamperes do correspond proportionately to voltages induced by lower amplitude lightning strokes. The oscillogram



24 kA/Div.

20 μ s/Div.

100 Kiloampere Simulated Lightning Stroke (13 x 23 μ s).
 (Appears negative due to placement of measurement shunt
 in impulse generator ground return circuit)



20 volts/Div.

5 μ s/Div.

b. Open Circuit Induced Voltage (Conductor 2L10E18 to Airframe)

FIGURE 30. - (a) 100 KILOAMPERE STROKE APPLIED TO LOCATION 1 AND
 (b) RESULTANT INDUCED VOLTAGE MEASURED BETWEEN CONDUCTOR 2L10E18
 AND AIRFRAME (CIRCUIT L.050 - POSITION LIGHT)

of the voltage induced by the 100-kiloampere stroke in the position lamp circuit is shown in Figure 30(b).

The effect of the subsequent lightning current oscillations, Figure 30(a), is simply to cause similar oscillations, or repetitions, of the induced voltages. Figure 30(b) shows the beginning of the second oscillation, which occurs simultaneous with the beginning of the second cycle of the lightning current (at $t = 44 \mu\text{s}$).

Transient Analyzer Comparison Tests

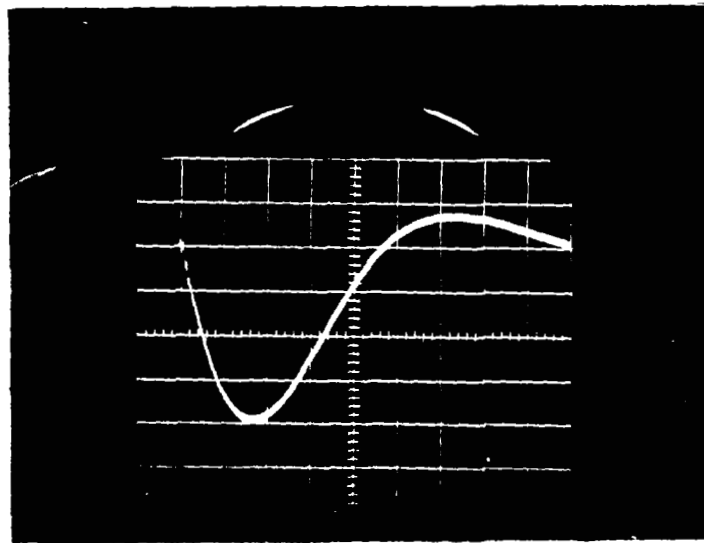
While this program has provided an excellent opportunity to thoroughly evaluate induced voltages in a major portion of a single type of aircraft, the practicality of doing so on a complete aircraft, or upon many different types of aircraft, is questionable. Yet, the need exists for similar information on existing aircraft, as well as prototype designs. Accordingly, it has become worthwhile to establish a more practical means of performing similar investigations economically and nondestructively. A possible instrument for this purpose is the transient analyzer, a device developed by the G.E. High Voltage Laboratory for applying nondestructive transients of desired wave shapes to power transformers. In transformers, the transient analyzer is used to determine the voltages induced at various locations within the windings which would result from lightning strokes to the external terminals of the transformer. It is an analog device, operating at non-destructive energy levels on the premise that if the system being tested is electrically linear, the results can be accurately scaled upward to full-scale levels. Extensive use of transient analyzer techniques for many years on transformers and some other systems has shown this to be the case.

Essentially, the transient analyzer generates a voltage or current pulse, the parameters of which may be easily selected and varied. This pulse is applied to the system being studied, and a related measurement system permits measurement of the pulse response anywhere in the system.

The transient response is then scaled upward by the ratio of a full-scale pulse amplitude to the transient analyzer output pulse amplitude.

To evaluate the effectiveness of the transient analyzer in the present application, it was set up to deliver a current pulse identical in wave shape to the $8.2 \times 14 \mu\text{s}$ "fast" lightning current applied for many of the 40 kiloampere (full scale) tests. This pulse was delivered to the tip of the pylon (for convenience) and measurements were made in the position lamp circuit (L.050) between conductor 2L10E18 and the airframe. A 40 kiloampere stroke of the same wave shape was then applied to the same location. These wave shapes are shown in Figure 31. The voltages and currents induced by each are shown on Figure 32. The oscillogram of Figure 32(a) shows that the 1 kiloampere current induced a maximum voltage of 1.8 volts in the circuit. Multiplication of this voltage by the scaling factor of 40 (the full-scale current amplitude divided by the transient analyzer current amplitude) indicates that a voltage of $1.8 \times 40 = 72$ volts would be induced by a 40-kiloampere stroke of the same wave shape. Figure 32(b) shows that an actual 40-kiloampere stroke induced 50 volts in the circuit, corresponding favorably with the value established by the transient analyzer.

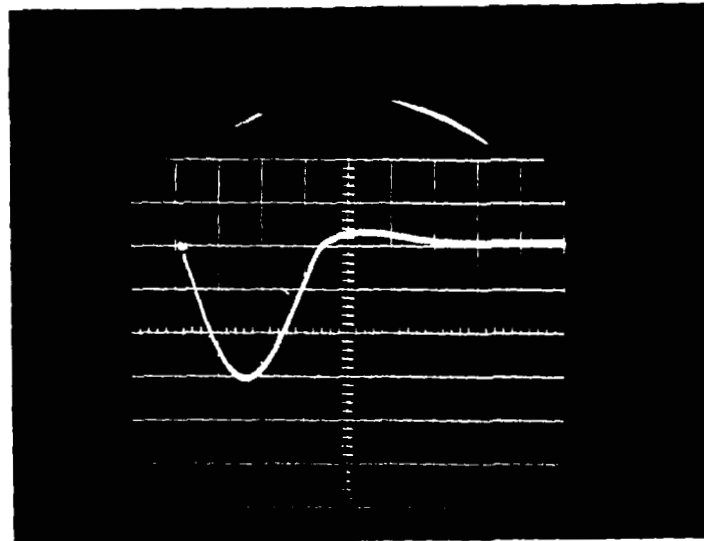
A similar correlation exists between the short-circuit currents, as would be expected. In this case, the transient analyzer induced a short-circuit current of 0.44 ampere, as shown in Figure 32(a). This current, when scaled upward, would predict a current of $0.44 \times 40 = 17.6$ amperes. The 40-kiloampere stroke did in fact cause a short-circuit current of 16 amperes to flow, as shown in Figure 32(b). The small differences between the results obtained from the transient analyzer and the full-scale tests are possibly the result of slight differences in the current wave shapes applied for each of these techniques. Similar comparisons were evident in the measurements obtained from other circuits.



260 amps/Div.

5 μ s/Div.

a. 1 Kiloampere $8.2 \times 17 \mu$ s Wave Form from Transient Analyzer.



13 kA/Div.

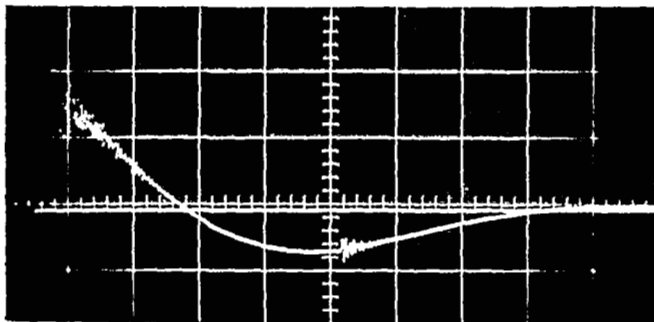
5 μ s/Div.

b. 40 Kiloampere $8.2 \times 14 \mu$ s Wave Form from Lightning Current Generator.

NOTE: Currents are actually positive but appear negative due to placement of current measurement shunt in impulse generator ground return circuit.

FIGURE 31. - SIMULATED LIGHTNING CURRENT WAVE SHAPES. COMPARISON OF WAVE SHAPES GENERATED BY (a) FULL SCALE LIGHTNING CURRENT GENERATOR AND (b) TRANSIENT ANALYZER.

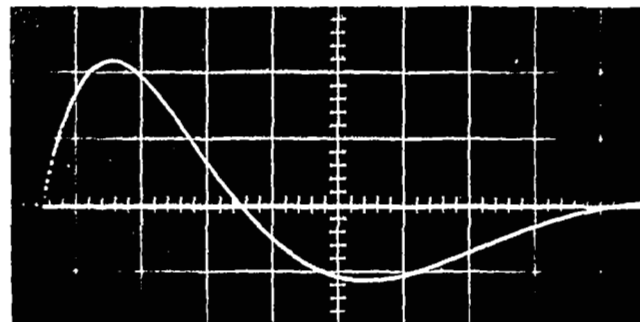
Open Circuit Induced Voltages



1 volt/Div.

5 μ s/Div.

Short Circuit Currents

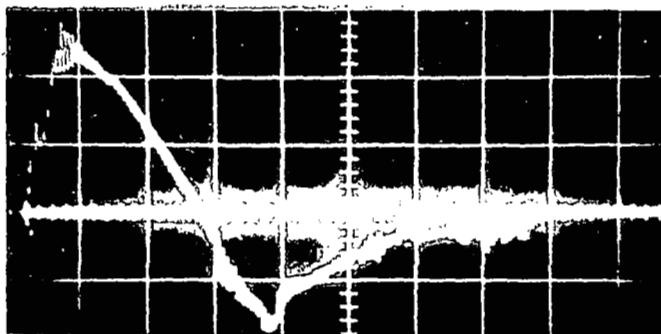


0.2 amp/Div.

5 μ s/Div.

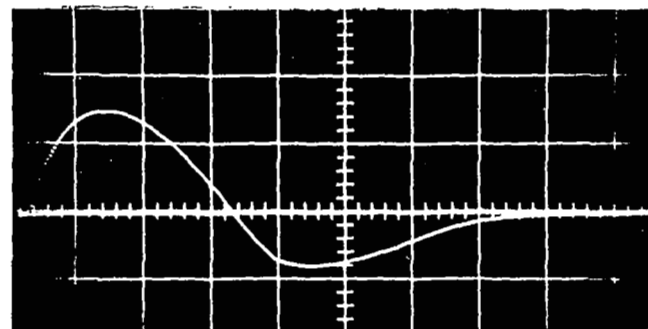
a. Induced Effects from 1 Kiloampere Stroke (Transient Analyzer).

88



20 volts/Div.

5 μ s/Div.



10 amps/Div.

5 μ s/Div.

b. Induced Effects from 40 Kiloampere Stroke (Full Scale).

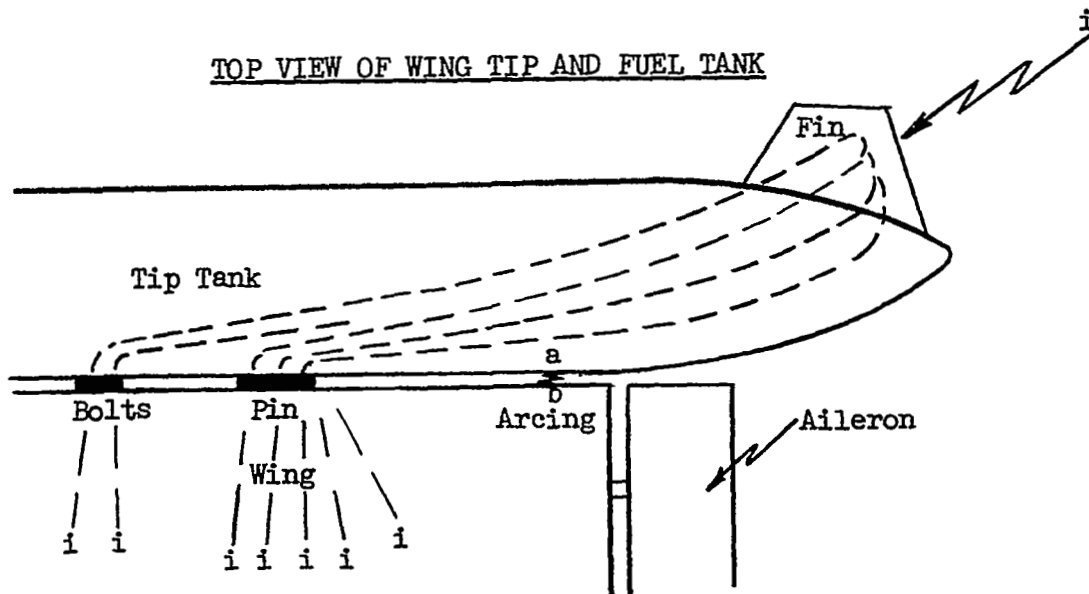
FIGURE 32. - COMPARISON OF INDUCED VOLTAGES AND CURRENTS INDUCED BY (a) 1 KILOAMPERE STROKE FROM TRANSIENT ANALYZER AND (b) 40 KILOAMPERE STROKE FROM SIMULATED LIGHTNING CURRENT GENERATOR. $8.2 \times 14 \mu$ s WAVE FORMS. MEASUREMENTS BETWEEN CONDUCTOR 2L10E18 AND AIRFRAME (CIRCUIT L.050 - POSITION LIGHT)

Other Observations

During the course of the testing, several other observations worthy of note were made, as follows:

Arcing Between Wing and Tip Tank

During the preliminary tests when a 14-kiloampere 11 x 22 μ s stroke was delivered to location 2 (trailing edge of tip tank fin), arcing was observed to occur between the tip tank and the adjacent wing tip. This arcing is visible in Figure 33, which also shows the stroke to the tank fin. When the tank is fastened to the wing tip, by means of attachment bolts and a pin, there is a slight gap between the tank wall and the wing tip, varying in length between about 1/8 inch and 1 inch. Electrical and fuel system connections to the tank are made via flexible connectors (one of which was conductor 2L10E18 leading to the position light). Close observation disclosed that the arcing occurred between the aft end of the wing tip and the adjacent fuel tank wall (between points a and b), across a gap of approximately 1/8 inch, as shown in the following sketch:



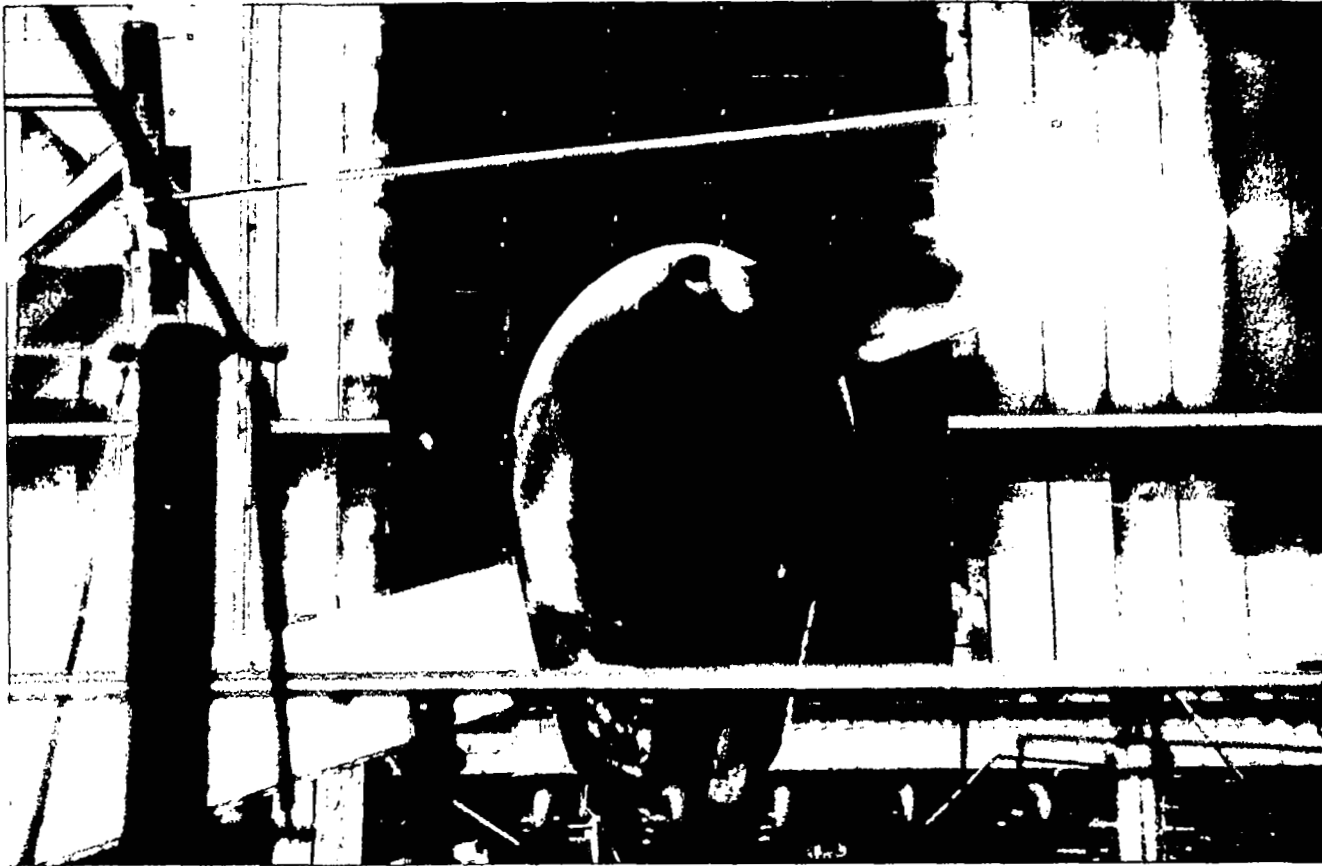


FIGURE 33. - 14 KILOAMPERE $11 \times 22 \mu\text{s}$ STROKE TO LOCATION 2 AT TRAILING EDGE OF FUEL TANK FIN. ARCING IS VISIBLE BETWEEN FUEL TANK AND WING TIP.

As shown in the previous sketch, the lightning current passes from the tip tank to the wing via the fastening bolts and pin. This apparently resulted in a sufficiently long current path between points a and b so that the inductive voltage rise between them was sufficient to break down the air gap between. The voltage rise would be

$$e = L \times \frac{di}{dt}$$

where L = effective inductance of path
a-b

i = lightning current flowing along
path a-b

Assuming that L was approximately 2 microhenrys and di/dt for the 14-kiloampere 11-microsecond wave front was approximately 2 kiloamperes per microsecond, then

$$e = (2 \times 10^{-6}) \times (2 \times 10^9) = 4,000 \text{ volts}$$

This voltage would be sufficient to cause an arc across such a gap.

This arcing occurred less regularly when strokes were delivered to other locations farther forward on the tank, and never occurred when strokes were delivered to the wing itself. The arcing caused no physical damage and was not associated with any wing electrical circuits. Its significance, however, should not be overlooked, since it occurred in an area near which fuel vapors may exist.

Stroke Damage to Wing Skin

Throughout the tests, observations were made of the simulated lightning stroke damage to the wing skin. Figure 34 shows markings made on the skin at location 7 (lower surface of wing at center) by a single 40-kiloampere stroke and by many similar strokes to the same point. This figure illustrates that very little damage was done to the skin by a single stroke. In fact, the tiny

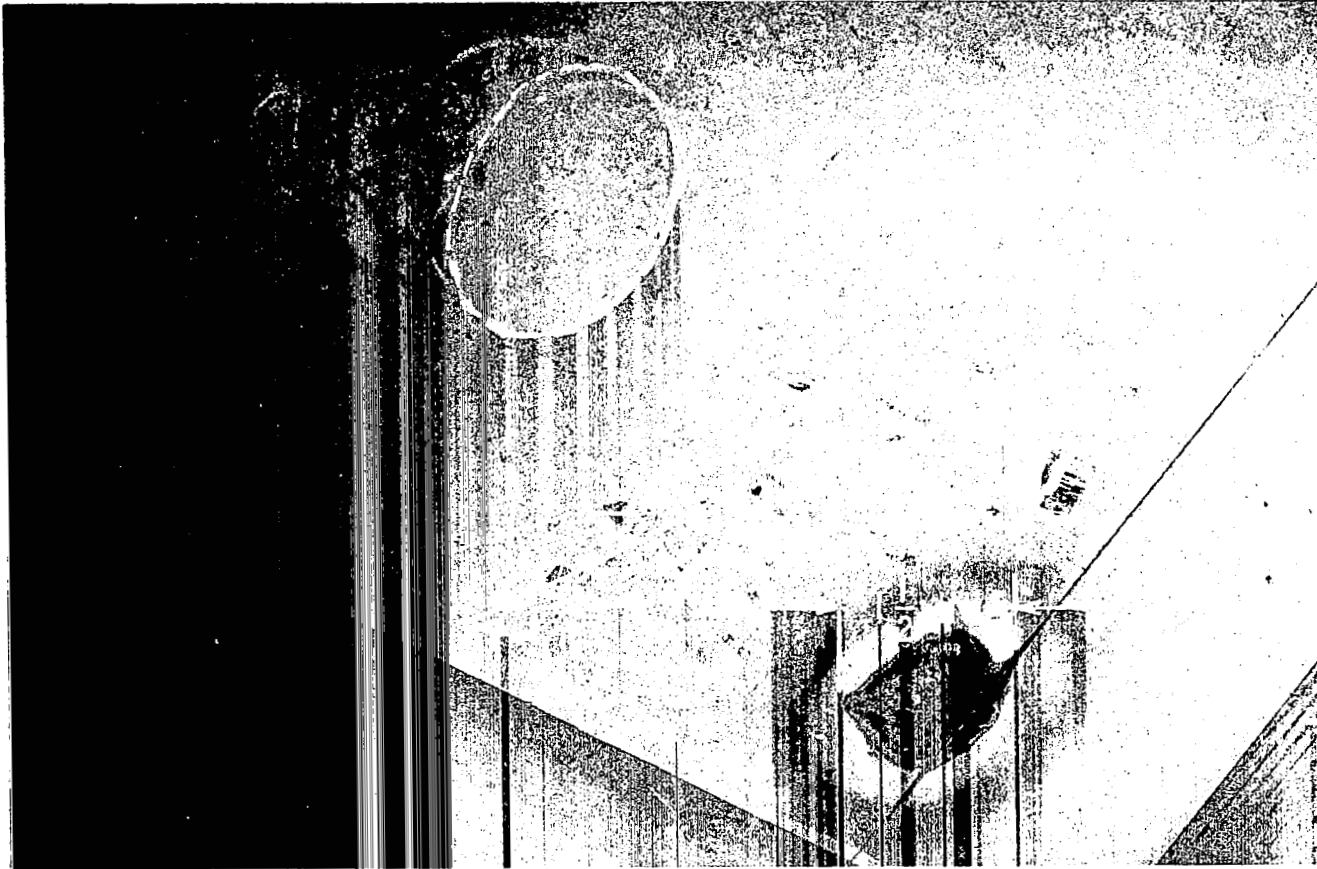


FIGURE 34. - 40 KILOAMPERE SIMULATED LIGHTNING STROKE DAMAGE TO WING SKIN. DARKENED AREA MADE BY 80 STROKES TO LOCATION 7. ENCIRCLED MARKS MADE BY A SINGLE STROKE. VIEW IS OF LOWER SURFACE OF WING, SHOWING WOODEN SUPPORT MEMBERS.

pit marks are almost undiscernible.

The low-amplitude, long-duration continuing currents which accompany a complete lightning flash were not simulated for these tests. These currents are the cause of most of the erosive damage inflicted so often upon aircraft skins (refs. 5 and 6). Comparatively little damage is done by a single high-amplitude, short-duration stroke. If many such strokes are delivered to the same location, more extensive damage results, as shown in Figure 34. This damage, however, is still mostly paint burning and metal surface pitting. In no case did one stroke cause a hole in the skin.

ANALYTICAL INVESTIGATION

The report thus far has described the experimental investigation and the induced voltages and currents measured in the electrical circuits within the wing of an F89J aircraft. Since the induced voltages were measured under open-circuit conditions, they are of course not the actual voltages which the circuits would develop across actual aircraft loads to which they are connected. Yet, it is necessary to determine the relationship between these and the open-circuit voltages actually measured. Rather than identify and simulate each of these for actual voltage measurements, it was decided to obtain sufficient measurements from the wing circuits alone, from which an equivalent circuit model of each wing circuit could be analytically established. From this equivalent circuit the voltage arising across any attached load impedance could be calculated by classical circuit analysis methods. One advantage of this technique is that it enables determination of the response across any selected impedance, thus permitting a more comprehensive understanding of the relationship between the voltage induced in a circuit and the amount of it actually impressed across the terminals of a piece of electrical equipment. Another advantage is that the analytical process of developing necessary mathematical descriptions of the measured induced voltages results in discovery of interesting relationships between these voltages and the causative lightning stroke parameters themselves. The following paragraphs describe the analytical processes applied. Several examples are described, and the remaining analytical results are tabulated.

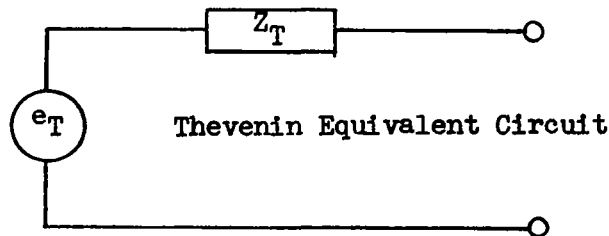
EQUIVALENT CIRCUITS

To derive the equivalent circuits, the wing circuits are considered as two-terminal networks viewed from the circuit terminals at the wing root (at which the actual measurements were made). The circuits are considered as being a combination of a voltage source, representing the induced voltage, and some impedances, and the equivalent circuit is actually the Thevenin

equivalent. Thevenin's theorem states:

"(1) Any active terminal pair composed of combinations of active and passive elements can, with respect to its terminals, be represented as the series connection of an ideal voltage source e_T and an operational element Z_T (an impedance) between the terminals. (2) The voltage source e_T referred to in (1) of this theorem is the voltage function found at the terminals of the active terminal pair (due to the sources within it) with no external elements connected to these terminals. The impedance function Z_T is the driving point impedance function at the terminals of the terminal pair when the ideal sources within the terminal pair are set to zero." (ref. 9)

The Thevenin equivalent circuit is therefore a series combination of an ideal voltage source, e_T , equal to the voltage measured across the open terminals of the actual circuit, and an impedance, Z_T , equal to this voltage divided by the current flowing through the actual short circuited terminals, as follows:



$$\text{Thevenin Voltage, } e_T = e_{oc}$$

$$\text{Thevenin Impedance, } Z_T = \frac{e_{oc}}{i_{sc}}$$

where e_{oc} = measured open circuit induced voltage

i_{sc} = measured short circuit current

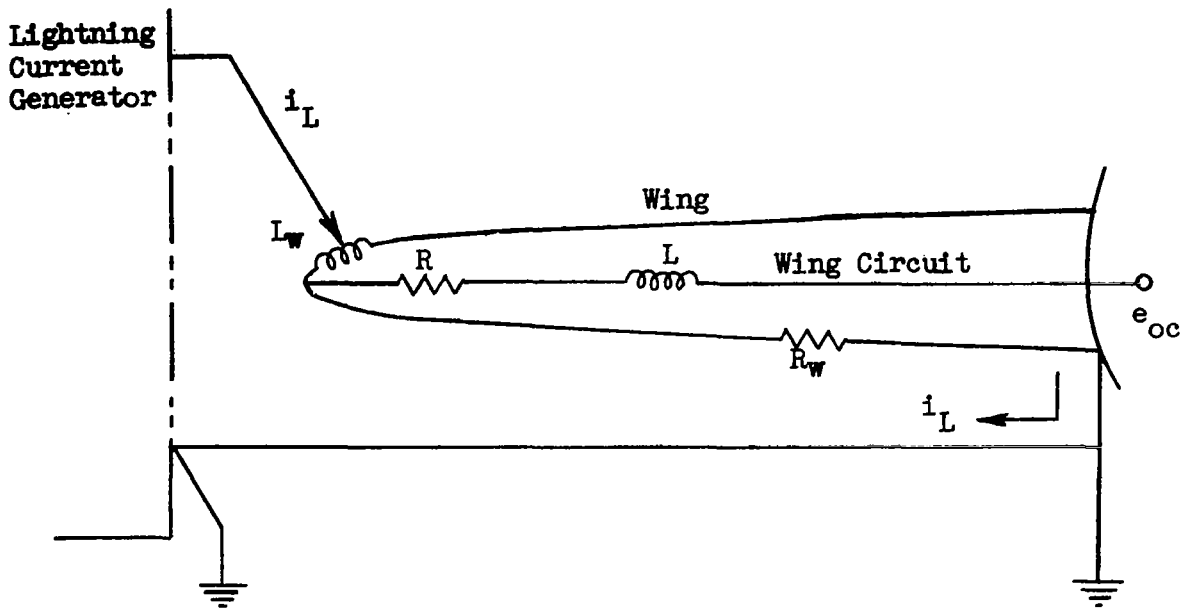


FIGURE 35 (a). - LUMPED CIRCUIT ELEMENT REPRESENTATION OF WING AND WING CIRCUIT

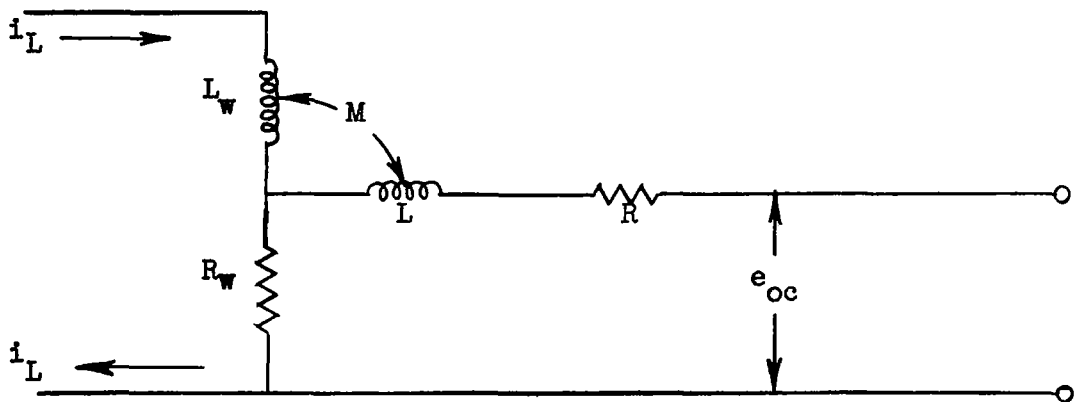


FIGURE 35 (b). - CIRCUIT REPRESENTATION OF WING STRUCTURE AND ELECTRICAL CIRCUIT

To establish the equivalent circuit, both e_T and Z_T (either of which may be complex functions) must be defined and expressed mathematically.

Thevenin Voltage Source, e_T

To determine an expression for the Thevenin voltage, e_T , first consider Figure 35(a), in which the wing and a hypothetical circuit are represented electrically by lumped impedances. The components R_w and L_w are the equivalent resistance and inductance, respectively, of the wing structure and skin, while the components R and L are representative of the electrical circuit within the wing. The circuit shown employs the airframe as its return path. The elements of Figure 35(a) are redrawn more clearly in the circuit representation shown in Figure 35(b). In this figure the magnetic coupling effect between the wing inductance and that of the electrical circuit within the wing is represented by the mutual inductance M . Also shown is the injection of the lightning current, i_L , and the resultant open circuit voltage, e_{oc} , measured at the circuit terminals. By Thevenin's theorem, this is the Thevenin voltage e_T . From Figure 35(b) it is apparent that this voltage is:

$$e_T = i_L R_w + M \frac{di_L}{dt} \tag{1}$$

This expression may then be substituted in the circuit of Figure 35(b) as the Thevenin voltage source, as shown in Figure 36.

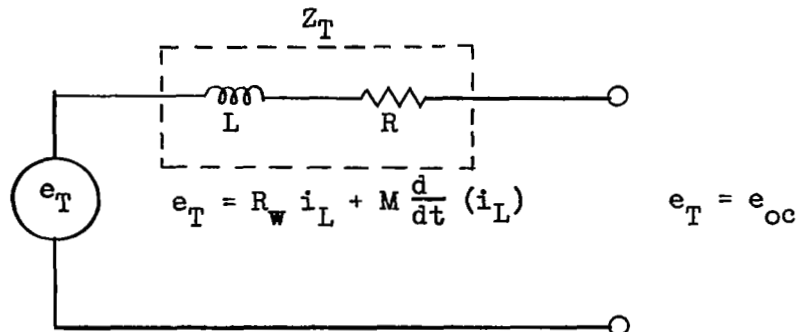


FIGURE 36. - THEVENIN EQUIVALENT CIRCUIT

From equation (1) it is apparent that the Thevenin impedance is the actual wing circuit impedance, consisting in this example of the circuit self inductance, L , and resistance, R . The Thevenin voltage source has been expressed in terms of the lightning current, i_L , as well as certain hypothetical wing parameters M and R_w . To express equation (1) in useful terms, it is necessary to have the mathematical description of the lightning current, i_L , as well as the parameters, R_w and M .

Assuming that the wave shape and amplitude of the lightning current is known, as was the case in this experimental investigation, then it can be expressed mathematically. Figures 37 and 38 show the actual 40-kiloampere slow ($36 \times 82 \mu s$) and fast ($8.2 \times 14 \mu s$) wave forms applied during this experimental investigation, together with the mathematical approximations used to describe each. Very close agreement is evident between the mathematically described approximations and the actual applied waves.

It will be noted that one mathematical expression does not apply to the wave shape throughout its entire time duration. Due to the particular nature of the wave shapes applied, it was not possible to find a single expression which would describe the entire wave forms. Accordingly, a combination of two expressions was utilized in each case.

Once the applied lightning current has been described, it is necessary to obtain values for the parameters R_w and M before an expression for e_T is completely defined. From the experimental results, it is obvious that e_T is not identical for all wing circuits or test conditions, even if the applied lightning stroke is unchanged. Therefore, the parameters R_w and M cannot be the same for all conditions, but must be dependent upon such factors as stroke location and circuit characteristics. They may, in fact, even be related to the lightning stroke wave shape.

If i_L is known and e_T is assumed to be equal to the experimental measurement e_{oc} , then equation (1) is an equation in two unknowns, R_w and M .

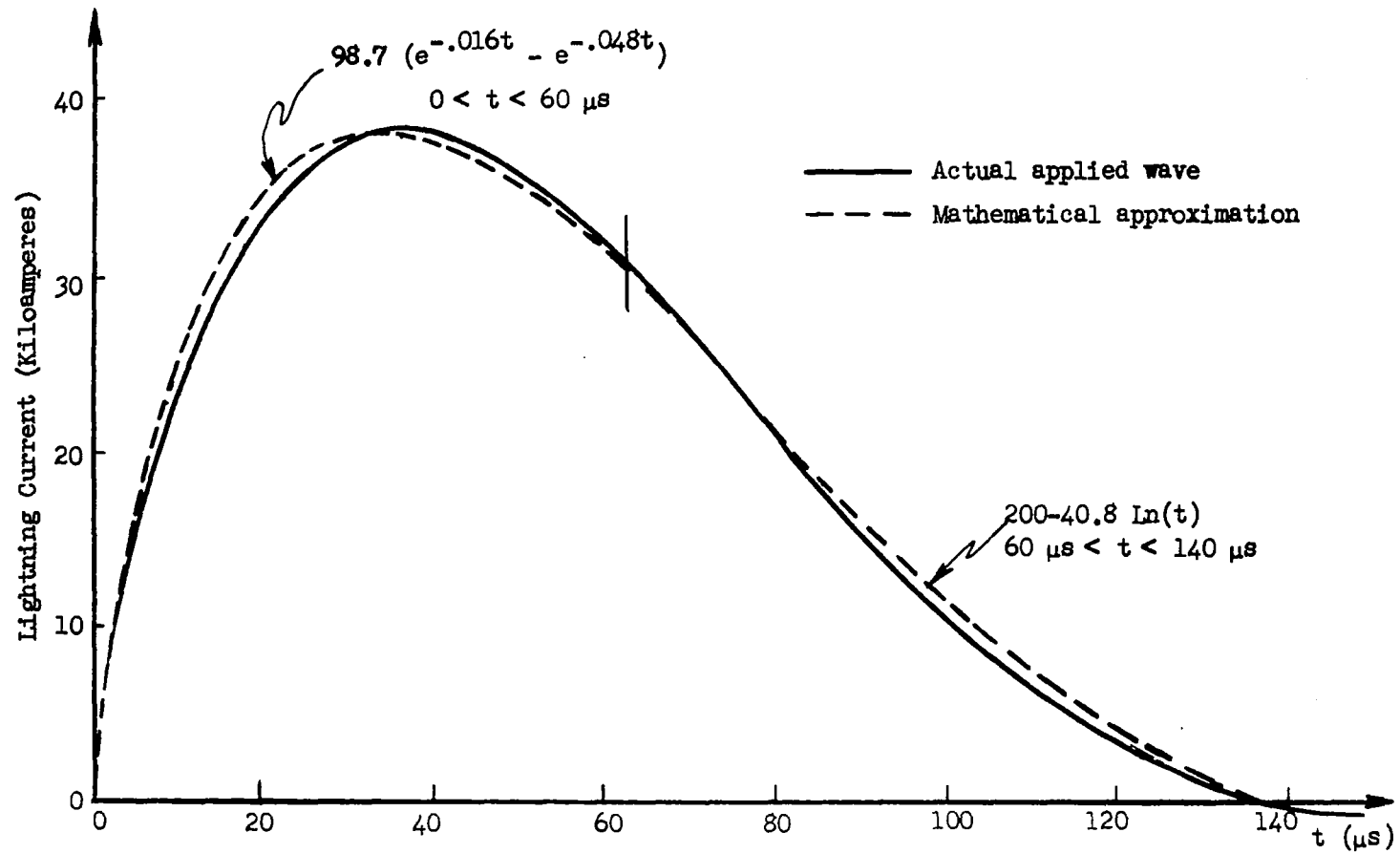


FIGURE 37. - MATHEMATICAL DESCRIPTION OF SIMULATED LIGHTNING CURRENT WAVE SHAPE
 $36 \times 82 \mu\text{s}$ (SLOW) WAVE SHAPE

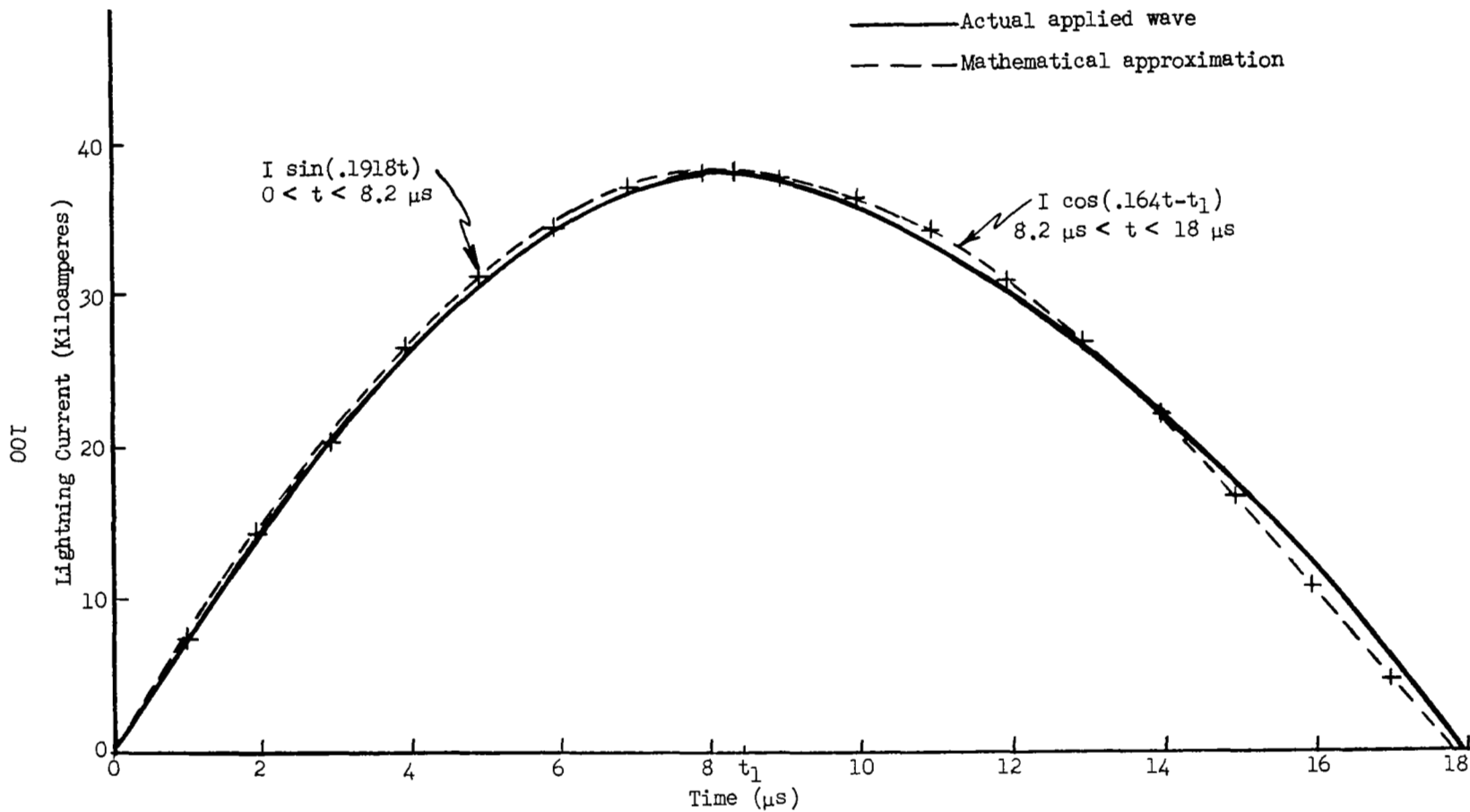


FIGURE 38. - MATHEMATICAL DESCRIPTION OF SIMULATED LIGHTNING CURRENT WAVE SHAPE
8.2 x 14 μs (FAST) WAVE SHAPE

Since e_{oc} and i_L are time varying functions, but R_w and M are presumably not, equation (1) can be written at two discrete times, resulting in a set of simultaneous equations which can be solved for R_w and M . Selection of appropriate discrete times is facilitated by reference to Figure 39, which shows a typical lightning current and resulting open-circuit induced voltage wave forms. If equation (1) is assumed to be valid for e_{oc} , then:

$$e_{oc} = R_w i_L + M \frac{di_L}{dt} \quad (1)$$

At $t = T_1$, the lightning current is unchanging; therefore

$$\frac{di_L}{dt} = 0 \quad (2)$$

and

$$e_{oc} = R_w i_L \Big|_{t = T_1} \quad (3)$$

from which

$$R_w = \frac{e_{oc}}{i_L} \Big|_{t = T_1} \quad (4)$$

which gives the solution for R_w . At $t = T_2$, the induced voltage is zero; therefore

$$e_{oc} = 0 \quad (5)$$

and

$$0 = R_w i_L + M \frac{di_L}{dt} \Big|_{t = T_2} \quad (6)$$

from which

$$M = -R_w \frac{di_L}{dt} \Big|_{t = T_2} \quad (7)$$

where R_w has been obtained from equation (4).

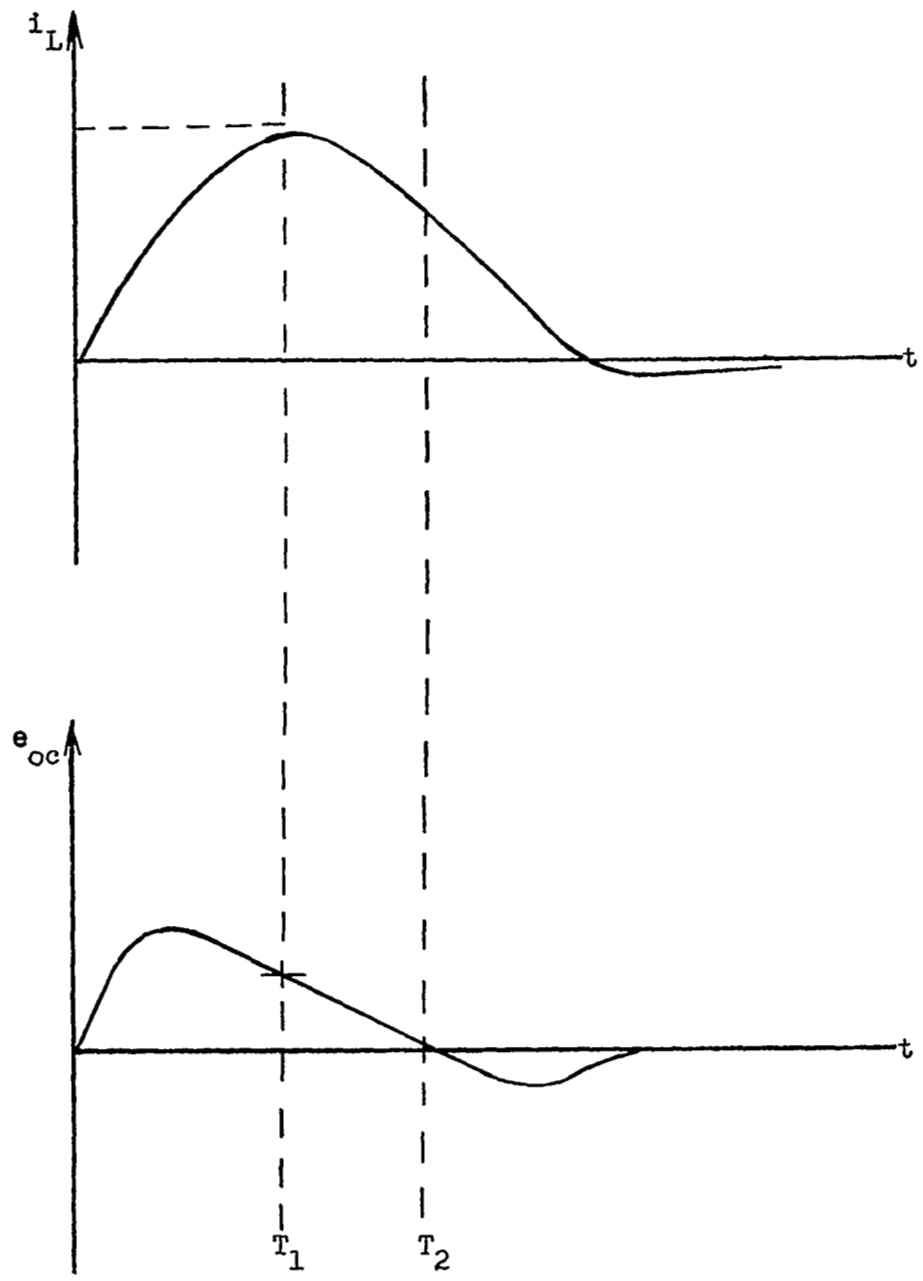


FIGURE 39. - TYPICAL LIGHTNING CURRENT AND INDUCED VOLTAGE WAVE FORMS

Thus, from an expression for the lightning current and two discrete voltage values from the measured open-circuit voltage oscillogram, a mathematical expression for the complete induced voltage wave form is obtained, in the form of equation (1). This expression was then used to calculate e_T for all values of time, and the resulting calculated wave form, e_T , was then compared with the actual measured wave form, e_{oc} , for verification. Close agreement between the calculated and measured wave forms in nearly all cases proved that this is a valid technique for generating an expression for the Thevenin voltage e_T . An example of this analysis is given in Figure 40, which shows both the measured and calculated wave forms of the voltage induced in the glide path antenna circuit (R.060) from a 40-kiloampere 8.2 x 14 μ s stroke to location-1 (forward end of tip fuel tank). In this case, equations (4) and (7) were solved for R_w and M respectively. The expression for i_L used in these solutions was that of Figure 38. Equation (4) states:

$$R_w = \left. \frac{e_{oc}}{i_L} \right|_{t = T_1} = 8.2 \mu s$$

From Figure 40 the measured value of e_{oc} at 8.2 μ s is 1.2 volts. i_L is equal to its maximum value of 40 kiloamperes at 8.2 μ s. Hence:

$$R_w = \frac{1.2 \text{ volts}}{40 \times 10^3 \text{ amperes}} = 3 \times 10^{-5} \text{ ohms}$$

Equation (7) states:

$$M = -R_w \left. \frac{di_L}{dt} \right|_{T = t_2}$$

From Figure 40 (e_{oc}), $t_2 = 9.1 \mu$ s. The value of $\frac{di_L}{dt}$ at 9.1 μ s is calculated from the expression of Figure 38 to be:

$$\frac{di_L}{dt} = -.863 \times 10^{-9} \text{ amperes per second}$$

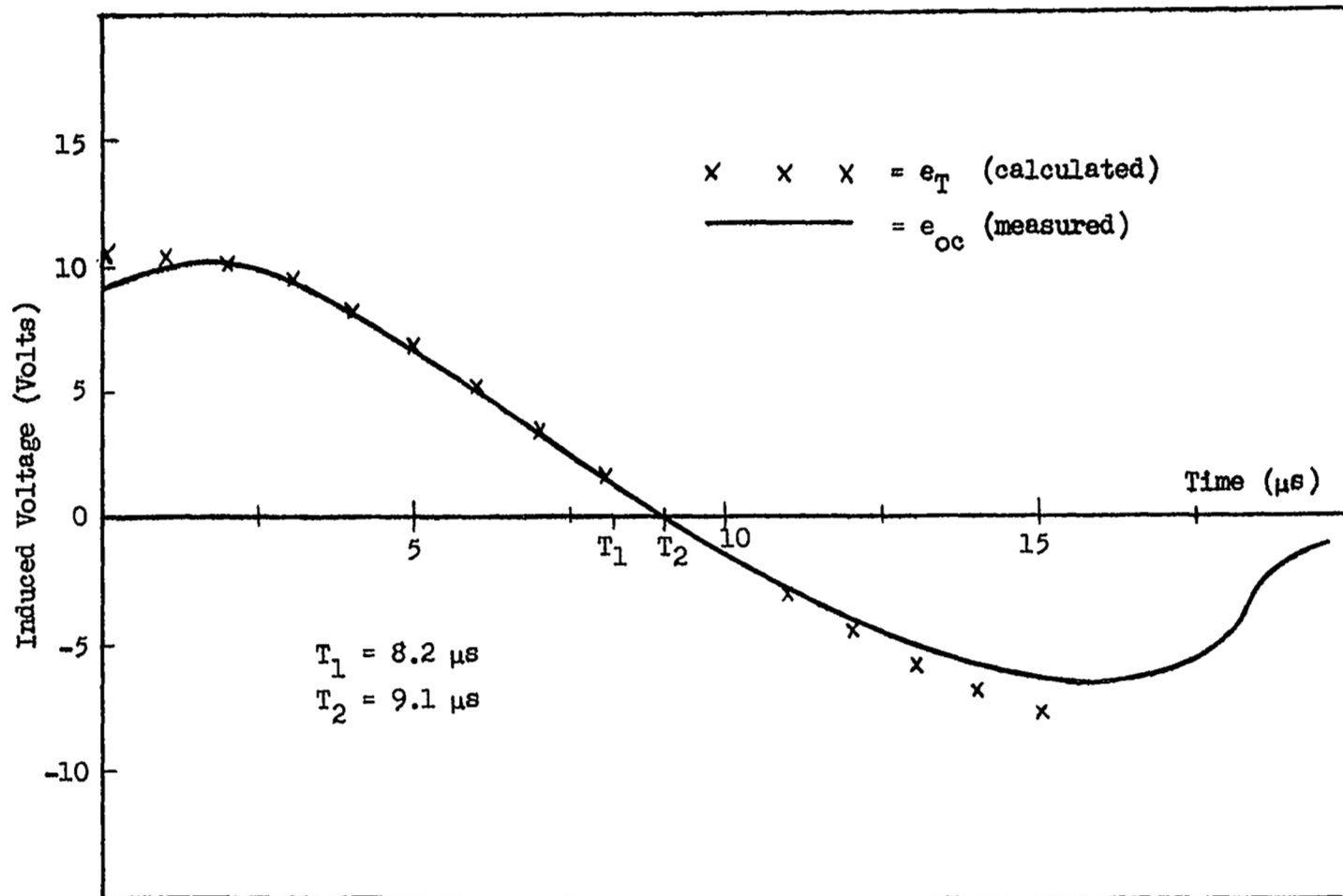


FIGURE 40. - COMPARISON OF MEASURED (e_{oc}) AND CALCULATED (e_T) INDUCED VOLTAGE WAVE SHAPES, RESULTING FROM 40 KILOAMPERE $8.2 \times 14 \mu s$ STROKE TO LOCATION 1. CIRCUIT R.060 (AN/ARN-18 GLIDE PATH RADIO RECEIVER ANTENNA - ANTENNA SHORTED)

Thus:

$$M = -3 \times 10^{-5} \text{ ohms} \times \frac{40 \times 10^3 \text{ amperes}}{-.863 \times 10^9 \frac{\text{amperes}}{\text{second}}}$$
$$M = 1.39 \times 10^{-9} \text{ henrys}$$

Substituting these values of R_w and M into equation (1) gives:

$$e_T = (3 \times 10^{-5}) i_L + (1.39 \times 10^{-9}) \frac{di_L}{dt} \quad (8)$$

which is an equation for e_T in terms of the lightning current i_L . The expression for i_L from Figure 38 was then substituted into this equation and values of e_T were calculated for $0 \leq t \leq 15$ microseconds. These are plotted on Figure 40, from which it is evident that there is very close agreement between the calculated and measured wave forms. Thus, the analytically derived equation (8) for e_T is valid.

The calculation just outlined and all similar ones made for other test conditions and circuits were performed by a computer. For this purpose, a computer program entitled "ETCAL" was written in the BASIC language of the General Electric time-sharing computer service. Using the expression for the lightning current and the value of e_{oc} measured at t_1 the computer program calculates the coefficients R_w and M of equation (1) and plots the solution of this equation over the time period of the complete wave form. The values of R_w and M are tabulated for each circuit and test condition in Tables VII through XIV.

Not only is the foregoing analysis an effective technique for establishing the expression for e_T , but it also expresses this voltage in terms of the lightning current itself. The latter affords an opportunity to study relationships between the lightning current characteristics, effective wing electrical parameters, and the resulting induced voltages.

Effective Wing Electrical Parameters

Equation (1) illustrates that the wave form of the complete "induced" voltage is really a combination of two component voltage wave forms. One is a resistive voltage rise proportional to and in phase with the lightning current wave form. The other is a magnetically induced voltage proportional to the time derivative (rate of change) of the lightning current. The proportionality constants are the effective wing electrical parameters R_w and M , which represent effectively a wing resistance and mutual inductance with the electrical circuit in question. As would be expected, these latter quantities are not the same for all test conditions (even for the same wing circuit). Tables VII through XIV show considerable variation among values of R_w and M for each of the 8 circuits, and also for different stroke locations when measurements were made upon the same circuit. Since both R_w and M must be functions of the effective lightning current path through the wing and its relation to the particular wing electrical circuit, these variations seem natural. Not as readily understood are the variations in R_w and M as a function of lightning current wave shape, with all other test conditions the same. The tables show that in some cases these variations are greater than in others. In particular, there is generally a greater difference in the values of M than in R_w . The explanation of this is unclear, although it is possible that lightning currents of different wave shapes themselves travel different paths through the airframe, which result in different effective wing resistances and mutual inductances with respect to the wing electrical circuit in question.

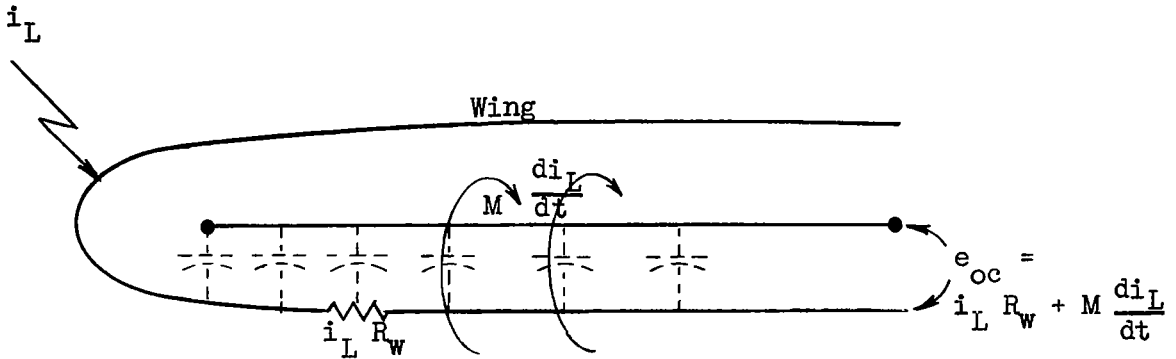
In spite of the unexplained variations mentioned above, Tables VII through XIV do exhibit some interesting relationships between values of R_w and M and the wing circuits or test conditions which appear logical. The first of these is the tendency for both R_w and M to increase as the lightning stroke is moved to locations farther out on the wing. This is logical since the lightning current must traverse a longer path of greater resistance

and mutual inductance with respect to wing electrical circuits. This effect was especially pronounced when strokes were delivered to the wing tip fuel tank, in which case the lightning current passes through the relatively high resistance of the tank fastening joint and the resultant concentrated magnetic flux more closely links the exposed circuit conductor passing between the wing tip and fuel tank. This relationship is particularly evident in the position light circuit (L.050, Table X) and the glide path receiver antenna circuit (R.060, Table XIII). It is not evident for the well shielded circuits or ones which do not employ the airframe as the return path.

It is noted that some of the values of R_w and M appear as negative numbers in the tables, indicating the existence of negative inductances or resistances. Since such elements are not possible, the appearance of the negative coefficients must be due to some other anomaly. Possibly they are the result of lightning currents flowing in a direction with respect to the wing circuit path opposite from that assumed for derivation of equation (1). In any event, it should be realized that R_w and M are effective wing resistances and mutual inductances and as such do not describe tangible wing characteristics. Further study should provide clarification of these phenomena and indicate relationships between R_w and M and wing physical characteristics.

Capacitive Coupling

Equation (1) for the induced voltage e_{oc} was derived for a circuit in which the airframe was actually used as the return path for the wing electrical circuit. Nevertheless, it has been possible to calculate values of R_w and M for an equation in the form of (1) which accurately describes the measured open-circuit voltages in circuits, the far ends of which are left 'floating' and are not terminated either directly or indirectly to the airframe. An example is the armament jettison circuit (A.140, Table VII) with the pylon removed, as shown on the following page.



The stray capacitance between this circuit conductor and the airframe is also present in other circuits which are terminated via low impedance paths to the airframe. In these cases, the low impedance path is preferential and the effect of the capacitance is comparatively minor. In the open-ended circuit, however, the capacitive coupling path is now the only one available to complete the circuit. Since an open-circuit voltage was measured in these circuits, a component of such voltage must have been the capacitive voltage between the conductor and the inside of the wing. However, since the voltage e_{oc} is expressed as a combination of resistive and inductive components only, the function of the capacitance might be visualized as simply connecting the apparent resistive voltage component arising in the airframe with the apparent magnetic component induced in the conductor itself. The effect of this coupling upon the calculated values of R_w and M as compared with those which would be calculated from a similar circuit connected via a low impedance to the airframe is not known; however, it is assumed to be significant. Accordingly, the calculated values of R_w and M for such open-ended circuits probably cannot be compared directly with their counterparts calculated from voltages measured in low impedance circuits. The negative coefficients of R_w and M may also be related to the capacitance effect. Further analysis should provide greater understanding of these relationships.

Voltage Components

The equation for the Thevenin voltage source,

$$e_T = i_L R_W + M \frac{di_L}{dt} \quad (1)$$

expresses this voltage as the combination of a resistive and an inductive voltage component. Both components are time-varying functions of the lightning current itself. It is of interest to study the factors affecting each of these voltages individually. Figures 41 and 42 show the magnetically induced and resistive voltage rises respectively as functions of the wing and lightning current parameters.

Figure 41 shows the resistive voltage, which is equal to the product of the effective wing resistance, R_W , and the lightning current amplitude. The range of wing resistances plotted covers those found in this investigation. The current amplitudes plotted encompass the range of currents believed to be possible in natural lightning. This figure can be used to determine the resistive voltage rise appearing in a wing electrical circuit (employing the airframe as the return path) for various combinations of R_W and lightning current amplitude. For example, a lightning current of 100 kiloamperes will cause a rise of 10 volts in a circuit with an associated wing resistance R_W of 100 microhms.

Figure 42 shows the magnetically induced voltages which may result from various lightning current and mutual inductance conditions. In this case the voltage is the product of the effective mutual inductance, M , and the rate of rise of the lightning current $\left(\frac{di_L}{dt}\right)$. From the figure, a lightning current rate of rise of 10 kiloamperes per microsecond, for example, will induce 100 volts in a circuit with an effective mutual inductance of 10 nanohenrys.

Since the resistive and inductive voltage components are each time-varying functions, proportional to the lightning current wave form and its differential respectively, they will not reach their maximum values at the

same time. Accordingly, the individual maximum voltages for each component as obtained from Figures 41 and 42 cannot be directly added to obtain the maximum voltage e_T which would appear in the circuit. Instead, equation (1) must be solved for e_T as a function of time and the resulting wave form plotted. Figures 41 and 42 do, however, serve the useful purpose of illustrating the range of resistive and magnetically induced voltages which can arise in circuits with various values of R_w and M .

Comparison of the possible resistive voltages of Figure 41 with the possible magnetically induced voltages of Figure 42, over the ranges of R_w and M found to be associated with the wing and circuits tested in this program, shows that the magnetically induced voltages are likely to be the most severe. For rates of rise of 10 to 20 kiloamperes per microsecond, for example, which are possible from lightning currents, some circuits in this wing would have induced voltages in excess of 1,000 volts.

TABLE VII. - CALCULATED EFFECTIVE WING RESISTANCES AND MUTUAL
INDUCTANCES FOR VARIOUS TEST CONDITIONS

Circuit A.140, Right Armament Jettison
Conductor 2A925G16 and Airframe. Location: Leading Edge
(Note: Pylon not attached)

i _L Wave Form: Stroke Location	Slow Wave Form (36 x 82 μs)		Fast Wave Form (8.2 x 14 μs)	
	R _w (microhms)	M (nanohenrys)	R _w (microhms)	M (nanohenrys)
1 Forward End of Tip Tank	13.7	0.0076	20.0	0.0597
4 Outboard Leading Edge	13.7	0.0076	13.7	0.0598
5 Trailing Edge of Aileron	11.2	0.1540	12.5	0.0450
7 Center of Wing Surface	12.5	0.2260	15.0	0.0545
10 Inboard Leading Edge	15.0	0.1380	18.7	0.134

TABLE VIII. - CALCULATED EFFECTIVE WING RESISTANCES AND MUTUAL
INDUCTANCES FOR VARIOUS TEST CONDITIONS
Circuit E.0711, Right Fuel Quantity Indication
Conductor 2E65B22 and Airframe

i _L Wave Form: Stroke Location	Slow Wave Form (36 x 82 us)		Fast Wave Form (8.2 x 14 us)	
	R _w (microhms)	M (nanohenrys)	R _w (microhms)	M (nanohenrys)
1 Forward End of Tip Tank	10	-0.00447	5.0	0.00649
4 Outboard Leading Edge	17.5	-0.00783	5.0	0.0258
5 Trailing Edge of Aileron	27.5	0.176	10.0	-0.27
7 Center of Wing Surface	1.25	-0.000559	25.0	-0.674
10 Inboard Leading Edge	32.5	-0.0145	5.0	0.0424
<u>Conductor 2E66B20 and Airframe</u>				
1 Forward End of Tip Tank	35.0	1.31	77.5	0.282
4 Outboard Leading Edge	30.0	1.19	45.0	0.232
5 Trailing Edge of Aileron	35.0	1.31	20.0	0.203
7 Center of Wing Surface	30.0	1.29	10.0	-0.0124
10 Inboard Leading Edge	45.0	-0.0201	25.0	0.185

(Continued)

TABLE VIII (Continued)

Conductor 2E67B22 and Airframe

i _L Wave Form:		Slow Wave Form (36 x 82 μs)		Fast Wave Form (8.2 x 14 μs)	
Stroke Location	R _w (microhms)	M (nanohenrys)	R _w (microhms)	M (nanohenrys)	
1 Forward End of Tip Tank	25.0	-0.0112	10.0	0.132	
4 Outboard Leading Edge	10.0	-0.00447	20.0	-0.141	
5 Trailing Edge of Aileron	12.5	-0.00559	5.0	0.0569	
7 Center of Wing Surface	30.0	-0.0134	15.0	0.0117	
10 Inboard Leading Edge	25.0	-0.0112	10.0	0.373	
<u>Conductor 2E68B20 and Airframe</u>					
1 Forward End of Tip Tank	55.0	1.71	95.0	0.372	
4 Outboard Leading Edge	22.5	2.23	42.5	0.25	
5 Trailing Edge of Aileron	50.0	1.78	55.0	0.24	
7 Center of Wing Surface	30.0	0.304	20.0	0.0598	
10 Inboard Leading Edge	65.0	-0.0291	57.0	0.349	

(Continued)

TABLE VIII (Continued)

Conductor 2E69B22 and Airframe

i _L Wave Form: Stroke Location	Slow Wave Form (36 x 82 μs)		Fast Wave Form (8.2 x 14 μs)	
	R _w (microhms)	M (nanohenrys)	R _w (microhms)	M (nanohenrys)
1 Forward End of Tip Tank	10.0	-0.00447	10.0	0.0709
4 Outboard Leading Edge	2.5	-0.00112	5.0	0.0354
5 Trailing Edge of Aileron	7.5	-0.00336	5.0	0.0354
7 Center of Wing Surface	10.0	-0.00447	7.5	0.0532
10 Inboard Leading Edge	15.0	-0.00671	5.0	-0.0228

TABLE IX. - CALCULATED EFFECTIVE WING RESISTANCES AND MUTUAL
INDUCTANCES FOR VARIOUS TEST CONDITIONS

Circuit F.0511, E-11 Autopilot
Conductors F572K18 and F755E18

i _L Wave Form: Stroke Location	Slow Wave Form (36 x 82 μs)		Fast Wave Form (8.2 x 14 μs)	
	R _w (microhms)	M (nanohenrys)	R _w (microhms)	M (nanohenrys)
1 Forward End of Tip Tank	0.75	-0.0185	4.5	-0.0698
4 Outboard Leading Edge	0.50	-0.0684	2.0	-0.187
5 Trailing Edge of Aileron	1.25	-0.0392	8.25	-0.107
7 Center of Wing Surface	0.375	-0.0169	10.0	-0.117
10 Inboard Leading Edge	2.25	-0.043	1.75	-0.0227

TABLE X. - CALCULATED EFFECTIVE WING RESISTANCES AND MUTUAL
INDUCTANCES FOR VARIOUS TEST CONDITIONS

Circuit L.050, Position Light
Conductor 2L1OE18 and Airframe

i _L Wave Form: Stroke Location	Slow Wave Form (36 x 82 μs)		Fast Wave Form (8.2 x 14 μs)	
	R _w (microhms)	M (nanohenrys)	R _w (microhms)	M (nanohenrys)
1 Forward End of Tip Tank	450.0	16.3	700.0	4.25
4 Outboard Leading Edge	57.5	0.032	70.0	0.5
5 Trailing Edge of Aileron	25.0	2.75	-100.0	1.55
7 Center of Wing Surface	45.0	1.68	- 40.0	0.244
10 Inboard Leading Edge	40.0	0.022	60.0	0.31

TABLE XI. - CALCULATED EFFECTIVE WING RESISTANCES AND MUTUAL
INDUCTANCES FOR VARIOUS TEST CONDITIONS

Circuit Q.0401, Fuel Vent Valves
Conductor 2Q331D14 and Airframe

i _L Wave Form:		Slow Wave Form (36 x 82 us)		Fast Wave Form (8.2 x 14 us)	
Stroke Location	R _w (microhms)	M (nanohenrys)	R _w (microhms)	M (nanohenrys)	
1 Forward End of Tip Tank	41.0	1.9	140.0	-0.71 * or -1.70 *	
4 Outboard Leading Edge	41.0	0.56	67.0	0.29	
5 Trailing Edge of Aileron	41.0	1.33	31.0	0.16	
7 Center of Wing Surface	61.5	1.99	36.0	0.066	
10 Inboard Leading Edge	61.5	0.034	46.0	0.33	

*Two zero-intersect times (T₁) were obtained from the measured induced voltage wave form. Hence, two values of M are obtained. The meaning of this is unclear.

TABLE XII. - CALCULATED EFFECTIVE WING RESISTANCES AND MUTUAL
INDUCTANCES FOR VARIOUS TEST CONDITIONS

Circuit Q.060, Right Wing Tank Booster Pump
Conductor 2Q78C12 and Airframe

i. Wave Form:		Slow Wave Form (36 x 82 μ s)		Fast Wave Form (8.2 x 14 μ s)	
Stroke Location	R_w (microhms)	M (nanohenrys)	R_w (microhms)	M (nanohenrys)	
1 Forward End of Tip Tank	47.5	0.86	60.5	0.12	
4 Outboard Leading Edge	45.5	0.46	55.5	0.24	
5 Trailing Edge of Aileron	45.2	0.778	-47.5	1.29	
7 Center of Wing Surface	37.5	0.89	60.0	0.36	
10 Inboard Leading Edge	30.0	0.0166	50.0	0.29	

TABLE XIII. - CALCULATED EFFECTIVE WING RESISTANCES AND MUTUAL
INDUCTANCES FOR VARIOUS TEST CONDITIONS

Circuit R.060, AN/ARN-18 Glide Path Radio Receiver
Conductor RA35C and Airframe

i _L Wave Form: Stroke Location	Slow Wave Form (36 x 82 μs)		Fast Wave Form (8.2 x 14 μs)	
	R _w (microhms)	M (nanohenrys)	R _w (microhms)	M (nanohenrys)
1 Forward End of Tip Tank	36.5	-1.82	30.0	1.39
4 Outboard Leading Edge	10.4	2.115	6.25	2.32
5 Trailing Edge of Aileron	6.25	-0.218	6.25	1.16
7 Center of Wing Surface	9.64	-0.729	-12.5	0.489
10 Inboard Leading Edge	24.7	-2.6	- 5.0	0.112

TABLE XIV. - CALCULATED EFFECTIVE WING RESISTANCES AND MUTUAL
INDUCTANCES FOR VARIOUS TEST CONDITIONS

Circuit S.220, Armament Power Supply
Conductor 2SF3886E20 and Airframe

i _L Wave Form: Stroke Location	Slow Wave Form (36 x 82 μs)		Fast Wave Form (8.2 x 14 μs)	
	R _w (microhms)	M (nanohenrys)	R _w (microhms)	M (nanohenrys)
1 Forward End of Tip Tank	0.625	-0.00028	2.5	0.0177
4 Outboard Leading Edge	0.50	-0.000224	2.5	0.0177
5 Trailing Edge of Aileron	0.75	-0.000336	0.88	0.0062
7 Center of Wing Surface	0.625	-0.00028	1.0	-0.00798
10 Inboard Leading Edge	0.50	-0.000224	0.25	0.00501

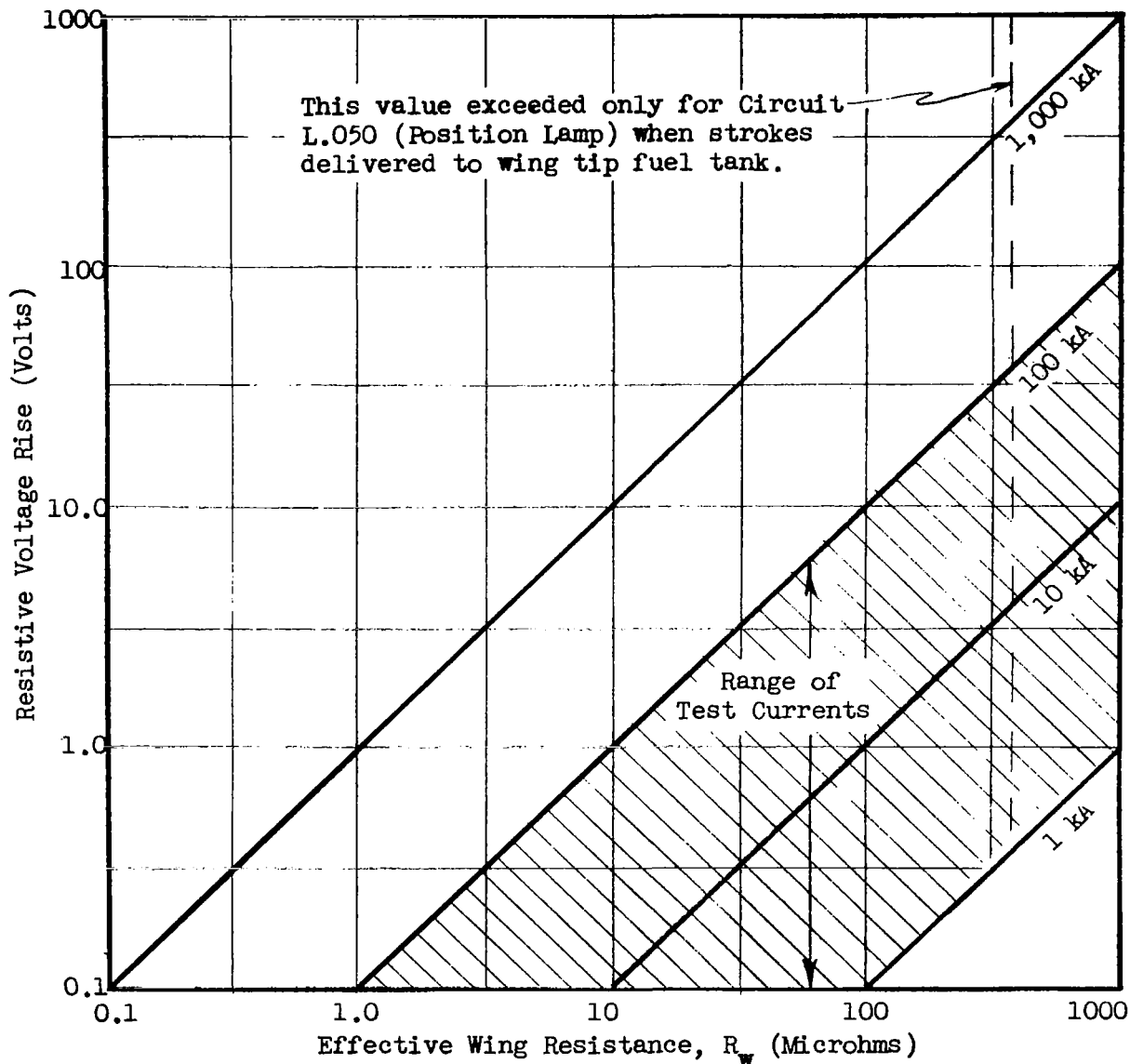


FIGURE 41. - RELATIONSHIP BETWEEN EFFECTIVE WING RESISTANCE (R_w) AND RESISTIVE VOLTAGE RISE IN ELECTRICAL CIRCUIT USING AIRFRAME AS RETURN PATH, FOR VARIOUS LIGHTNING CURRENT AMPLITUDES.

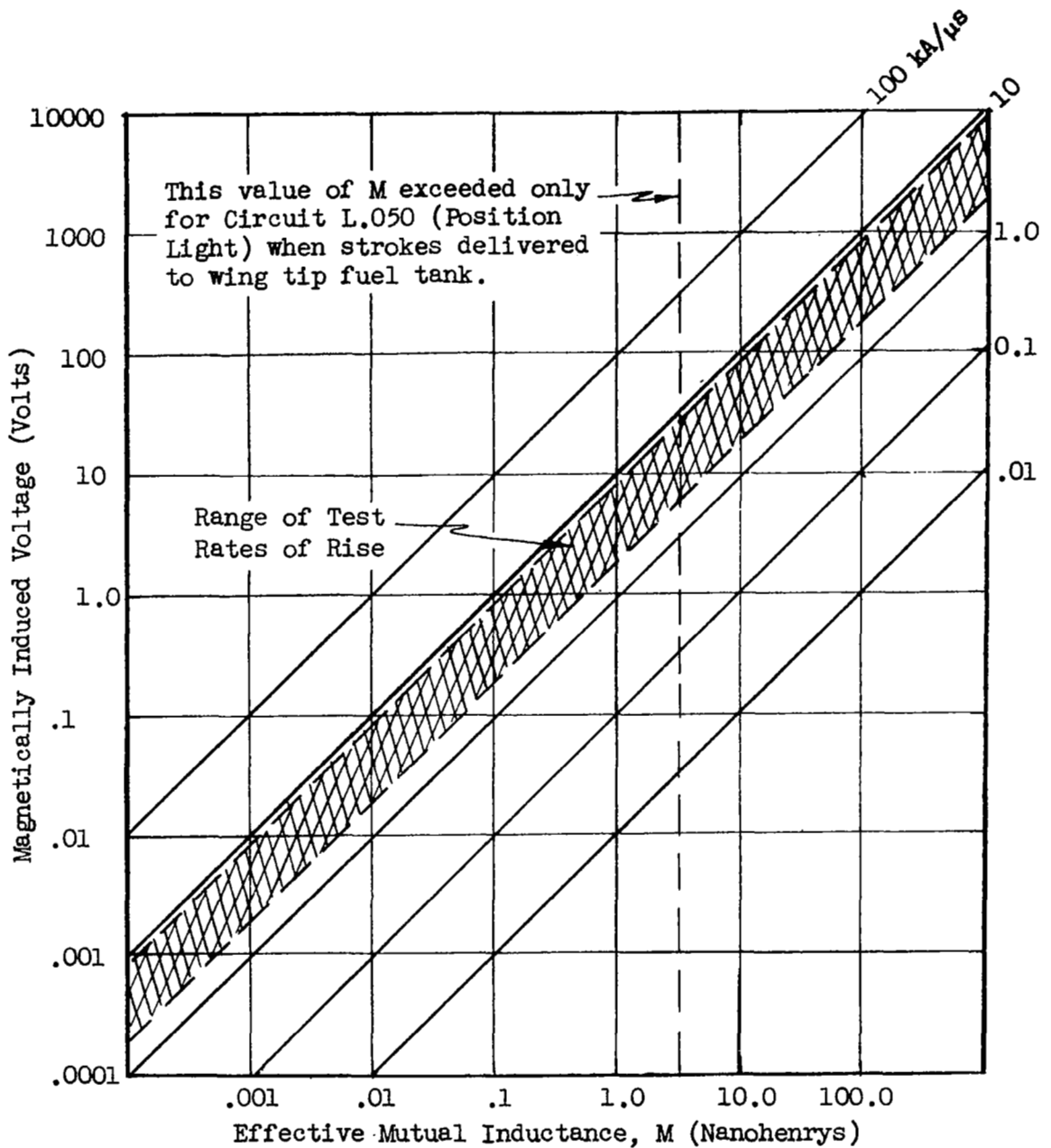


FIGURE 42. - RELATIONSHIP BETWEEN EFFECTIVE MUTUAL INDUCTANCE (M) AND MAGNETICALLY INDUCED VOLTAGE IN WING ELECTRICAL CIRCUIT FOR VARIOUS RATES OF LIGHTNING CURRENT RISE (di/dt).

Thevenin Impedance, Z_T

As described earlier in this report, measurements were made of both the open-circuit voltages, e_{oc} , and short-circuit currents, i_{sc} , so that sufficient data would be available from which to calculate the Thevenin impedance, Z_T , by:

$$Z_T = \frac{e_{oc}}{i_{sc}} = \frac{e_T}{i_{sc}} \quad (9)$$

The calculations were made by first writing mathematical expressions for both e_{oc} and i_{sc} . The expression for e_{oc} is equation (1) derived previously for the Thevenin voltage. An approximate mathematical expression for the short-circuit currents, i_{sc} , was obtained from the oscillogram using standard curve-fitting techniques. Calculation of the impedance Z_T then proceeded. The procedure used is illustrated by the following example, in which the Thevenin impedance of the glide path antenna circuit (R.060) with the antenna coupling capacitor shorted will be calculated, for an 8.2 x 14 μ s stroke delivered to location 1.

The equation for e_T has been written as

$$e_T = e_{oc} = R_w i_L + M \frac{di_L}{dt} \quad (1)$$

For these test conditions, i_L , R_w and M are as follows:

$$i_L \approx (40 \times 10^3) \sin (0.2 \times 10^6 t) \text{ amperes (from Figure 38)} \\ (t \leq 18 \times 10^{-6} \text{ seconds})$$

$$R_w = 30 \times 10^{-6} \text{ ohms} \quad (\text{from Table XIII})$$

$$M = 1.39 \times 10^{-9} \text{ henrys} \quad (\text{from Table XIII})$$

Substitution of these quantities into (1) and simplification gives:

$$e_{oc} = 1.2 \sin (0.2 \times 10^6 t) + 11.1 \cos (0.2 \times 10^6 t) \quad (10)$$

From the oscillogram of Figure 43,

$$i_{sc} \approx 19 \sin (0.2 \times 10^6 t) \quad (11)$$

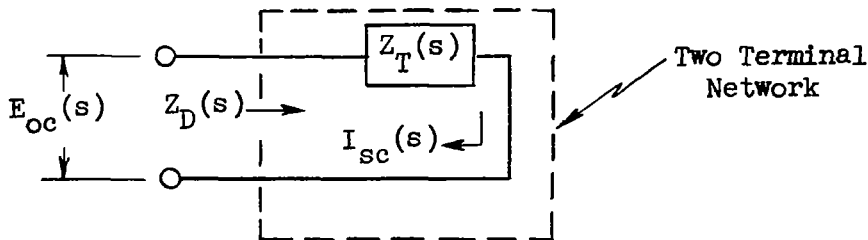
($t \leq 18 \mu s$)

The problem is next transformed into the complex frequency domain, where it can be viewed as a problem in passive network synthesis, where,

$$Z_T(s) = \frac{E_{oc}(s)}{I_{sc}(s)} \quad (12)$$

where s is the Laplace operator

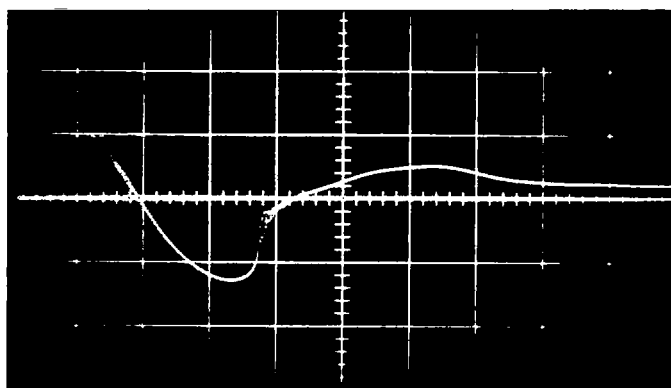
with the circuit output terminals shorted. In this case, $Z_T(s)$ can be considered as $Z_D(s)$, the driving point impedance function of a two-terminal network.



Rewriting equations (10) and (11) in the complex frequency domain,

$$E_{oc}(s) = \frac{0.2 \times 10^6}{s^2 + (0.2 \times 10^6)^2} + \frac{11.1s}{s^2 + (0.2 \times 10^6)^2} \quad (13)$$

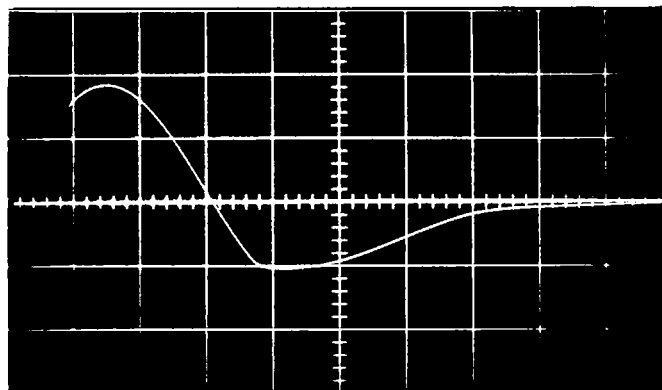
Open Circuit Voltage, e_{oc}



5 volts/Div.

5 μ s/Div.

Short Circuit Current, i_{sc}



10 volts/Div.

5 μ s/Div.

FIGURE 43. - OPEN CIRCUIT INDUCED VOLTAGE AND SHORT CIRCUIT CURRENT MEASURED IN CIRCUIT R.060 (GLIDE PATH ANTENNA - COUPLING CAPACITOR SHORTED)

$$E_{oc}(s) = \frac{11.1s + 0.2 \times 10^6}{s^2 + (0.2 \times 10^6)^2} \quad (14)$$

and

$$I_{sc}(s) = \frac{3.80 \times 10^6}{s^2 + (0.2 \times 10^6)^2} \quad (15)$$

Therefore

$$Z_D(s) = \frac{E_{oc}(s)}{I_{sc}(s)} = \frac{11.1s + 0.2 \times 10^6}{3.80 \times 10^6} \quad (16)$$

$$= 2.92 \times 10^{-6}s + .0632 \quad (17)$$

which can be considered as a series R-L network such that

$$Z_D(s) = Ls + R = Z_T(s) \quad (18)$$

where, from (17),

$$L = 2.92 \text{ microhenrys}$$

$$R = 0.0632 \text{ ohm}$$

which are the series inductance and resistance of the Thevenin impedance, Z_T .

This process was repeated with the use of the digital computer for other test conditions applied to this circuit. Calculations of the R and L components for nearly all test conditions were possible. The few cases in which solutions were not possible are apparently the result of anomalies in the measured e_{oc} or i_{sc} oscillograms, attributable to loose connectors, etc. in the aircraft circuits.

Under some test conditions, an adequate mathematical description of i_{sc} could not be obtained. In these cases, a graphical approach was used, in which the measured e_{oc} and i_{sc} wave forms were plotted graphically, and

values of R and L were obtained by dividing the ordinate of the e_{oc} wave form by that of the i_{sc} wave form at discrete times, derived as follows:

Since

$$e_{oc} = R i_{sc} + L \frac{di_{sc}}{dt} \quad (19)$$

then, at a time $t = t_0$ when

$$\frac{di_{sc}}{dt} = 0 \quad (20)$$

$$R = \left. \frac{e_{oc}}{i_{sc}} \right|_{t = t_0} \quad (21)$$

Also, at time $t = t_1$ when

$$e_{oc} = 0 \quad (22)$$

Then

$$L = - \left. \frac{R i_{sc}}{\frac{di_{sc}}{dt}} \right|_{t = t_1} \quad (23)$$

where R is the value obtained from (21). For several circuits $\frac{di_{sc}}{dt}$ is zero at more than one value of t. In these cases, R was calculated at each value of t and then averaged. The calculated values of R and L for circuit R.060 under all test conditions are listed in Table XV.

As was noted earlier, measurements of i_{sc} in some circuits were not possible because these circuits had very high impedance or open-ended terminations within the wing. In such cases, while a voltage, e_{oc} , was measured, no short-circuit currents above the sensitivity of the measurement system (about 10 milliamperes) could be detected. As a result, calculations

of Z_T were not possible. This indicates, however, that these circuits would deliver little or no current to such finite load impedances as would be associated with most avionics equipment, to which the circuits might be connected. As a result, little chance of damage would be expected to occur in this equipment. The circuits for which measurements of i_{sc} and calculations of Z_T were possible included:

R.060 (Glide Path Antenna - with coupling capacitor shorted only)

L.050 (Position Light)

Q.060 (Right Wing Tank Booster Pumps)

Calculations of Z_T for circuit L.050 were performed using the same techniques as outlined above. The series R and L components of Z_T for the various test conditions are listed in Table XVI.

In the case of circuit Q.060 (Right Wing Tank Booster Pump), many of the measured voltages, e_{oc} , were nearly unidirectional. As a result, accurate definition of the times, t_2 , at which the e_{oc} wave forms intersected the zero line, and subsequent calculations of reliable values of R_w and M , were not always possible. The result was that some expressions obtained for e_{oc} did not approximate the measured wave form of e_{oc} closely enough to permit accurate calculation of Z_T . In these cases, an alternate approach was applied, in which an equation for the e_{oc} wave form was obtained by standard curve-fitting techniques.

Examples of the e_{oc} and i_{sc} measurements obtained from circuit Q.060, for a 40-kiloampere $36 \times 82 \mu s$ lightning current delivered to location 1, are shown in Figure 44. These wave shapes are plotted together on Figure 45, along with the wave shapes of the mathematical expressions arrived at for approximation. These expressions are:

$$e_{oc} = 0.75 + 1.2 \sin(0.0392t) \quad (24)$$

$$i_{sc} = 1.38e^{-0.025t} \left(\sin(0.0785t \times 10^{-6}) + 0.33 \sin(0.275t \times 10^{-6}) \right) \quad (25)$$

Since these are time-varying functions, transformation into the complex frequency domain yields

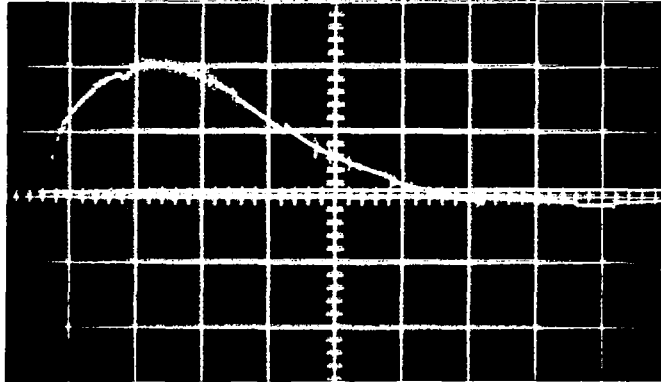
$$E_{oc}(s) = \frac{0.75 (s^2 + 0.0627s + 0.00154)}{s(s^2 + 0.00154)} \quad (26)$$

$$I_{sc}(s) = \frac{0.235 (s^2 + 0.0362s + 0.0281)}{(s^2 + 0.05s + 0.00683) (s^2 + 0.05s + 0.076)} \quad (27)$$

from which the driving point impedance function $Z_D(s)$ can be found as stated earlier. Once this impedance function is obtained, a suitable network for Z_T can be found using the principles and methods of passive network synthesis.

Because the expression obtained for $Z_D(s)$ from (26) and (27) will have complex roots, it becomes apparent that the network involved is one containing elements of resistance, inductance and capacitance. The techniques available for two-terminal R-L-C network synthesis are those of (1) Brune, and (2) Bott and Duffin (ref. 10). Since each Brune cycle ultimately requires the use of a transformer, the most useful technique to apply in the present analysis would be the Bott-Duffin. For the circuit under consideration (Q.060) a network for Z_T was not actually obtained since the process would be quite involved. This circuit is known to have a radio noise filter in it, which in fact has both inductance and capacitance elements in it. For the present investigations, the investment of time to obtain a complex solution to this circuit was not warranted. The techniques are available, should it be desirable to pursue this synthesis in the future.

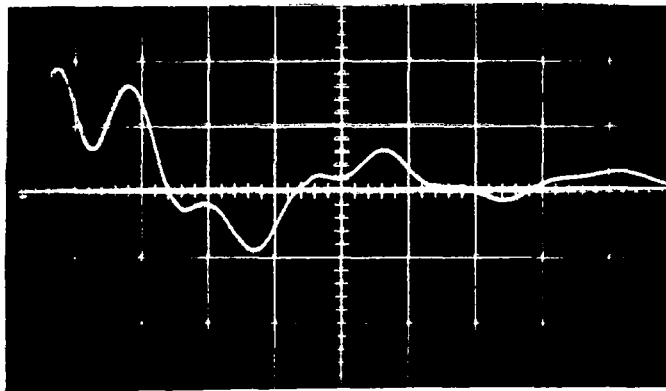
Open Circuit Voltage, e_{oc}



1 volt /Div.

20 μ s/Div.

Short Circuit Current, i_{sc}



0.5 amp/Div.

20 μ s/Div.

FIGURE 44. - OPEN CIRCUIT VOLTAGE AND SHORT CIRCUIT CURRENT MEASURED BETWEEN CONDUCTOR 2Q78C12 AND AIRFRAME. 40 KILOAMPERE, 36 x 82 μ s LIGHTNING CURRENT APPLIED TO LOCATION 1. CIRCUIT Q.060 (RIGHT WING TANK BOOSTER PUMP).

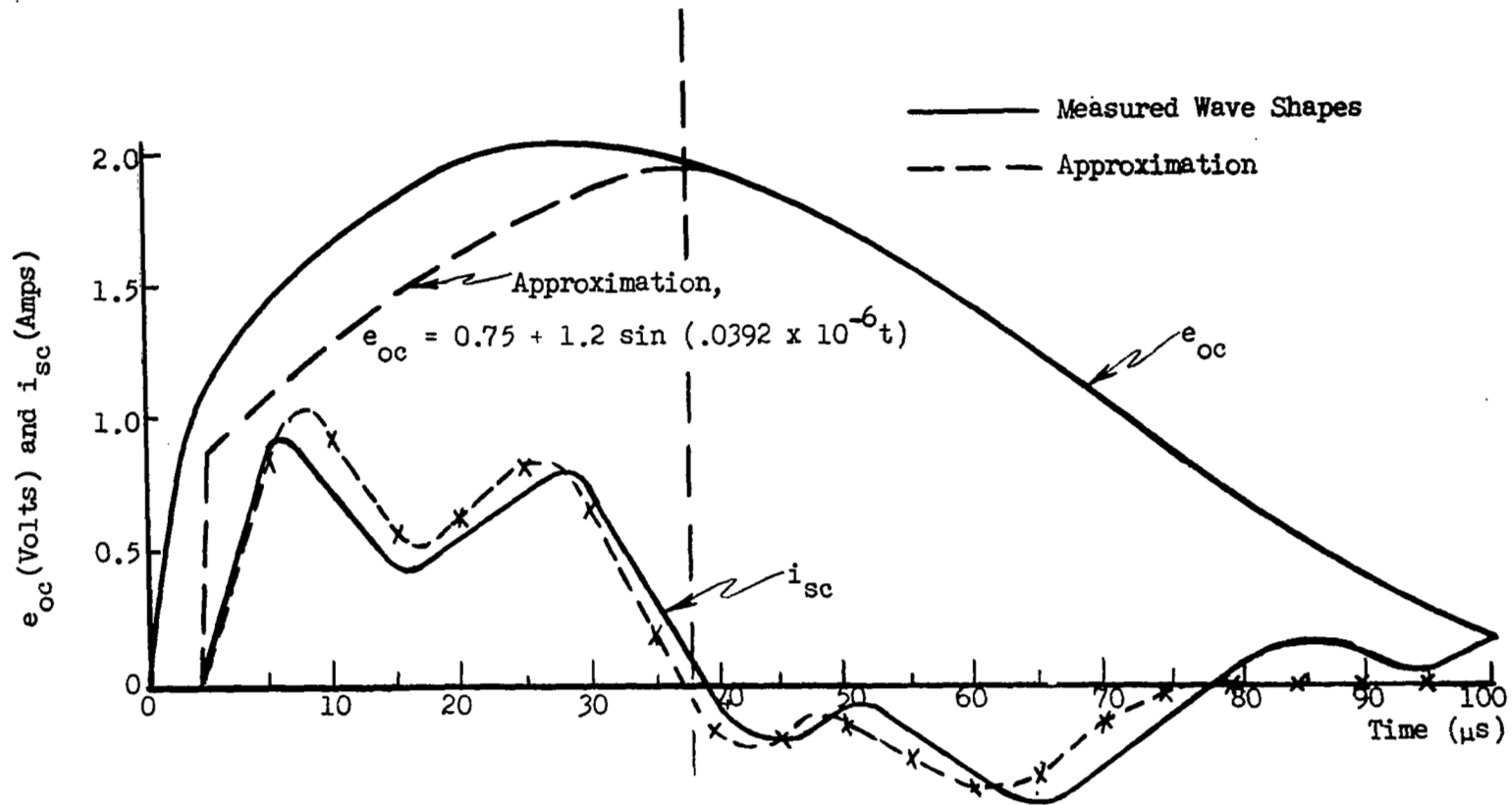


FIGURE 45. - WAVE SHAPES OF MEASURED OPEN CIRCUIT VOLTAGE, e_{oc} , AND SHORT CIRCUIT CURRENT, i_{sc} , OBTAINED FROM FIGURE 44, TOGETHER WITH MATHEMATICAL APPROXIMATIONS. CIRCUIT Q.060 (RIGHT WING TANK BOOSTER PUMP).

TABLE XV. - CALCULATED THEVENIN IMPEDANCE SERIES R AND L COMPONENTS FOR VARIOUS TEST CONDITIONS
 Circuit R.060, Glide Path Radio Receiver
 Conductor RA35C and Airframe
 (Note: Coupling Capacitor Shorted)

Lightning Current Wave Shape:	8.2 x 14 μ s		36 x 82 μ s	
Stroke Location	R (ohms)	L (microhenrys)	R (ohms)	L (microhenrys)
1 Forward End of Tip Tank	0.0632	2.92	--	--
4 Outboard Leading Edge	0.1956	2.25	0.2	2.03
5 Trailing Edge of Aileron	0.377	3.14	0.12	0.62
7 Center of Wing Surface	0.131	2.33	0.164	--
10 Inboard Leading Edge	--	--	0.491	--

TABLE XVI. - CALCULATED THEVENIN IMPEDANCE SERIES R AND L COMPONENTS FOR VARIOUS TEST CONDITIONS
 Circuit L.050, Position Light
 Conductor 2L10E18 and Airframe

Lightning Current Wave Shape:	8.2 x 14 μ s		36 x 82 μ s	
	R (ohms)	L (microhenrys)	R (ohms)	L (microhenrys)
1 Forward End of Tip Tank	1.98	11.2	--	--
4 Outboard Leading Edge	3.33	0.39	2.65	-7.8
5 Trailing Edge of Aileron	1.23	8.0	2.3	36.2
7 Center of Wing Surface	--	--	2.63	8.37
10 Inboard Leading Edge	3.09	5.7	2.29	9.56

Characteristics of Z_T

Tables XV and XVI show that there is some variation in Z_T as a function of stroke location and lightning current wave shape; however, the variation is not as great as was the variation in calculated values of R_w and M for identical sets of test conditions. It is possible that some or all of the variations in Z_T are simply the result of slight experimental inconsistencies or analytical imperfections. Such a conclusion is possible because the values of R and L generated seem to approximate the actual characteristics of the particular wing circuits. For example, the resistances calculated for circuit R.060 are all very low, as would be expected from a circuit connected directly (through the shorted coupling capacitor) to the airframe. The variations obtained may only be the result of a poor connection through the shorted coupling capacitor. Similarly, the values of inductance (2 - 3 microhenrys) are the same order of magnitude as might be expected for a coaxial cable circuit the length of R.060 (17 feet).

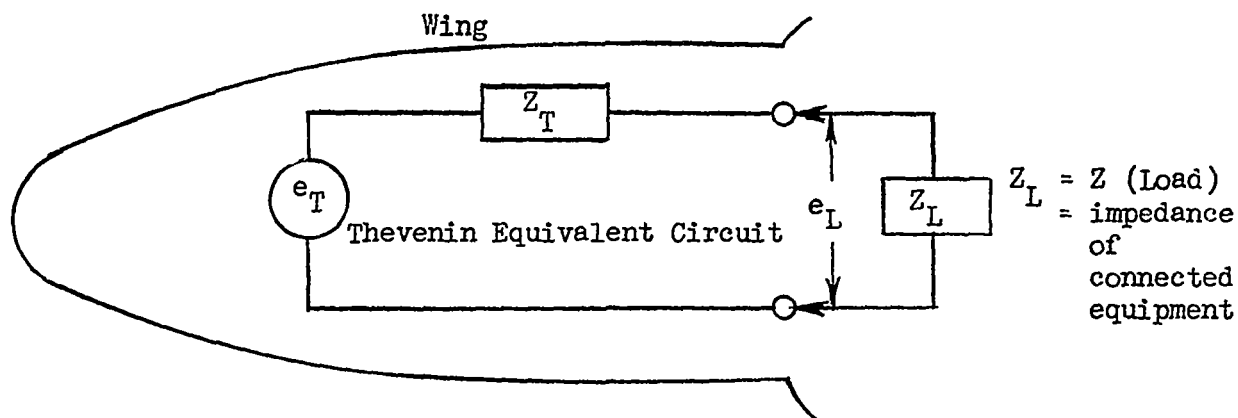
For the position light circuit (L.050), values of resistance between 1.23 and 3.09 ohms were calculated. These compare favorably with the resistance of the light bulb, which was 2.5 ohms. The inductances calculated for this circuit, which extends longer than the antenna circuit, are larger.

Finally, the impedance Z_T for the booster pump circuit (Q.060), while not fully defined, does appear to be a combination of R , L and C elements. Such is actually the case, since the circuit possesses an RFI filter which has all of these elements.

Further study may uncover more definite relationships than these; however, it does appear that the Thevenin impedances closely approximate the actual impedances already existing in the wing circuits. If this is the case, the problem of determining the impedances of other aircraft circuits would be simplified.

Voltages Across Circuit Load Impedances

Once the Thevenin equivalent circuits have been defined, they may be used to calculate the amount of voltage which would be impressed upon any connected loads (avionics equipment, etc.), the terminal impedances of which are known, by:



$$e_L = \frac{Z_L}{Z_L + Z_T} e_T \quad (28)$$

No attempt was made in this program to identify or simulate the impedances of the equipment to which each wing circuit was connected; however, actual measurements were made in most cases of the voltages arising across 1-ohm resistive loads connected to the wing circuits. These measurements were made to verify the reliability of the measurements system, as previously described, and also to confirm the Thevenin equivalent circuit method of calculating the load voltage, by comparison with actual measurements of voltages across a known load. An example of this confirmation is now presented.

Using the Thevenin equivalent circuit of the example described on Page 123 (circuit R.060), the voltage appearing across a 1-ohm resistive load, Z_L , will be calculated as follows:

The expression for e_T in the complex frequency domain is, from equation (14),

$$E_T(s) = E_{oc}(s) = \frac{11.1s + 0.2 \times 10^6}{s^2 + (0.2 \times 10^6)^2} \quad (29)$$

From equation (17), the expression for $Z_T(s)$ is,

$$Z_T(s) = Z_D(s) = 2.92 \times 10^{-6}s + 0.0632 \quad (30)$$

In this example, the load impedance Z_L is one ohm of resistance; thus,

$$Z_L(s) = 1 \quad (31)$$

The voltage e_L across load Z_L is obtained by substituting (29), (30) and (31) into equation (28) as follows:

$$E_L(s) = \left(\frac{1}{2.92 \times 10^{-6}s + 1.0632} \right) \left(\frac{11.1s + 0.2 \times 10^6}{s^2 + (0.2 \times 10^6)^2} \right) \quad (32)$$

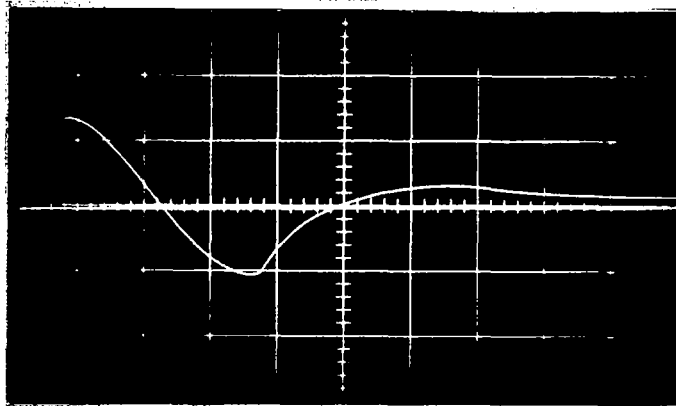
which, when simplified and expressed in the time domain yields,

$$e_L = 9.8 \left(\cos (0.2 \times 10^6 t) - e^{-0.364 \times 10^6 t} \right) + 1.13 \sin (0.2 \times 10^6 t) \quad (33)$$

The wave form described by this equation is plotted on Figure 46(b), together with the wave form of the voltage actually measured across the 1-ohm resistor, taken from the oscillogram of Figure 46(a). It is evident that the amplitude and wave shape of the voltage e_L calculated from the Thevenin equivalent circuit compare favorably with those of the measured voltage.

This example verifies that the Thevenin equivalent circuit is in fact a valid means of determining the voltage which would arise across the input

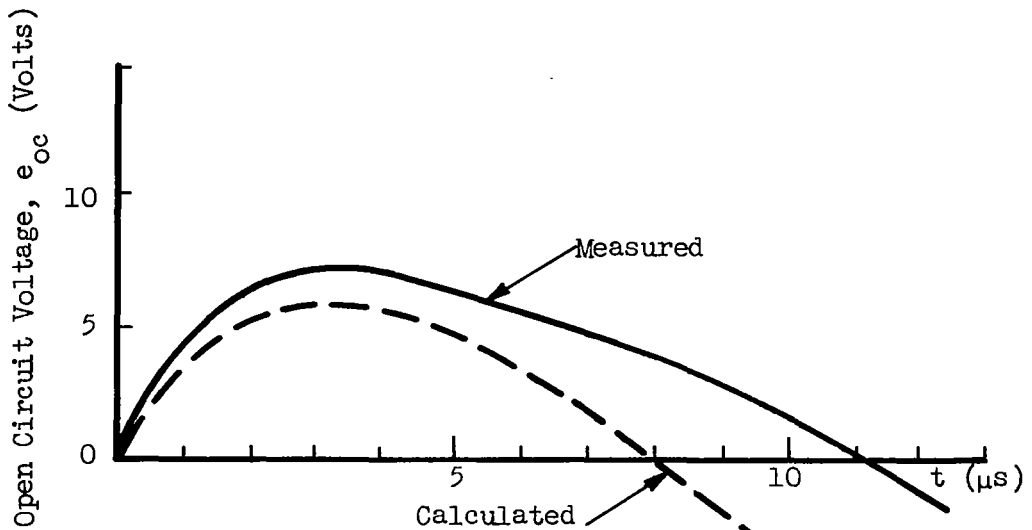
impedance of a piece of avionic equipment. The degree of accuracy associated with this technique is of course dependent upon the authenticity of the previously determined Thevenin circuit parameters. The Thevenin circuits derived in this investigation are comparatively simple circuits, the synthesis of which was straightforward. It should be realized, however, that these circuits are in fact simplified approximations of highly complex circuits. Thus, care should be taken not to attach undue significance to the Thevenin circuit parameters themselves. In particular, the same significance given the Thevenin impedance, Z_T , should not be given the R_L and M quantities in equation (1) for the Thevenin voltage, e_T . While Z_T does appear to simply represent the actual wing circuit impedances, analysis has not proceeded to the point of being able to relate the parameters R_L and M to tangible wing (or lightning) characteristics. The value of the Thevenin circuit is therefore its usefulness as a means of determining the approximate level of lightning induced voltages which a wing circuit would impress upon various load impedances.



5 volts/Div.

5 μ s/Div.

(a) Voltage measured across 1-ohm resistive load.



(b) Comparison of measured load voltage from (a) with load voltage calculated by Thevenin equivalent circuit

FIGURE 46. - VERIFICATION OF THEVENIN CIRCUIT CALCULATION OF VOLTAGE ACROSS 1-OHM RESISTIVE LOAD. CIRCUIT R.060 (GLIDE PATH RADIO ANTENNA). 40 KILOAMPERE, $8.2 \times 14 \mu$ s LIGHTNING CURRENT TO LOCATION 1.

CONCLUDING DISCUSSION

This research program was based on measurement of the voltages induced in electrical circuits within an aircraft wing by lightning currents flowing through its skin and structural members. The measured voltages were then subjected to analysis, from which equivalent circuits were derived for use in determining the amount of induced voltage which would be applied to aircraft loads to which the circuits may be connected.

Conclusions derived from this program which are associated with particular wing circuits or test conditions have been included when warranted in the preceding discussions. However, some general conclusions pertaining to the investigation as a whole are now discussed.

Voltages Induced by Lightning

It has been found that lightning currents flowing through a metallic aircraft structure can cause transient voltages to appear in electrical circuits within the structure. These voltages are a combination of a resistive voltage rise caused by lightning currents passing through the finite resistance of the aircraft structure, and a magnetically induced voltage arising in the electrical circuit as a result of linkage of magnetic flux created by the lightning current. In nearly all cases this voltage, appearing across the open-circuit terminals of the circuit, could be expressed as a mathematical combination of these two voltage components, where each in turn is expressible as a function of the lightning current itself, as follows:

$$e_{oc} = R_w i_L + M \frac{di_L}{dt}$$

where:

e_{oc} = voltage appearing across open wing circuit terminals at root of wing

R_w = an effective wing (structure) resistance

M = an effective mutual inductance between
the lightning current and the particular
wing electrical circuit

i_L = lightning current (a time-varying function)

Because the induced voltages are dependent upon the lightning current, they vary considerably in amplitude and wave shape according to the lightning current parameters of wave shape and amplitude. Induced voltages are also dependent upon the characteristics of the circuit in which they are measured, and the location at which the lightning stroke attaches to the wing.

Simulated lightning currents of 40 kiloamperes were used for most of these tests, with wave shapes resulting in rates of current rise, to which the magnetically induced voltage is proportional, of between 2 and 8 kiloamperes per microsecond. These currents resulted in induced voltages of between several millivolts and one hundred volts, depending upon the particular circuit and test conditions applied. Initially, it may appear that transient overvoltages of 100 volts or less may not be damaging to avionics equipment to which the wing circuits are connected, particularly since only a portion of the total voltage induced in the circuit can actually arise across the input impedance of the equipment in question. It is not possible to compare these voltages with known equipment withstand levels, however, since there exist no universal lightning induced transient voltage withstand requirements for aircraft electronic equipment. Such aircraft manufacturers' specifications as do exist (ref. 11) apply only to aircraft power circuits and generally require that transient overvoltages of up to 600 volts be withstood by these circuits and connected equipment. These specifications are intended to assure that the equipment will be undamaged by aircraft power system transients resulting from system switching operations or other sources within the aircraft power system. As such, they are not considered as applying to other circuits interconnecting

various equipment within the aircraft. Voltages induced in some of these other circuits, which operate at the very low signal voltage levels characteristic of solid-state devices, may damage or interfere with the operation of such equipment to a considerably greater extent than would similar voltages induced in the circuit supplying aircraft power to the equipment, to which the power system transient overvoltage requirements apply. The transient overvoltage withstand capability of most avionics equipment is unknown; however, the frequent reports of interference or malfunctions of avionics equipment while an aircraft is within a thunderstorm environment suggest that such equipment is susceptible to induced voltages as a result of lightning currents flowing through the aircraft.

Taken in perspective, the results of this investigation indicate that voltages induced in similar circuits of other aircraft are likely to be greater than those measured in this investigation. The lightning current amplitudes and rates of current rise applied for most of these measurements, for example, are those of more moderate strokes when compared with the range of similar characteristics of lightning strokes to ground, as shown on Figures 47 and 48. While considerably less is known of the characteristics of cloud-to-cloud lightning strokes, aircraft may be struck by either type of stroke, and it is apparent that strokes of considerably greater magnitude than those simulated in this program may pass through an aircraft. From knowledge of the relationship between lightning current and induced voltage learned from this investigation, increases in stroke current amplitude and rate of rise will result in corresponding increases in the resistive and magnetically induced components, respectively, of voltages induced in aircraft circuits. From a study of Figures 47 and 48 it is evident that natural lightning may induce voltages several times greater than those induced by the simulated strokes used in this investigation. Further, when comparing the voltages induced in circuits within the F89J wing with those which might appear in other aircraft, the relative size of the wings, as

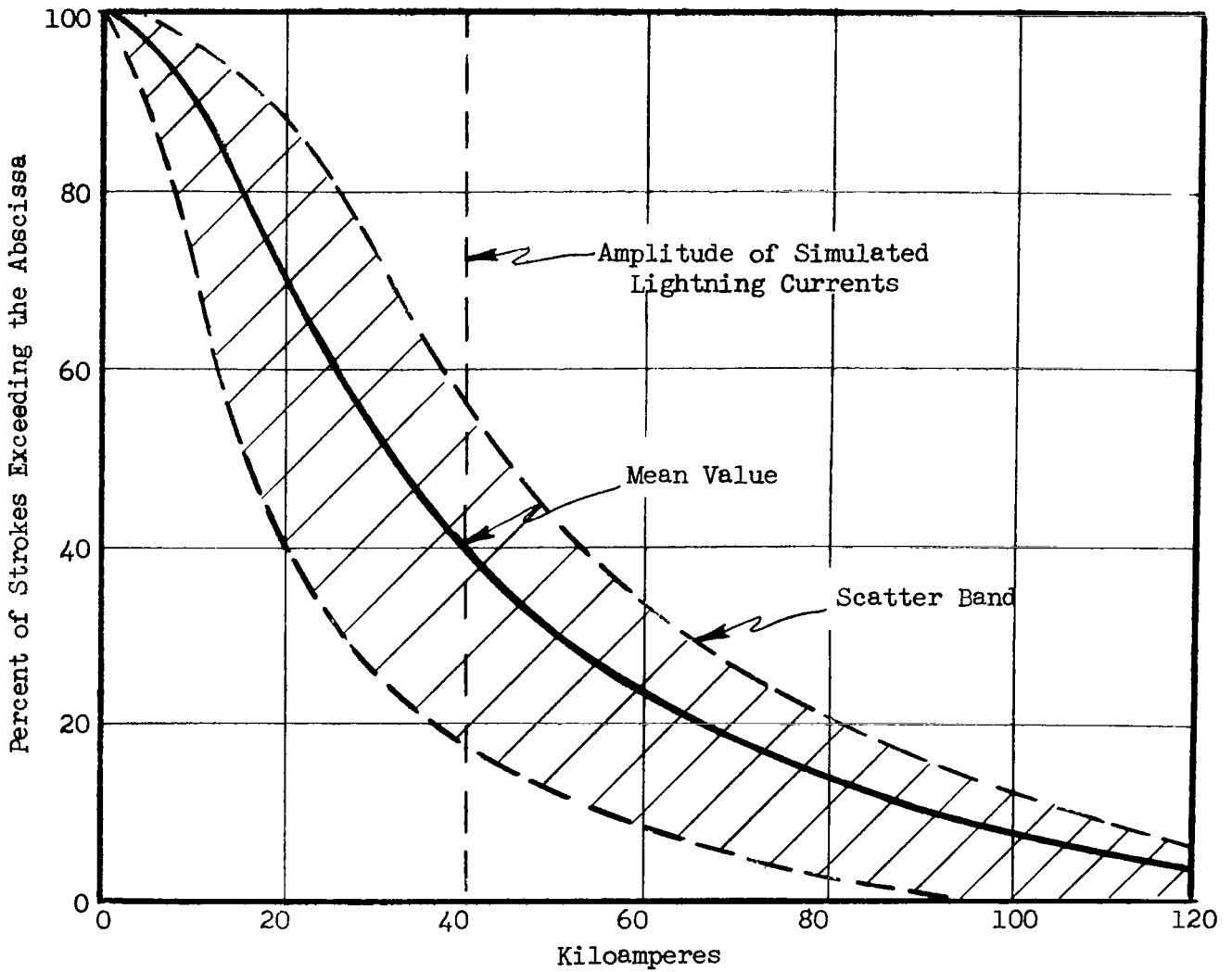


FIGURE 47. - PROBABILITY DISTRIBUTION OF LIGHTNING STROKE PEAK VALUES
 (From Bibliography - General Lightning Characteristics)

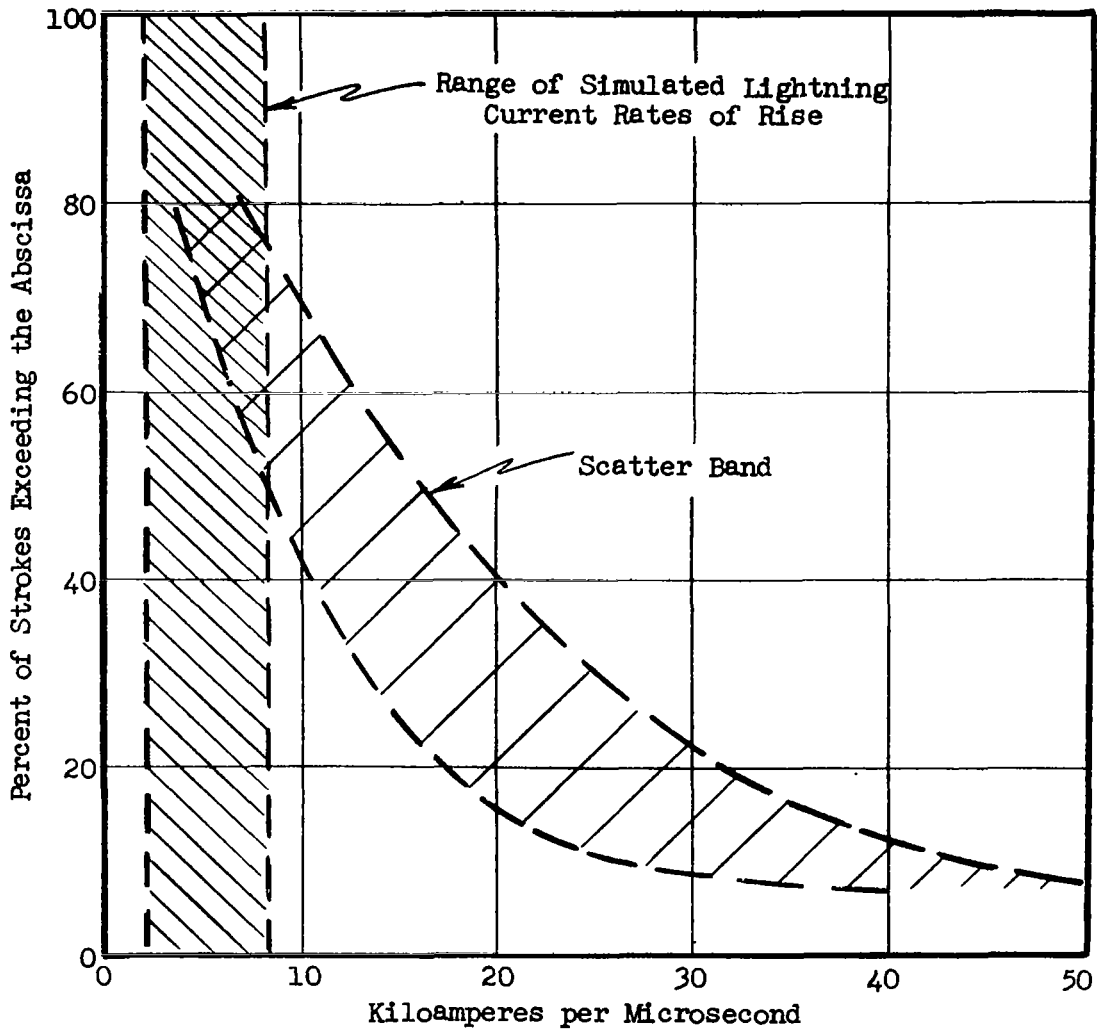


FIGURE 48. - PROBABILITY DISTRIBUTION OF LIGHTNING STROKE RATES OR RISE
 (From Bibliography - General Lightning Characteristics)

well as thickness of their skins, must be considered. The F89J wing, with a 26-foot length, is considerably shorter than similar dimensions of modern jet transport aircraft. Since the greatest voltages measured in this investigation appeared in the longest circuits, it is probable that circuits extending the length of longer wings would receive greater induced voltages than those measured in the F89J. The extent to which the thickness of wing skin is related to the level of induced voltages in circuits within could not be evaluated in this program; however, skin thickness is known to be significant in determining the electromagnetic shielding effectiveness of other enclosures. Generally, the thicker the skin the greater the shielding effectiveness. It should thus be noted that the skin plating of the F89J ranged in thickness from 50 to over 250 mils, which in some cases is greater than corresponding thicknesses on other aircraft. The F89J is also an all-metallic aircraft, and there are no panels or sections covered with nonmetallic materials, as is the case in some aircraft of more modern design. It should also be realized that the resistive voltage component was kept comparatively low in circuits within this wing due to the very low resistance of the metallic skin and structure. If similar circuits were utilized in an aircraft constructed of the poor conducting composite material, the resulting resistive voltage rises may be many orders of magnitude greater. These materials would also have considerably less magnetic shielding ability, which would result in increases in the magnetically induced component as well.

Circuit Characteristics

Considerable variation was evident in voltages induced in the various circuits. An identical lightning stroke could induce up to 100 volts in some circuits, while only a few millivolts in others. The characteristics of the circuits which received the greatest and the least induced voltages are therefore of interest. In general these characteristics can be summarized as follows:

Circuit Characteristics:	Circuit Return Path	Circuit Termination (Within Wing)	Shielding	Routing	Length
Highest voltages	Use airframe as return	Through low impedance component to airframe	Unshielded and exposed to outside of wing	Exposed to outside and routed across joints to mechanically attached assemblies	Extending through full length of wing
Lowest voltages	Use separate conductor as return	Through high impedance element to separate return conductor	Shielded and completely enclosed by wing	Unexposed and entirely within wing enclosure	Extending only short distances in wing

Particular relations and characteristics are discussed in detail in the report. From the above summary, it is apparent, however, that the level of lightning induced voltages is considerably dependent upon the characteristics of the individual circuits. As a result, rearrangement or modification in aircraft electrical circuits where possible in the light of the above findings may be an effective means of minimizing the effects of lightning on aircraft electrical systems.

Analytical Method

The method of analysis of data utilized in this program has proven to be effective as a means of determining the amount of open-circuit induced voltage actually impressed upon a load impedance to which the circuit is connected, provided reliable open-circuit and short-circuit measurements can be made. Of equal or greater significance, however, is the

ability to analytically relate, in nearly all cases, the measured induced voltages to the lightning current wave shape and amplitude, as well as some effective wing parameters. While the effective wing parameters of resistance (R_w) and mutual inductance (M) have yet to be expressed in terms of tangible wing characteristics, they do shed light upon the qualitative effects of these electrical characteristics of the wing. These relationships enable greater understanding of the factors permitting lightning to induce significant voltages in aircraft electrical circuits.

Measurement of Induced Voltages in Operational Aircraft

During this program, a series of tests were made in which the transient analyzer was utilized to provide low-amplitude nondestructive current surges to the wing. The transient analyzer is a device developed by the High Voltage Laboratory for similar transient response studies of large power transformers. In this series of tests, the induced voltage response to low-level currents from the transient analyzer was compared with similar measurements of voltages induced by full-scale lightning currents. The comparison was favorable, indicating that the results of low-level tests can be scaled proportionately upward to determine the results obtainable from full-scale lightning currents.

These tests indicated that the transient analyzer has validity as a method of determining induced voltage levels in aircraft circuits. In fact, it has several advantages over the full-scale technique. Aside from being physically portable, it has an electrical versatility lacked by most full-scale impulse generators, and can generate a much wider range of wave shapes. For example, it can generate currents with rise times many times faster than those obtainable with a full-scale impulse generator. This will enable evaluation of induced voltages resulting from a much wider range of lightning current wave shapes than possible with full-scale tests.

A system analysis technique such as this is theoretically valid as long as the system electrical characteristics are linear. This will be

true for an essentially nonsaturable (nonferrous) system like an aircraft as long as the patterns of lightning current flow are identical throughout the range of current amplitudes in question. This was apparently so for the F89J wing, and can be expected to be so unless arcing contacts occur somewhere in the structure, which would render the path of full-scale current flow different from that at reduced levels. In some aircraft this may be a possibility; however, careful study of the physical system before performance of transient analysis tests should enable appropriate identification of this possibility.

Thus, this practical and nondestructive technique may be applicable to the determination of possible induced voltages in the circuits of operational aircraft. In such a case, the actual voltages and currents associated with the normal aircraft equipment would be measurable, since this equipment would of course already be connected to the circuits.

APPENDIX

This section includes tables of all test results not otherwise specifically tabulated in the text of this report. All measurements made on a particular circuit are tabulated together, and the tables are arranged in the order in which the circuits have been discussed in the text.

The numerical values listed in the tables are the peak or maximum values reached by a particular induced voltage or current wave. In some cases, two values are given in the form, X/Y. In this case the quantity (X) above the line is the maximum amplitude of the high-frequency oscillations sometimes superimposed on the initial part of the measured induced voltage wave form. The number below the line (Y) is the maximum amplitude of the induced voltage or current wave form itself.

All measurements tabulated have been the result of simulated lightning strokes with amplitudes of 40 kiloamperes, unless otherwise noted in the table.

TABLE XVII. - MAXIMUM AMPLITUDES OF MEASURED INDUCED VOLTAGES AND CURRENTS

Circuit A.140, Right Armament Jettison

Conductor 2A925G16 and Airframe

(Note: Pylon not attached)

i_L Wave Form:		Slow Wave Form (36 x 82 μ s)			Fast Wave Form (8.2 x 14 μ s)			
Stroke Location	Open Circuit Voltage, e_{oc} (volts)	Short Circuit Current, i_{sc} (amps)	Voltage Across 1-ohm Load, e_L (volts)	Current Through 1-ohm Load, i_L (amps)	Open Circuit Voltage, e_{oc} (volts)	Short Circuit Current, i_{sc} (amps)	Voltage Across 1-ohm Load, e_L (volts)	Current Through 1-ohm Load, i_L (amps)
1 Forward End of Tip Tank	0.5	0	---	---	0.9	0	---	---
4 Outboard Leading Edge	0.58	0	---	---	0.78	0	---	---
5 Trailing Edge of Aileron	0.55	0	---	---	0.64	0	---	---
7 Center of Wing Surface	0.5	0	---	---	0.75	0	---	---
10 Inboard Leading Edge	0.7	0	---	---	1.0	0	---	---

(Continued)

TABLE XVII (Continued)

Circuit A.140, Right Armament Jettison
 Conductor 2A925G16 and Airframe
 Pylon attached

Jettison safety relay de-energized - explosive bolt not in circuit

i_L Wave Form:		Slow Wave Form (36 x 82 μ s)				Fast Wave Form (8.2 x 14 μ s)			
Stroke Location	Open Circuit Voltage, e_{oc} (volts)	Short Circuit Current, i_{sc} (amps)	Voltage Across 1-ohm Load, e_L (volts)	Current Through 1-ohm Load, i_L (amps)	Open Circuit Voltage, e_{oc} (volts)	Short Circuit Current, i_{sc} (amps)	Voltage Across 1-ohm Load, e_L (volts)	Current Through 1-ohm Load, i_L (amps)	
1 Forward End of Tip Tank	--	--	--	--	-13/-6	0	--	--	
Pylon Tip	--	--	--	--	90/70	0	--	--	
Jettison safety relay energized - explosive bolt connected									
1 Forward End of Tip Tank	--	--	--	--	-7/-2	0	(Excursion from 16-volt Battery Voltage)		
Pylon Tip	--	--	--	--	40/15	0	(Excursion from 16-volt Battery Voltage)		
Wing Panel	--	--	--	--	28.0	--	--	--	
Aluminum foil applied over leading edge seam									
1 Forward End of Tip Tank	--	--	--	--	5.2	--	--	--	
1 kiloampere strokes from transient analyzer									
1 Forward End of Tip Tank	--	--	--	--	0.1	--	--	--	

(Continued)

TABLE XVII (Continued)

Circuit E.0711, Right Fuel Quantity Indication
Open Circuit Voltage, e_{oc} (volts)

i_L Wave Form:		Slow Wave Form (36 x 82 μ s)							
Stroke Location	Circuit Conductor								
	2E69B22 & Airframe	2E70B20 & Airframe	2E69B22 & 2E70B20	2E67B22 & Airframe	2E68B20 & Airframe	2E67B22 & 2E68B20	2E65B22 & Airframe	2E66B20 & Airframe	2E66B20 & 2E65B22
1 Forward End of Tip Tank	0.6	0.8	-1.1	1.1	2.4	-1.4	0.7	1.9	1.4
4 Outboard Leading Edge	0.6	1.2	-0.9	0.4	1.8	-1.2	0.9	1.3	0.5
5 Trailing Edge of Aileron	0.6	0.8	-0.8	0.6	2.1	-0.8	1.2	1.4	0.5
7 Center of Wing Surface	0.6	0.8	-0.6	1.3	1.3	-0.7	0.3	1.6	0.5
10 Inboard Leading Edge	0.9	1.3	-1.1	1.1	2.7	-0.5	1.8	1.8	0.5

(Continued)

TABLE XVII (Continued)

Circuit E.0711, Right Fuel Quantity Indication
Open Circuit Voltage, e_{oc} (volts)

Stroke Location	Fast Wave Form (8.2 x 14 μ s)								
	Circuit Conductor								
	2E69B22& Airframe	2E70B20& Airframe	2E69B22& 2E70B20	2E67B22& Airframe	2E68B20& Airframe	2E67B22& 2E68B20	2E65B22& Airframe	2E66B20& Airframe	2E66B20& 2E65B22
1 Forward End of Tip Tank	0.8	1.3	-1.0	0.6	4.0	-3.3	0.3	3.7	2.3
4 Outboard Leading Edge	0.5	1.0	-1.0	0.8	2.2	-1.6	0.2	2.2	0.9
5 Trailing Edge of Aileron	0.6	0.8	-0.8	0.4	2.4	-0.8	0.5	1.7	0.55
7 Center of Wing Surface	0.8	1.3		0.6	1.0	-0.5	1.0	0.8	0.55
10 Inboard Leading Edge	0.5	1.6	-1.6	0.4	2.7	-1.1	0.2	1.8	0.4

(Continued)

TABLE XVII (Continued)

Circuit E.0711, Right Fuel Quantity Indication
Conductor 2E69B22 and Airframe

Stroke to removable panel on top of wing (panel completely bolted)

i _L Wave Form:		Slow Wave Form (36 x 82 μs)				Fast Wave Form (8.2 x 14 μs)			
Stroke Location	Open Circuit Voltage, e _{oc} (volts)	Short Circuit Current, i _{sc} (amps)	Voltage Across 1-ohm Load, e _L (volts)	Current Through 1-ohm Load, i _L (amps)	Open Circuit Voltage, e _{oc} (volts)	Short Circuit Current, i _{sc} (amps)	Voltage Across 1-ohm Load, e _L (volts)	Current Through 1-ohm Load, i _L (amps)	
Wing Panel	--	--	--	--	0.9	0	--	--	
Conductor 2E70B20 and Airframe									
Wing Panel	--	--	--	--	1.7	0	--	--	
Stroke to removable panel on top of wing (panel fastened by 8 volts) Conductor 2E69B22 and Airframe									
Wing Panel	--	--	--	--	0.8	0	--	--	
Conductor 2E70B20 and Airframe									
Wing Panel	--	--	--	--	1.6	0	--	--	
Stroke to removable panel on top of wing (panel completely unbolted and elevated 1/4" by fiber spacers) Conductor 2E69B22 and Airframe									
Wing Panel	--	--	--	--	0.9	--	--	--	
Conductor 2E70B20 and Airframe									
Wing Panel	--	--	--	--	1.75	--	--	--	
Stroke to just outboard of the top panel (panel completely unbolted and elevated 3/4" by fiber spacers) Conductor 2E69B22 and Airframe									
Wing Panel	--	--	--	--	0.95	--	--	--	

(Continued)

TABLE XVII (Continued)

Circuit F.0511, E-11 Autopilot

i_L Wave Form:		Slow Wave Form (36 x 82 μ s)				Fast Wave Form (8.2 x 14 μ s)			
Conductor	Stroke Location	Open Circuit Voltage, e_{oc} (volts)	Short Circuit Current, i_{sc} (amps)	Voltage Across 1-ohm Load, e_L (volts)	Current Through 1-ohm Load, i_L (amps)	Open Circuit Voltage, e_{oc} (volts)	Short Circuit Current, i_{sc} (amps)	Voltage Across 1-ohm Load, e_L (volts)	Current Through 1-ohm Load, i_L (amps)
F572K18 and Airframe	1	2	0.1	--	--	3	--	--	--
	4	1	--	--	--	2.5	--	--	--
	5	2	--	--	--	2	--	--	--
	7	2	--	--	--	5/2	--	--	--
	10	2	--	--	--	2	--	--	--
F755E18 and Airframe	1	--	--	--	--	3	--	--	--
	4	5/1	--	--	--	2.5	--	--	--
	5	1	--	--	--	2	--	--	--
	7	2	--	--	--	2	--	--	--
	10	2	--	--	--	2	--	--	--
F572K18 and F755E18	1	0.07	0.3	.068	.075	0.4	0.2	.23/.23	0.2
	4	27/0.1	0.25	0.2/0.12	0.1	3/.48	0.5	0.26	0.2
	5	2/0.2	0.25	.4/0.13	0.1	0.6	0.5	0.3	0.25
	7	0.1	0.25	0.12	0.1	6/.5	0.5	0.3	0.25
	10	0.1	0.25	0.04	0.04	1.5/.2	0.1	0.1	0.1
100 Kiloampere Oscillatory Current, Wave Shape of First Half Cycle: 13 x 23 μ s									
F572K18 and Airframe	1	--	--	--	--	4.0	--	--	--
	5	--	--	--	--	3.8	--	--	--
F755E18 and Airframe	1	--	--	--	--	4.6	--	--	--
	5	--	--	--	--	3.6	--	--	--
F572K18 and F755E18	1	--	--	--	--	1.8	1.6	--	--
	5	--	--	--	--	2.5	2.0	--	--

(Continued)

TABLE XVII (Continued)

Circuit L.050, Position Light
Conductor 2L10E18 and Airframe

i _L Wave Form:		Slow Wave Form (36 x 82 μs)				Fast Wave Form (8.2 x 14 μs)			
Stroke Location	Open Circuit Voltage, e _{oc} (volts)	Short Circuit Current, i _{sc} (amps)	Voltage Across 1-ohm Load, e _L (volts)	Current Through 1-ohm Load, i _L (amps)	Open Circuit Voltage, e _{oc} (volts)	Short Circuit Current, i _{sc} (amps)	Voltage Across 1-ohm Load, e _L (volts)	Current Through 1-ohm Load, i _L (amps)	
1 Forward End of Tip Tank	40/20	9.0	6.0	6.0	96/48	15.0	12.0	11.0	
4 Outboard Leading Edge	6/2.2	0.8	3/0.6	0.6	15/4	1.1	0.7	0.65	
5 Trailing Edge of Aileron	15/3.8	1.3	1.0	1.0	30/12	4.0	3.0	3.0	
7 Center of Wing Surface	10/2.4	0.8	0.8	0.7	20/2	1.5	1.2	1.2	
10 Inboard Leading Edge	10/1.8	0.7	0.8	0.5	17/2.8	1.7	2.8/0.7	0.65	

(Continued)

TABLE XVII (Continued)

Circuit L.050, Position Light
Conductor 2L10E18 and Airframe

i_L Wave Form:		Slow Wave Form (36 x 82 μ s)				Fast Wave Form (8.2 x 14 μ s)			
Stroke Location	Open Circuit Voltage, e_{oc} (volts)	Short Circuit Current, i_{sc} (amps)	Voltage Across 1-ohm Load, e_L (volts)	Current Through 1-ohm Load, i_L (amps)	Open Circuit Voltage, e_{oc} (volts)	Short Circuit Current, i_{sc} (amps)	Voltage Across 1-ohm Load, e_L (volts)	Current Through 1-ohm Load, i_L (amps)	
Stroke to removable panel on top of wing (panel completely bolted)									
Wing Panel	--	--	--	--	1.6	0.6	--	--	
Stroke to removable panel on top of wing (panel fastened by 8 bolts)									
Wing Panel	--	--	--	--	2.0	0.65	--	--	
1 Kiloampere stroke from transient analyzer									
1 Forward End of Tip Tank	--	--	--	--	1.4	0.44	--	--	
100 Kiloampere oscillatory current, wave shape of first half cycle: 13 x 23 μ s									
1 Forward End of Tip Tank	--	--	--	--	70.0	23.0	--	--	
5 Trailing Edge of Aileron	--	--	--	--	21.0	6.0	--	--	

(Continued)

TABLE XVII (Continued)

Circuit Q.0401, Fuel Vent Valves
Conductor 2Q331D14 and Airframe

i_L Wave Form:	Slow Wave Form (36 x 82 μ s)				Fast Wave Form (8.2 x 14 μ s)			
	Stroke Location	Open Circuit Voltage, e_{oc} (volts)	Short Circuit Current, i_{sc} (amps)	Voltage Across 1-ohm Load, e_L (volts)	Current Through 1-ohm Load, i_L (amps)	Open Circuit Voltage, e_{oc} (volts)	Short Circuit Current, i_{sc} (amps)	Voltage Across 1-ohm Load, e_L (volts)
1 Forward End of Tip Tank	2.8	.019	2.6	.01	6.5	0.1	0.5	0.1
4 Outboard Leading Edge	1.8	0.1	0.4	.05	3.1	0.1	0.5	.05
5 Trailing Edge of Aileron	1.8	.05	0.7	.05	1.6	.05	?	.05
7 Center of Wing Surface	2.2	.05	0.6	.05	7/1.9	.05	7/1.0	.05
10 Inboard Leading Edge	2.4	.05	0.8	.05	5.4/2.4	.05	0.35	.05

(Continued)

TABLE XVII (Continued)

Circuit Q.060, Right Wing Tank Booster Pump
Conductor 2Q77C8 and Airframe

i_L Wave Form:	Slow Wave Form (36 x 82 μ s)				Fast Wave Form (8.2 x 14 μ s)			
	Stroke Location	Open Circuit Voltage, e_{oc} (volts)	Short Circuit Current, i_{sc} (amps)	Voltage Across 1-ohm Load, e_L (volts)	Current Through 1-ohm Load, i_L (amps)	Open Circuit Voltage, e_{oc} (volts)	Short Circuit Current, i_{sc} (amps)	Voltage Across 1-ohm Load, e_L (volts)
1 Forward End of Tip Tank	1.0	0.7	0.3	0.3	1.2	1.7	0.7	0.7
4 Outboard Leading Edge	1.4/1.0	0.75	0.25	0.25	1.3	1.8	0.75	0.7
5 Trailing Edge of Aileron	1.0/0.9	0.5	0.25	0.25	1.3	1.7	0.7	0.7
7 Center of Wing Surface	0.9	0.25	0.3	0.25	1.4	1.9	0.7	0.6
10 Inboard Leading Edge	1.4	0.85	0.4	0.35	1.6	2.4	0.95	0.9

(Continued)

TABLE XVII (Continued)

Circuit Q.060, Right Wing Tank Booster Pump
Conductor 2Q78C12 and Airframe

i_L Wave Form:	Slow Wave Form (36 x 82 μ s)				Fast Wave Form (8.2 x 14 μ s)			
	Stroke Location	Open Circuit Voltage, e_{oc} (volts)	Short Circuit Current, i_{sc} (amps)	Voltage Across 1-ohm Load, e_L (volts)	Current Through 1-ohm Load, i_L (amps)	Open Circuit Voltage, e_{oc} (volts)	Short Circuit Current, i_{sc} (amps)	Voltage Across 1-ohm Load, e_L (volts)
1 Forward End of Tip Tank	2.3/2	0.9	0.5	0.5	2.5	2.6	1.2	1.2
4 Outboard Leading Edge	6/1.8	0.9	0.5	0.5	2.6	2.8	1.2	1.2
5 Trailing Edge of Aileron	4/1.8	1.0	--	--	3.2/1.5	2.7	1.0	0.9
7 Center of Wing Surface	1.7	1.3	0.7	0.7	7/3	3.8	1.6	1.6
10 Inboard Leading Edge	2.0	0.9	0.5	0.5	2.4	2.6	1.2	1.1
Using transient analyzer as lightning current source - 1 kiloampere crest applied wave								
1	--	--	--	--	0.1	0.1	--	--

(Continued)

TABLE XVII (Continued)

Circuit R.060, AN/ARN-18 Glide Path Radio Receiver
Conductor RA35C and Airframe

i_L Wave Form:	Slow Wave Form (36 x 82 μ s)				Fast Wave Form (8.2 x 14 μ s)			
	Stroke Location	Open Circuit Voltage, e_{oc} (volts)	Short Circuit Current, i_{sc} (amps)	Voltage Across 1-ohm Load, e_L (volts)	Current Through 1-ohm Load, i_L (amps)	Open Circuit Voltage, e_{oc} (volts)	Short Circuit Current, i_{sc} (amps)	Voltage Across 1-ohm Load, e_L (volts)
1 Forward End of Tip Tank	2.0*	0.012*	1.0*	--	30/7	18.0	7.0	6.5
4 Outboard Leading Edge	9/4	12.0	2.8	2.6	40/20	20.0	7.5	7.0
5 Trailing Edge of Aileron	3/.8	4.0	2/1	0.8	28/3	7.5	7.0	6.0
7 Center of Wing Surface	6/.6	3.0	0.6	0.6	30/2.4	6.0	2.4	2.2
10 Inboard Leading Edge	6/2	5.0	1.0	0.5	14/1	1.6	3/.8	0.8

* Antenna coupling capacitor opened for these measurements. Capacitor shorted for all other measurements.

(Continued)

TABLE XVII (Continued)

Circuit R.060, AN/ARN-18 Glide Path Radio Receiver
Conductor RA35C and Airframe

i_L Wave Form:	Slow Wave Form (36 x 82 μ s)				Fast Wave Form (8.2 x 14 μ s)			
	Open Circuit Voltage, e_{oc} (volts)	Short Circuit Current, i_{sc} (amps)	Voltage Across 1-ohm Load, e_L (volts)	Current Through 1-ohm Load, i_L (amps)	Open Circuit Voltage, e_{oc} (volts)	Short Circuit Current, i_{sc} (amps)	Voltage Across 1-ohm Load, e_L (volts)	Current Through 1-ohm Load, i_L (amps)
Wing Panel	--	--	--	--	5.0	1.9	--	--
Stroke to removable panel on top of wing (panel completely unbolted and elevated 1/4" by insulating spacers)								
Wing Panel	--	--	--	--	6.0	1.6	--	--
Stroke to removable panel on top of wing (panel completely unbolted and elevated 3/4" by insulating spacers)								
Wing Panel	--	--	--	--	8.5	2.0	--	--
Wing Panel	--	--	--	--	7.0	--	--	--
Aluminum foil applied over leading edge seam								
1 Forward End of Tip Tank	--	--	--	--	--	17.0	--	--
10 Inboard Leading Edge	--	--	--	--	8.5	2.4	--	--

(Continued)

TABLE XVII (Continued)

Circuit S.220, Armament Power Supply
Open Circuit Voltage, e_{oc} (volts)

i_L Wave Form:	Slow Wave Form (36 x 82 μ s)						Fast Wave Form (8.2 x 14 μ s)					
	Circuit Conductor											
Stroke Location	2SF3886E20 & Airframe	2SF3887E20 & Airframe	2SF3819J20 & Airframe	2SF3861D20 & Airframe	2SF3821J20 & Airframe	2SF3885D20 & Airframe	2SF3886E20 & Airframe	2SF3887E20 & Airframe	2SF3819J20 & Airframe	2SF3861D20 & Airframe	2SF3821J20 & Airframe	2SF3885D20 & Airframe
1 Forward End of Tip Tank	.045	.045	.045	.045	.055	.05	0.2	0.18	0.18	0.2	0.15	0.2
4 Outboard Leading Edge	.03	.03	.03	.025	.04	.035	0.1	--	--	--	--	--
5 Trailing Edge of Aileron	.03	.02	.025	.03	.03	.025	.045	--	--	--	--	--
7 Center of Wing Surface	.025	.02	.02	.025	.03	.025	.045	--	--	--	--	--
10 Inboard Leading Edge	.04	.045	.045	.04	.06	.025	.02	.03	.02	.025	.025	.04

REFERENCES

1. Morgan, G.E.: "Investigation of Inadvertent Firing of Electroexplosive Subsystems on Aerospace Vehicles", Interim Technical Report: AF-33(615)-3853, North American Aviation Inc., August, 1966.
2. USAF Technical Order 1F-89J-2-10: "Maintenance Instructions: Wiring Diagrams and Data", February 1960.
3. Peterson, B.J., Wood, A.R.: "Measurements of Lightning Strikes to Aircraft", Final Report No. DS-68-1 Federal Aviation Administration, January, 1968.
4. Hagenguth, J.H., Anderson, J.G.: "Lightning to the Empire State Building -- Part III", AIEE Trans., vol. 71, Part III (Power Apparatus and Systems), pp. 641-649, August 1952.
5. Hagenguth, J.H.: "Lightning Stroke Damage to Aircraft", AIEE Trans., vol. 68, Part II, pp. 1036-1044, 1949.
6. Kesler, F.L., Gerstein, M., Plumer, J.A.: "A Study of Aircraft Fire Hazards Related to Natural Electrical Phenomena", NASA Publication No. CR 1076, 1967.
7. McEachron, K.B.: "Lightning to the Empire State Building", AIEE Trans., vol. 60, pp. 885-890, 1941.
8. Bewley, L.V.: "Traveling Waves on Transmission Systems", Dover Publications, Inc., New York, N.Y., 1963.
9. Brenner, E., Javid, M.: "Analysis of Electric Circuits", McGraw-Hill Book Co., Inc., 1959.
10. Chen, W.H.: "Linear Network Design and Analysis", McGraw-Hill Book Co., Inc., 1964.
11. Aeronautical Radio Inc.: "Guidance for Aircraft Electrical Power Utilization and Transient Protection", ARINC Specification No. 413, May, 1967.

BIBLIOGRAPHY

Technical papers and articles covering subjects related to the research described in this report are listed below. Items listed below have not been utilized as specific references in this report.

General Lightning Characteristics

1. McEachron, K.B.: "Lightning to the Empire State Building", The Journal of the Franklin Institute, vol. 227, No. 2, pp. 149-217, February, 1939.
2. McEachron, K.B.: "Wave Shapes of Successive Lightning Current Peaks", Electrical World, vol. 113, pp. 56-58, 126-127, February 10, 1940.
3. Newman, M.M., Stahmann, J.R., Robb, J.D.: "Experimental Study of Triggered Natural Lightning Discharges", FAA Report No. DS-67-3, March, 1967.
4. Schonland, Sir Basil: "Lightning and the Long Electric Spark", an address delivered to the August 31, 1962 meeting of the British Association for the Advancement of Science. Available as a preprint from The Advancement of Science XIX, 1962-63.
5. Wilson, C.T.R.: "Some Thunderstorm Problems", The Journal of the Franklin Institute, vol. 2, p. 1, 1929.
6. Wilson, C.T.R.: "Investigations on Lightning Discharges on the Electrical Field of Thunderstorms", Proceedings of the Royal Society, Series A, vol. 221, pp. 73-115, 1929.
7. Simpson, Sir George: "The Mechanism of a Thunderstorm", Proceedings of the Royal Society, Series A, vol. 114, p. 376, 1927.
8. Evans, E.A., McEachron, K.B.: "The Thunderstorm", General Electric Review, pp. 413-425, September 1936.
9. Simpson, G.C.: "Lightning", Journal of the Institution of Electrical Engineers, vol. 67, No. 395, pp. 1269-1282, November 1929.
10. Simpson, G.C., Scrace, F.J.: "The Distribution of Electricity in Thunderclouds", Proceedings of the Royal Society, Series A, vol. 161, pp. 309-352, 1937.

11. Robertson, L.M., Lewis, W.W., Foust, C.M.: "Lightning Investigations at High Altitudes in Colorado", AIEE Trans., vol. 61, pp. 201-208, April 1942.
12. Lewis, W.W.: "The Protection of Transmission Lines Against Lightning", Chapters 1 and 2, John Wiley, New York, N.Y., 1950.
13. Westinghouse Electric Corp.: "Electrical Transmission and Distribution Reference Book", Chapter 16, East Pittsburgh, Pa., 1950.
14. Alexander, W.H.: "Distribution of Thunderstorms in the United States", Monthly Weather Review, vol. 52, p. 337, 1924.
15. McCann, G.D.: "The Measurement of Lightning Currents in Direct Strokes", AIEE Trans., vol. 63, pp. 1157-1164, 1944.
16. Berger, K.: "Front Time (Rise Time) and Current Steepness of Lightning Strokes to the Earth", Central Electricity Generating Board, Central Electricity Research Laboratories, Leatherhead, England. International Conference, May 1962. Gas Discharges and the Electricity Supply. Preprint Paper No. 27.

Effects of Lightning on Aircraft Electrical Systems

17. Conference Papers, Lightning and Static Electricity Conference, Dec. 3-5, 1968, Technical Report AFAL-TR-68-290, Part II, May, 1969.
18. "Protection of Nonmetallic Aircraft from Lightning - IV. Electro-cution Hazards from Inductive Voltages", NACA ARR No. 4128, March 1945.
19. Newman, M.M., Robb, J.D., Stahmann, J.R.: "Electromagnetic Hazards Inside Aircraft - I", AFAL-TR-66-215, Part I, September, 1966.